NTNU
Norwegian University of
Science and Technology

Semiclassical theory of a disordered two-dimensional SNS-junction

Nicolai Gerrard

MSc in Physics
Submission date: May 2018
Supervisor: Jeroen Danon, IFY

Norwegian University of Science and Technology
Department of Physics

Abstract

Two-dimensional hybrid superconductor-semiconductor structures provide a promising platform for realising networks of Majorana fermions for fault-tolerant quantum computing, and, as such, are attracting a lot of attention. Recently, two-dimensional superconductor-normal material-superconductor (SNS) junctions created in such hybrid systems, exhibited dramatic asymmetries in their Fraunhofer-like patterns of the critical current as a function of applied magnetic field. It was proposed that, apart from spin-orbit interaction and Zeeman effects, disorder inside the junction can play an important role in the appearance of these asymmetries.

This thesis investigates the role of disorder in two-dimensional SNS-junctions by developing a toy model in a semiclassical picture. This model assumes two distinct paths across the junction, connected by beamsplitters at the normal material-superconductor (NS) interfaces, enclosing a magnetic flux. By describing these paths as ballistic, one-dimensional nanowires, and using a scattering matrix approach to describe the beamsplitters, we develop a method for calculating the transmission and reflection coefficients of the junction as a whole. This allows us to control the coupling between the nanowires and the NS-interfaces, as well as to introduce an asymmetric probability injection into the two arms and to incorporate a difference in the two path lengths.

The supercurrent through the junction is found from the energy of the Andreev bound states, which allows us to investigate the critical current as a function of the magnetic flux penetrating the surface enclosed by the two paths. We find that, in the absence of spin-dependent effects such as spin-orbit interaction and the Zeeman effect, none of the combinations of asymmetric probability injection, different path lengths, modifications of the chemical potential or NS coupling strength produces asymmetries in the critical current, such as observed in the experiment. We thus conclude that either our toy model is not sufficiently complex, e.g., one would need more than two interfering trajectories, or that disorder alone is not sufficient to produce asymmetric patterns of critical currents. Further research is required to in order to to determine which conclusion is correct.

Sammendrag

Todimensjonale hybridstrukturer av superledere - halvledere er lovende plattformer for å skape majoranafermion-nettverk, som er en mulig byggestein for kvantedatamaskiner. Nylig har man oppdaget asymmetriske Fraunhofermøsntre i den kritiske strømmen som en funksjon av magnetisk felt i todimensjonale superledere - normalt materiale - superleder (SNS) koblinger, av nettopp slike hybridstrukturer. Det har blitt foreslått at uorden, i tillegg til spinn-bane-kobling og Zeemaneffekter, kan spille en avgjørende rolle i mekanismen bak disse asymmetriene. Denne masteroppgaven fokuserer på å utforske uorden i SNS-koblinger ved å bygge opp en forenklet modell for uordnede, todimensjonale SNS-koblinger i en semiklassisk tilnærming. Modellen består av to mulige baner over koblingen, koblet sammen med strålespredere på normalt material - superleder (NS) overflaten. På denne måten kan man ha en innesluttet magnetfluks og en Aharanov-Bohm-effekt. Ved å beskrive banene som ballistiske, endimensjonale nanotråder kan vi finne transmisjon- og refleksjonskoeffisientene i koblingen. Vi tar i bruk en spredningsmatrisemetode for strålesprederne, noe som tillater oss å kontrollere koblingen mellom nanotrådene og NS-overflaten, samt mulige asymmetriske sannsynligheter for valg av bane. Asymmetriske banelengder er også inkludert. Superstrømmen gjennom koblingen blir funnet via Andreev-bundende tilstander, noe som tillater oss å utforske den kritiske strømmen som en funksjon av magnetfluks. Vi finner at, i fraværet av spinneffekter som spinn-bane-kobling og Zeemaneffekter, ingen mulige kombinasjoner av kobling mellom NS-overflatene og banene, asymmetrisk sannsynlighet, asymmetrisk banelengde eller endringer i det kjemiske potensialet klarer å gjenskape de nevnte asymmetriene i den kritiske strømmen.Vi må derfor konkludere med at den forenklede modellen vår enten ikke er kompleks nok, ved at to baner ikke er nok, eller at uorden alene ikke er nok til å skape asymmetriske Fraunhofermønstre i den kritiske strømmen.Et endelig svar krever

videre forsking.

Preface

This thesis is submitted as the conclusion of a two-year Master of Science in Physics program at the Norwegian University of Science and Technology (NTNU). I want to extend my gratitude to my supervisor, Prof. Jeroen Danon, for his invaluable support and guidance over the last two years. His patience, helpfulness and understanding has been an inspiration. I would also like to extend my appreciation to Stian H. Hartman, Erik Liodden, Martin Hornkjøl, Jonas L. Willadsen, Frode T. Børseth og Sandra Suciu for companionship, exchange of ideas and general support during the work on this thesis.

Dedication

To Sandra, for all her support and love

Table of Contents

List of Figures

List of Tables

Abbreviations and conventions

Abbreviations

SNS - Superconductor - Normal material - Superconductor

NS - Normal material - Superconductor

N-region - Normal region

SC - Superconducting, superconductor

SC-region - Superconducting region

SOI - Spin-Orbit Interaction

SO - Spin-Orbit

MF - Majorana Fermion

ABS - Andreev Bound State

NW - Nanowire

BdG - Bogoliubov - de Gennes

AB - Aharanov - Bohm

1D - one dimension, one-dimensional

Conventions

E - energy

μ - chemical potential

$\hat{\mathbf{p}}$ - quantum mechanical momentum operator

Δ - superconducting gap

$\mathbf{k}$ - wavevector

v_F - Fermi velocity

k_F - Fermi wavenumber

$\mathbf{A}$ - magnetic potential, vector potential

g - gyromagnetic factor, g-factor

$\mathbf{B}$ - magnetic field

$\boldsymbol{\alpha}$ - SO-field

σ_i - Pauli matrix

$\hat{H}$ - Hamiltonian

t, r - transmission, reflection

1 — Introduction

Technological development and growing improvement of crystal growth methods over the last few decades have allowed researchers to investigate tailor-made quantum structures. This has led to an intense research activity into the field of spintronics, or spin electronics. The central theme of this field is the manipulation of spin degrees of freedom; to understand the interaction between the spin of a particle and its environment and how this can be applied to create useful devices. The most important areas of study are spin transport in electronic systems, spin dynamics and spin relaxation in different environments [1].

Among the most significant spin effects is the spin-orbit interaction (SOI), also known as spin-orbit coupling. SOI is a relativistic effect where the spin of the electron couples to the orbital movement in the presence of an electric field. In crystals lacking an inversion center, SOI has the effect of spin splitting the electronic energy bands, even without a magnetic field, thus removing the spin degeneracy in momentum space [2]. A Lorentz transformation of an electric field $\mathbf{E}$, arising from e.g. a confinement potential (caused by inversion asymmetry) or the electrostatic gate potential, to the rest frame of a particle moving through said field, yields a term which couples $\mathbf{E} \times \hat{\mathbf{p}}$ to the spin of the particle, i.e. an effective magnetic field. $\hat{\mathbf{p}}$ is the quantum mechanical momentum operator. The importance of this effective field lies in the possibility to manipulate and control the spin of an electron using electric fields rather than actual magnetic fields [3, 4, 5]. A conceptually simple example of of such control is the fact that the electric field can be used as a control knob for the spin precession through materials. The effective magnetic field will make the spin of the electron precess around it. Thus, by controlling the electric field with e.g. a gate voltage, one can alter the angular frequency of the Larmor precession of the spin and therefore the angle through which it precesses while it moves through the material. This has been demonstrated in for example InGaAs/InAlAs heterostructures [6] and HgTe quantum wells [7]. The control over spin polarisation is extremely important for spintronic devices, like those based on spin currents and information storage with spins. Figure 1.1 shows some areas of study where this is realised by the means of the SOI. Electric control of spin states is an enticing alternative to magnetic control based on ferromagnetic elements, as electric control is superior to magnetic control because of more accurate scalability, lower power consumption and the capability of locale spin manipulation [8]. For example, electronic separation of spin states has been demonstrated in quantum point contacts [9]. Methods like this are also a demonstrated way to create spin-filters [10].

One exciting example of a proposed spintronic application that relies on the ability to separate and control the spin states of electrons electrically, is quantum bits, or qubits. Qubits are two-level quantum systems intended for use in quantum information processing, and they are the quantum analogue to the classical bits, representing units of quantum information. The great advantage qubits have over conventional bits is that

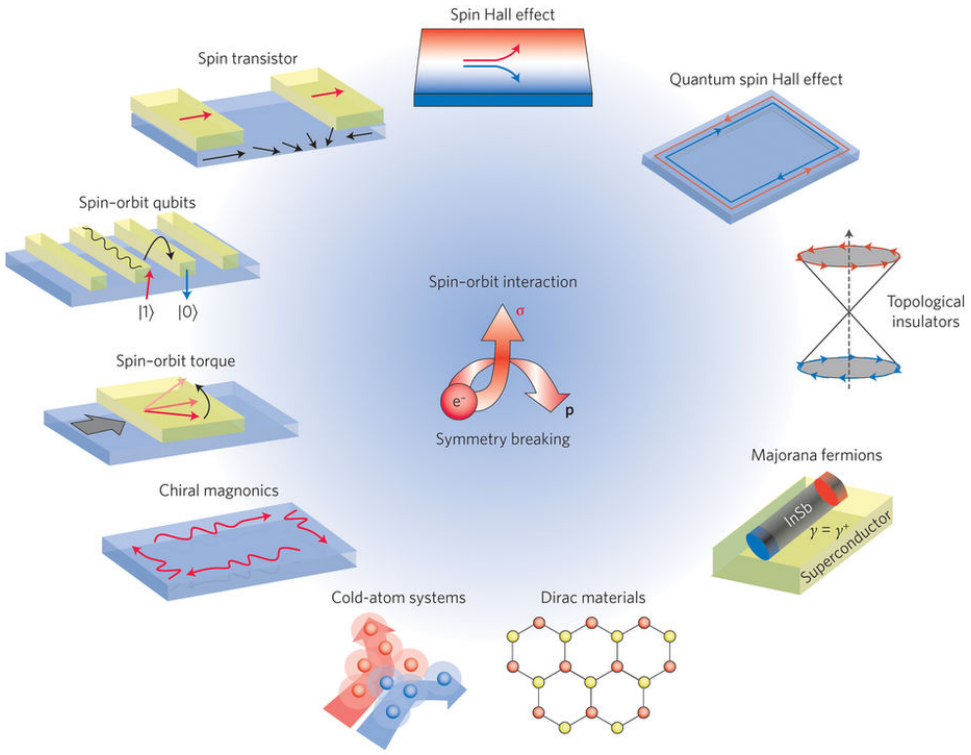

Figure 1.1: This figure shows various sub-fields of spin-orbitronics, where the SOI is responsible for electrical control over spin and magnetisation. Adapted from [8].

they can exist in superpositions, they can be both "0" and "1" at the same time, as well as entangled with each other. The Hilbert space of a set of N qubits will have dimensions 2^N, which means that the number of classical bits required to represent the information stored in N qubits is proportional to $(2^N - 1)$ [11]. This is a staggering gain in information storage capabilities compared to classical bits. One proposed qubit implementation is an electron confined in a quantum well, where spin up and down are the two levels. It is a so-called spin qubit, where electrical control is preferred over magnetic control. SOI provides such a control method, and such "spin-orbit" qubits have been realised in quantum dots [12] and in quantum wires [13].

An inherent problem with qubits is decoherence. Quantum systems become decoherent when interacting with their surroundings, by randomisation of the phase of the system. The implementation of qubits is a challenge from this perspective, since they require both good interaction with their surroundings for reliable quantum control; as well as isolation to ensure suffucient coherence times [14]. One proposed way for fault-tolerant quantum computing is by encoding the qubits into Majorana fermions (MF) [15], fermions which are their own antiparticles. These fermions can then be used to manipulate quantum information in topologically protected procedures [16]. MF's can theoretically appear in a wide variety of solid state materials, such as p-wave superconductors [17]. Let us quickly introduce superconductivity and how MF's appear in superconductors.

Superconductivity is an effect discovered at the beginning of the 20th century and is mainly characterised by complete zero-resistivity conduction (the so-called "supercurrent") and the expulsion of magnetic fields. At a critical temperature, a phase transition takes place, from a normal conducting phase to a superconducting one. The phase transition normally takes place in the range between 0 and 40 kelvin (K) [18], yet critical

temperatures up to 203K have been experimentally proven in exotic compounds [19]. Supercurrents can prevail up until either too strong of a current is passed through the material or a too strong external magnetic field is applied, which are called the critical current and the critical magnetic field, respectively. Both of these events suppress the superconducting phase state and cause the transition to a normal state of matter. Single-particle excitations in a superconductor are Bogoliubov quasiparticles, or excitations, coherent superpositions of electrons and holes, mirroring the particle-antiparticle representation of particle physics. Electrons (holes) are filled (empty) states with energy E above (below) the chemical potential μ with negative (positive) charge. Energy is conventionally measured from μ when discussing quasiparticles, giving $E = 0$ at μ. If there is an odd number of states, particle-hole symmetry ensures that one of these lies at zero energy (at the Fermi level) [8], a neutrally charged eigenstate. This state is called a MF, since it is its own antiparticle. The creation $\hat{\gamma}^\dagger(E)$ and annihilation $\hat{\gamma}(E)$ Bogoliubov operators for excitations are related through

$$\hat{\gamma}(E) = \hat{\gamma}^\dagger(-E), \tag{1.1}$$

which at zero energy means that the electron (particle) and hole (anti-particle) coincide; and therefore it is a Majorana fermion [20].

Such MF zero modes ($E = 0$) are strictly forbidden to take place in conventional s-wave superconductors, but can occur in rare p-wave superconductors. However, when s-wave superconductivity is induced by the proximity effect onto topological insulators with strong SOI, MF's can appear. They will be located in Abrikosov vortices and at edges of the topological insulator [21]. This type of vortex serves as a topological defect, which, when hosting a MF, follows non-Abelian statistics. The underlying physical ingredient allowing for the theoretical existence of MF's is the strong SOI, which gives rise to an odd number of states [17]. Thus topological superconductors is a promising way of creating MF's [22]. As already mentioned, the importance of MF's in condensed matter physics is most appreciated when trying to minimise the errors that can occur in quantum computing. Small cumulative perturbations cause the states to decohere, which introduces errors in computations based on qubits. This decoherence problem can be solved by hiding the phase of the qubits through a procedure called braiding; adiabatic interchange of two Majorana bound states in closed loops around each other in three-dimensional spacetime [20]. As a result, the computing operations are topologically protected, which is the premise of topological quantum computers. Experiments have been performed in semiconducting nanowires [23, 24], topological insulators [25] and magnetic atom chains [26]. These experiments provide convincing arguments for the existence of Majorana fermions. However, the correlation between MF's and these results is still up for debate. The ongoing work faces challenges on how to implement networks of Majorana fermions to create logical gates for quantum computing (analogous to transistor gates in classical computing). One proposal is a two-dimensional electron gas on a superconducting layer as a platform for networks of Majorana fermions [27, 28]. Frameworks for how to implement these networks into quantum computing by Majorana fermion codes are also being developed [29]. The spin-orbit plays a crucial role in all of this, since it ensures an odd number of states [8] while also playing a critical role in the search for MF's in nanowires on superconductors [30, 31]. MF's are supposed to manifest themselves as peaks in the conductance at zero gate voltage at finite magnetic fields.

We can conclude from all of the above that SOI is not only important for realisation of spintronic devices, but it also plays a crucial role in proposals to establish fault-tolerant

quantum computing. Also, the recent interest in hybrid heterostructures (involving superconductors and non-superconducting materials), spurred by the aforementioned development of advanced nanostructures, has called for a more thorough understanding of transport phenomena in these structures and their respective properties. The Josephson effect and the possibility offered by nanostructures to control appropriate parameters present a convenient way to investigate transport and other properties of several materials by studying the supercurrent [32]. Properties of 2D-epitaxial structures (which are more amendable for quantum computing with MF's), such as the SOI-strength, the effective SO-field, the importance of impurities and how to disentangle SOI-effects and other mechanisms, are not yet well understood. For example, experiments claiming MF-existence are somewhat controversial, since other mechanisms may also be responsible for the reported results [17]. Also, many applications require magnetic fields, so understanding the behaviour of structures when applying magnetic fields of different orientations, can be essential. Superconductor - normal material - superconductor junctions (SNS-junction) with strong SOI form a well-known base from which to study these properties further, for example by studying the supercurrent as a function of magnetic field. Let us therefore introduce SNS-junctions and the Josephson effect here.

Normal material - superconductor (NS) interfaces, such as topological insulator - superconductor interfaces, can cause a rather special reflection. Low-energy electrons that are incident on the interface will cause the injection of a Cooper pair into the superconductor, and the generation of a reflected hole. This process is known as Andreev reflection [33, 34] and gives rise to Andreev bound states (ABS) if the normal material is sandwiched between two superconducting leads. The ABS arises when excitation (electron- or hole-like) carries out a periodic motion, resulting in resonant standing waves between the superconducting leads. This leads to quantisation of the excitation energy levels [35]. This kind of structure is called a SNS-junction, where the ABS supports supercurrent through the normal material by "tunneling" of Cooper pairs. The effect where a supercurrent flows across a SNS-junctions withput external electric fields is the so-called DC Josephson effect [36], where the supercurrent is often referred to as the Josephson current. The interplay between SOI and magnetic fields in SNS-junctions is of special interest, for example in heterostructures consisting of semiconducting nanowires and superconducting leads, which are promising platforms for realising Majorana modes [15]. The interplay is also responsible for phenomena in Josephson currents, such as the anomalous Josephson effect, where a finite current can persist even at zero phase difference, $I(\phi = 0) \neq 0$, where ϕ is the phase difference between the two superconductors [37, 38].

SNS-junctions with strong SOI have been proposed as a way to study topological phase transitions [27, 39] and to quantify the strength of the SOI for different materials [38, 40]. Josephson currents can therefore provide insight to the physics of the junction via, for example, investigation of the critical current. As an example, a rectangular junction with uniform current density results in a critical current resembling that of a single-slit Fraunhofer pattern from optics [41]. Current deviations from this pattern may contain information about the system and its properties [42, 43]. Recent experimental advances on 2D epitaxial Al/InAs-heterostructures have attained NS-interfaces with high electron mobility and Andreev reflection probability very close to unity [44, 45]. A recent article by Suominen et. al. [46] on an InAs/InGaAs heterostructure with an epitaxial Al layer, has studied the critical current as a function of magnetic fields both perpendicular and in-plane of the junction. When both a perpendicular magnetic field and an in-plane magnetic field were included, Suominen et. al. discovered asymmetries with respect to

the magnetic field. They found first a gradual transformation from a Fraunhofer pattern in the critical current to a pattern of a superconducting quantum interference device. It was argued that this was due to expulsion of magnetic flux form the superconducting Al-leads by the Meissner effect, which lead to an effective out-of-plane flux dipole. This dephases contributions in the central region and forces coherent transport to the edges. In contrast, the in-plane field induced striking asymmetries in the interference pattern upon inversion of the perpendicular field, as shown in Figure 1.2. The asymmetries depend on both magnitude and direction of the in-plane field, as well as varying between lobes and samples. This second result conceals information about the interplay of SOI and the Zeeman effect, effectively concealing system properties.

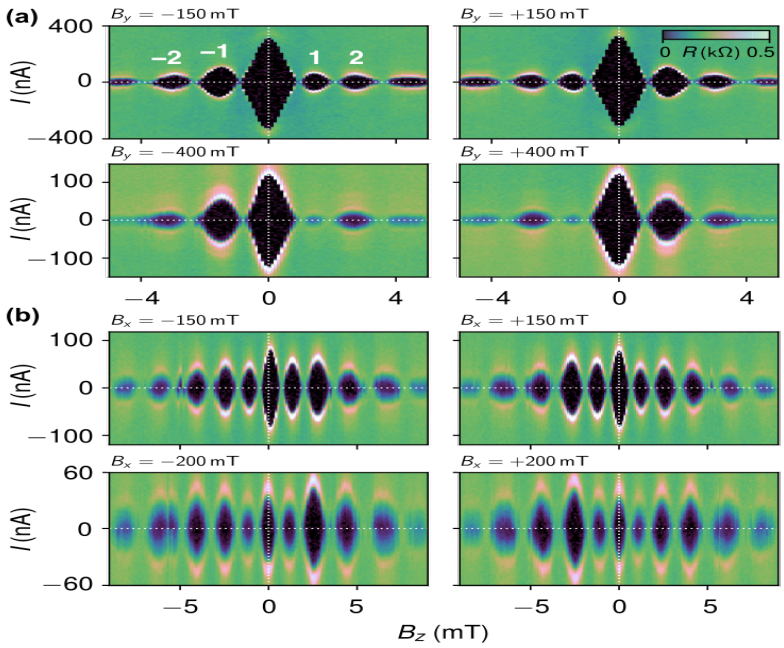

Figure 1.2: Differential resistance as a function of current I and perpendicular magnetic field B_z through the SNS-junction. Disregard the white numbers. a) is for an in-plane magnetic field in the $\pm y$-direction of two different magnitudes, b) is the same, only for the $\pm x$-direction. Adapted from [46].

A more detailed investigation of several samples pointed to an interplay of several device-dependent factors, such as SOI, disorder, interface coupling and the microscopic size of the samples. The authors argue that disorder plays a crucial role in the mechanisms responsible for the asymmetries. It was therefore unclear whether measurements of the asymmetries can be used to disentangle SOI and the Zeeman effect. Rasmussen et. al. [47] did an analysis of symmetries of the Hamiltonian for a 2D SNS-junction, relating them to the interference pattern of the critical current. They took into account both Rashba and Dresselhaus SOI, magnetic field, disorder and structural asymmetries. Their analysis supports the view that disorder, band bending and NS-interface barriers are influential ingredients contributing to the asymmetries in the interference patterns.

1.1 Motivation

The results of the experiments from [46] and the analysis of [47] serve as the motivation for this thesis. A more thorough understanding of SOI's effects and disorder on SNS-junctions might shed light on how to interpret the asymmetries arising in the interference patterns. If the effects of SOI, magnetic fields and disorder where to be disentangled, their individual effects on the asymmetry of the critical could current become apparent. This would clarify how to interpret the asymmetry of the measurements, and thus elucidate if the asymmetries can be used to arrive at quantitative conclusions about the SOI of the system, its strength, the effective SO-field and the interplay between SOI and the Zeeman effect.

A proper understanding of SOI and its effects is a prerequisite in the search and understanding of MF-hosting effective topological superconductors. The creation and employment of such devices for fault-tolerant quantum computing would bring us one step closer to the realisation of quantum computers.

1.2 Outline of thesis

The outline of the thesis is as follows: Chapter 2 will give the necessary background theory, where we start by introducing superconductivity, its characteristics and two theoretical models. We will so derive the BdG-equation before we introduce Andreev scattering and SNS-junctions. We end the chapter by explaining in detail the spin-orbit interaction. In Chapter 3, we will start our own work by deriving the Andreev reflection coefficients and show explicitly how the reflections follow naturally from the Bogoliubov - De Gennes equation. We will also find the Andreev energy levels and the supercurrent for 1D SNS-junctions at zero temperature for three cases: for no fields at all, magnetic field and magnetic field with SOI. The understanding of the Andreev reflection and the Josephson effect for 1D SNS-junctions will serve as a basis for expanding to a 2D SNS-junction in Chapter 4. Here we will allow for disorder at the interfaces, by developing a toy model for two paths across the junction, connected by beamsplitters. By applying a magnetic field perpendicular to the junction we can investigate the critical current through the junction as a function of magnetic field. This allows us to look for results which would indicate that disorder at the interfaces could be a possible reason for the asymmetries in the critical current discussed above. Chapter 5 will summarise the results in a conclusion, followed by an outlook and proposals for future work.

2 — Theory

Section 2.1 is supposed to give an introduction to the phenomenon superconductivity. We start out with a list of basic experimental facts in 2.1.1, supposed to give an overview over the nature of a superconductor, its properties and what distinguishes it from regular conductors. Section 2.1.2 I will go through the early theoretical models describing superconductivity, London-Pippard electrodynamics and Ginzburg-Landau theory. They are all essentially phenomenological, although surprisingly accurate. We so move over to the Bardeen-Cooper-Schrieffer (BCS) theory in Section 2.1.3, the first microscopic theory of superconductivity, before we in the end derive the Bogoliubov-de Gennes equation in Section 2.2. These sections will all in large parts draw from [11, 18, 35, 41, 48]. Sections 2.3 and 2.4 will present the Andreev reflection and SNS-junctions in more detail, as well as the Josephson effect and a derivation for the Fraunhofer pattern described in Chapter 1. Wrapping up the theory chapter will be Section 2.5, which will introduce spin-orbit interaction for charged particles. Qualitatively spin-orbit interaction mixes spin up and spin down states and splits the energy spectrum of spin-dependent systems, even without magnetic fields.

2.1 Superconductivity

2.1.1 Basic phenomena

Superconductivity is a phenomenon that occurs in solids, such as metals, alloys and intermetallic compounds below a certain critical temperature T_C. The solids undergo a phase transition from a normal state above the critical temperature to a state characterised by several fundamental properties. We will list some of these properties here, adopted from [18] and [48].

- *Sudden disappearance of electrical resistance.* This is maybe the most striking characteristic of superconductivity, and was first discovered by Dutch physicist Kamerlingh Onnes in 1911 in his pursuit towards ultra-low temperatures by exploitation of the Hampson-Linde cooling cycle [49]. When cooled below T_C, a transition from a state of finite resistivity to one of zero resistivity takes place. This transition is not associated with any change of structure or property of the lattice and as such it is interpreted as an electronic transition, where the electrons enter a more ordered state. This interpretation is supported by the fact that the entropy of superconductors decreases markedly below T_C, indicating a transition to a more ordered state. The supercurrent carried by a superconductor has an upper limit, the critical current I_C, above which superconductivity becomes suppressed.

- *Exclusion of magnetic flux* from the bulk of the material. This fundamental property was first discovered by German physicists Walther Meissner and Robert Ochsenfeld in 1933 [50], in their work on magnetic fields outside superconducting samples. It was later named *the Meissner effect*. It should be noted, however, that magnetic fields do penetrate superconductors. The typical penetration depth is the London penetration depth, λ_L, which, albeit oversimplified, gives an inclination to the actual penetration depth. $\lambda_L = \sqrt{\frac{\epsilon_0 mc^2}{nq^2}}$ for superconducting particles of charge q and mass m in concentration n, where c is the speed of light and ϵ_0 is the vacuum permittivity [18]. λ_L is usually not greater than that magnetic fields only penetrate a short distance into the surface (compared to the bulk size). This proves a unique way to define the superconducting state: The combination of the Meissner effect and zero resistivity provide a clear distinction between the thermodynamical state of superconductivity and the so-called "perfect conductor". A perfect conductor has the transport property of zero resistance, same as for superconductors. However, perfect conductors trap the flux inside them, i.e. the magnetic field in the bulk must remain at a fixed value [51]. If the initial flux is zero, it will remain zero. This is not the same as expelling the flux though, as happens in superconductors. Thus, superconductors are a distinct state and not an example of a perfect conductor.

- Superconductors exhibit a *discontinuous increase of specific heat* at T_C, followed by an exponential decline when cooling beneath T_C. This is a signature sign of second order phase transitions, adding weight to the argument for a specific thermodynamical phase.

- The Meissner effect occurs only for sufficiently low magnetic fields. The *critical magnetic field* H_C that separates the superconducting state (SCS) and the normal state (NS) has roughly a parabolic connection to the temperature, as in Figure 2.1. When the magnetic field is larger than this critical value, the superconductivity will become suppressed. Also, superconductors are perfect diamagnets when the field is below H_C.

- It is possible to create *persistent currents* in superconductors, either by cooling a current-carrying material below T_C or by entrapment of external flux, maintained by the supercurrents. Lifetimes up to over 10^5 years have been proposed [52]. Furthermore, the trapped flux is *quantised* in units of $\Phi_0 = \frac{2\pi\hbar}{q}$, where $q = -2e$. The fact that the $q = -2e$, and not just $-e$, is usually ascribed to the fact that electrons pair up into so-called Cooper pairs in the SCS.

- All superconductors exhibit an *energy gap* E_g for single-particle excitations around the Fermi level, which is of an entirely different origin than those for semiconductors and insulators. The energy gap is a forbidden region for excitation in the solid. As we will see in the next sections, the energy gap can originate from an attractive electron-electron potential, for example mediated by electron-phonon interaction, which orders the electrons in **k**-space. This interpretation is supported by the fact that when T goes to T_C continuously, $E_g \to 0$, indicating thermal breaking of some collective nature of the electrons. In BCS-theory, this is interpreted as thermal fluctuations becoming too prominent and the electron-electron attraction breaks down.

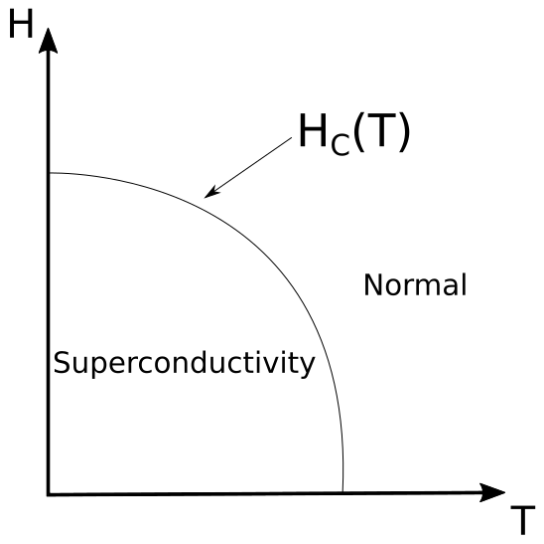

Figure 2.1: Illustration of the phase diagram in the H-T plane, distinguishing between the normal and the superconducting phases. Adapted from [41].

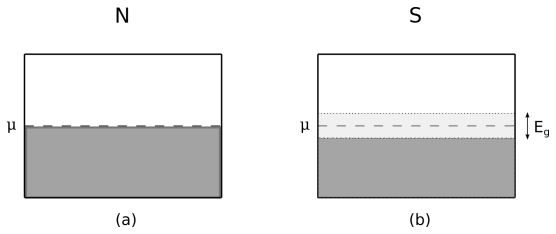

Figure 2.2: Illustration of (a) the conduction band in a normal metal (N) and (b) the energy gap E_g in superconductors (S). Dark, grey areas are filled electron states with energies less than the Fermi level μ. Adapted from [18].

2.1.2 Phenomenological theory

We will here present two theories based on phenomenological aspects of superconductivity. They were both developed before the first microscopic theory of superconductivity was developed. Adapted from [41, 48]. The first theoretical description of the Meissner effect was put forward by Fritz and Heinz London in 1935. Their derivation was simple and only based on classical theory. Assume that the electrons are considered as an incompressible, nonviscous charged fluid. By starting out from the Drude-Lorentz equation of motion for electrons in a metal for a perfect conductor and employing Maxwell's equations, one will end up at

$$\nabla \times \mathbf{j} = -\frac{1}{\mu_0 \lambda_L^2}\mathbf{B} \tag{2.1}$$

and

$$\nabla \times (\nabla \times \mathbf{B}) = -\nabla^2 \mathbf{B} = \mu_0 \nabla \times \mathbf{j}, \tag{2.2}$$

where $\mathbf{B}$ is the magnetic field, $\mathbf{j}$ is the current density and μ_0 is the magnetic susceptibility. λ_L is still the London penetration depth. Combination of these two equations leads to

$$\nabla^2\mathbf{B} = \mathbf{B}/\lambda_L^2. \tag{2.3}$$

This equation accounts for the Meissner effect, as it doesn't allow for a solution uniform in space (unless it is zero), but a field which is exponentially damped over length scales λ_L. This screens the superconductor from magnetic fields, but it also implies that the supercurrents have to flow in a region of depth λ_L from the surface of the superconductor to satisfy Maxwell's fourth equation.

This theory was generalised by Brian Pippard in the 1950's. His theory is based on a quantity called the *coherence length* $\xi_0 = \frac{\hbar v_f}{\pi\Delta}$, where Δ is the superconducting energy gap. It can be interpreted as a characteristic length that measures the spatial response to some external disturbance. In the London picture $\mathbf{j} = \frac{\mathbf{A}}{\mu_0\lambda_L^2}$, where $\mathbf{A}$ is the magnetic potential. Pippard assumed instead that the current density $\mathbf{j}(\mathbf{r})$ at point $\mathbf{r}$ should involve contributions from $\mathbf{A}$ at points neighbouring $\mathbf{r}$ in a volume of radius ξ_0, resulting in a new expression for $\mathbf{j}(\mathbf{r})$ called the Pippard equation. The concept of this coherence length can be used to define a quantity ξ, which again can be used to part the magnetic response of superconductors into two regimes. In the limit $\lambda_L << \xi_0$, $\mathbf{A}(\mathbf{r})$ will drop sharply on a scale much shorter than ξ_0, leading to a weak response in $\mathbf{j}(\mathbf{r})$. Assuming it drops over a distance equal to the effective penetration depth, λ, we can rewrite the Pippard equation into a "London-like" form, which decays in the same way by setting $\lambda^3 \propto \lambda_L^2\xi_0$. By defining an effective coherence length ξ, differing from ξ_0 because of impurities and such, we have two regimes, designated in Table 2.1.

Type I	$\lambda < \xi$
Type II	$\lambda > \xi$

Table 2.1: Regimés defining the Type I and Type II superconductors

Lastly, it should be noted that each of these models considers the charge carries (the electrons) to be single, i.e. $m = m_e$ and $q = -e$. As it will become apparent later, the superconducting charge carriers are pair of electrons.

Let us take a closer look at the two types of superconductors indicated in Table 2.1. There are no differences in the superconducting mechanisms, both have similar properties in the transition point at zero magnetic field, but the Meissner effect is, on the other hand, quite distinct for each type. A good type I superconductor completely expels fields up until the critical magnetic field H_C, after which the magnetic fields penetrate it completely, suppressing the supercurrent. Typically, a type II superconductor acts like a type I up until a critical field H_{c1}, after which it is partially penetrated. This intermediate state prevails until H_{C2}, where superconductivity breaks down completely. Analysis of the surface energy of superconductor-normal metal interfaces reveals that the system can lower its energy by maximising the interfacial area. Type II superconductors can avoid the transition to the normal state, i.e. still have lower energy than in the normal state, by allowing the entry of magnetic flux lines into the bulk. The bulk will then be filled with filaments of normal metal where the flux lines can penetrate, so that the superconducting regions still obey the Meissner effect. These normal regions increase the interfacial area, allowing the superconducting state to prevail. We call these normal regions *vortices* and the intermediate state the *vortex state*, or the Abrikosov mixed state. The vortex state

persists by inclusion of more and more vortices, up until they start to overlap, meaning there are no more superconducting regions. This happens at H_{C2}. As it can be seen from Figure 2.3, the Meissner effects are quite different for the two regimes, as already noted.

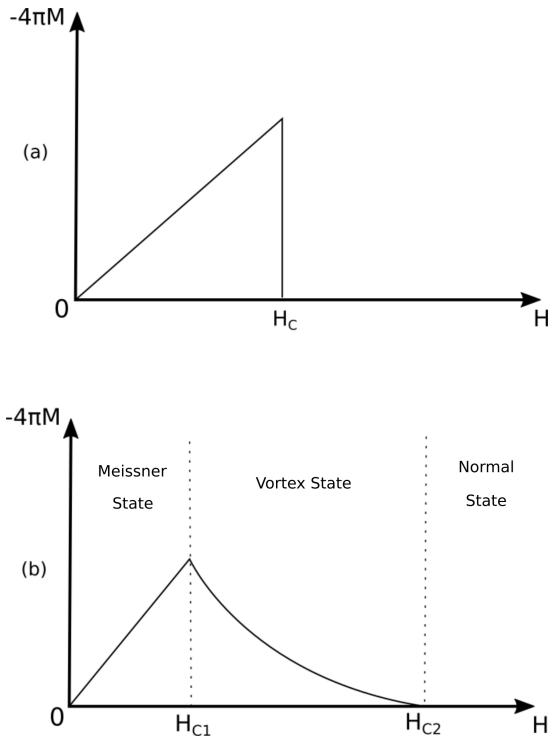

Figure 2.3: Illustrations of magnetisation vs magnetic field for (a) Type I and (b) Type II superconductors. Critical fields and intermediate states are indicated. Adapted from [41].

From here, let us take another approach, based on the fact that the appearance of superconductivity below T_C indicates the transition to a more ordered state. In *Ginzburg-Landau's theory*, this is envisioned as a partial condensation of the electrons into a frictionless superfluid, described by a macroscopic wave function ψ. This was built into Landau second-order phase transition theory (a theory for transitions involving no latent heat) by taking ψ as being the order parameter. It is conventional to choose a particular normalisation for the order parameter, namely $|\psi|^2 = n$. n is the density of superconducting charge carriers. In Landau second-order phase transition theory, the free energy can be written as an expansion of the order parameter. So, by limiting the expansion to the fourth order, we write

$$\mathcal{F} = \mathcal{F}(T) + \alpha|\psi|^2 + \frac{1}{2}\beta|\psi|^4. \tag{2.4}$$

Thermodynamical stability requires $\beta > 0$. Minimalisation will give that, if $\alpha > 0$, $|\psi|^2 = 0$ and if $\alpha < 0$, $|\psi|^2 \neq 0$. The second order phase transition takes place at $T = T_C$, where the more ordered state is at $T < T_C$. Therefore, we can model it by setting $\alpha(T) = a(T - T_C)$, a is a constant, and it is sufficient to regard β as a positive constant.

For a inhomogeneous state we need a more detailed expression for the free energy, namely

$$\mathcal{F} = \mathcal{F}_0 + \int d^3r \left\{ \alpha|\psi(\mathbf{r})|^2 + \frac{1}{2}\beta|\psi(\mathbf{r})|^4 + \frac{\hbar^2}{2m^*}\left| \left[\nabla - \frac{ie^*}{\hbar c}\mathbf{A}(\mathbf{r})\right]\psi(\mathbf{r})\right|^2 + \frac{1}{8\pi}H^2(\mathbf{r}) \right\}, \tag{2.5}$$

where e^* and m^* are the charge and the mass, respectively, of the supercunducting charge carriers. As will become clear in Section 2.1.3, these are $e^* = -2e$ and $m^* = 2m_e$, where m_e is the mass of an electron. $\mathcal{F}_0$ is the free energy of the spatially homogenous system. The third term in the integrand models the increase in energy from the spatial distortion of the order parameter in a magnetic field, and the last term is the contribution to the energy density from the magnetic field. $\mathcal{F}$ is a functional, so we can perform a variational minimalisation with respect to $\psi^*(\mathbf{r})$, which yields

$$-\frac{\hbar^2}{2m^*}\left[\nabla - \frac{ie^*}{\hbar c}\mathbf{A}(\mathbf{r})\right]^2 \psi(\mathbf{r}) + \alpha\psi(\mathbf{r}) + \beta|\psi(\mathbf{r})|^2\psi(\mathbf{r}) = 0, \tag{2.6}$$

called the first G-L equation. Minimalisation with respect to $\mathbf{A}$ yields Ampère's law, as long as we identify the current density as

$$\mathbf{j}(\mathbf{r}) = \frac{-ie^*\hbar}{2m^*}\left[\psi^*(\mathbf{r})\nabla\psi(\mathbf{r}) - \psi(\mathbf{r})\nabla\psi^*(\mathbf{r})\right] - \frac{(e^*)^2}{m^*c}|\psi(\mathbf{r})|^2\mathbf{A}(\mathbf{r}), \tag{2.7}$$

called the second G-L equation. An important result of Ginzburg-Landau theory is that the symmetry-breaking in superconductors is the gauge symmetry (or phase symmetry), similar to the broken rotational symmetry in ferromagnets when crossing the Curie point. This means that superconductors with different phases, when written as $\psi(\mathbf{r}) = ae^{i\Phi(\mathbf{r})}$, are in a physical sense distinct, although only phase differences $\Delta\Phi$ are measurable. This randomness of the phase is analogous to the fact that the magnetisation of a ferromagnetic, isotropic liquid may point in any direction.

These equations can be used to find a few useful relations. Let us examine a simple case of an inhomogeneous order parameter that disappears at the interface between a superconductor occupying the region $x > 0$ and a normal material at $x < 0$ in the absence of a magnetic field. The one-dimensional (1D) version of (2.6) is, for $\mathbf{A} = 0$,

$$-\frac{\hbar^2}{2m^*}\frac{d^2\psi}{dx^2} + \alpha\psi + \beta\psi^3 = 0. \tag{2.8}$$

Defining the G-L coherence length as $\xi^2 = \frac{\hbar^2}{2m^*|\alpha|}$, one can solve this by setting $\frac{\beta}{|\alpha|}\psi^2 = f(x)^2$, so that (2.8) becomes

$$-\xi^2 f''(x) - f(x) + f^3(x) = 0. \tag{2.9}$$

Solving this with the correct boundary conditions would yield an expression which justifies our earlier characterisation of the coherence length ξ as the distance over which the order parameter responds to external perturbations (the interface being the disturbance). Also, since $\alpha = a(T - T_C)$, we have

$$\xi(T) = \left(\frac{\hbar^2}{2m^*aT_C}\right)^{1/2}\left(1 - \frac{T}{T_C}\right)^{-1/2}. \tag{2.10}$$

The second G-L equation, in a limit where the first two terms can be negated, reproduces the London equation, where $|\psi|^2 = n$. This supports the normalisation choice done earlier,

allowing us to identify ψ as a condensate wave function belonging to the superconducting electrons. It follows immediately that the London penetration depth is

$$\lambda_L = \left(\frac{m^* c^2 \beta}{4\pi (e^*)^2 a T_C}\right)^{1/2} \left(1 - \frac{T}{T_C}\right)^{-1/2}. \tag{2.11}$$

Comparison between (2.10) and (2.11) gives a very useful parameter, $\kappa = \frac{\lambda_L}{\xi}$. More detailed analysis reveals that one can distinguish between type I and type II at $\kappa = 1/\sqrt{2}$, where we have a Type I superconductor for $\kappa < 1/\sqrt{2}$.

2.1.3 BCS theory

Here, we present the first microscopic theory for superconductivity, developed in the 1950's by John Bardeen, Leon Cooper and Robert Schrieffer, adapted from [11, 41].

In 1956, Leon Cooper made an important calculation, where he showed that in the presence of an (arbitrary weak) attractive potential, electrons will start forming bound states of pairs, nowadays called Cooper pairs. Based on this intuition, one can calculate the mean square radius of the pair, which turns out to be of the same order as Pippard's coherence length ξ_0, spawning another interpretation of ξ_0 as the size of a Cooper pair. If one is to compute the binding energy, one would find that the lowest energy comes with pairs that have equal but opposite momentum and spin. Robert Schrieffer expanded Cooper's idea, thinking that if all electrons form pairs, then one needs to describe the behaviour of all pairs at the same time, not just focusing on one pair at the time. They published their work together with John Bardeen in 1957 [53], a theory later known as the BCS-theory.

One can understand the basics of BCS-theory by working with an ansatz wavefunction,

$$|\Psi_{\text{BCS}}\rangle = \prod_{\mathbf{k}} \left(u_{\mathbf{k}} + v_{\mathbf{k}} \hat{c}^\dagger_{\mathbf{k},\uparrow} \hat{c}^\dagger_{-\mathbf{k},\downarrow}\right) |\phi_0\rangle \,, \tag{2.12}$$

which creates electrons only in Cooper pairs with opposite momentum and spin. Here, $\hat{c}^\dagger$ is the usual second quantisation creation operator, $|\phi_0\rangle$ is the vacuum state and $u_{\mathbf{k}}$ and $v_{\mathbf{k}}$ are (in general complex) adjustable parameters used to minimise the energy. The modulo squares $|u_{\mathbf{k}}|^2$ and $|v_{\mathbf{k}}|^2$ describe the probability to find zero particles or one Cooper pair in the levels with $\mathbf{k}, \uparrow$, $-\mathbf{k}, \downarrow$, respectively. Thus, they have the relationship

$$|u_{\mathbf{k}}|^2 + |v_{\mathbf{k}}|^2 = 1. \tag{2.13}$$

This wavefunction is "weird", in the sense that it does not describe a state with a fixed number of electrons. A more correct, many-body wavefunction which defines a state with an well-defined number of electrons can, of course, be found. However, if one were to evaluate the variance of the number of electrons N, one would find that it is proportional to $1/\sqrt{N} \sim 10^{-11}$. Thus, the error of not fixing N is very small. Since (2.13) is much easier to work with than the more correct wavefunction, this is what we will use.

The ground state energy is found by operating with the Hamiltonian $\hat{H}$ on the (translationally invariant) system of electrons,

$$\hat{H} = \sum_{\mathbf{k},\sigma} \frac{\hbar^2 k^2}{2m} \hat{c}^\dagger_{\mathbf{k},\sigma} \hat{c}_{\mathbf{k},\sigma} + \frac{1}{2\mathcal{V}} \sum_{\mathbf{k},\mathbf{k}',\mathbf{q};\sigma,\sigma'} V_{\mathbf{k},\mathbf{k}',\mathbf{q};\sigma,\sigma'} \hat{c}^\dagger_{\mathbf{k}+\mathbf{q},\sigma} \hat{c}^\dagger_{\mathbf{k}'-\mathbf{q},\sigma'} \hat{c}_{\mathbf{k}',\sigma'} \hat{c}_{\mathbf{k},\sigma}, \tag{2.14}$$

where the first term is the kinetic energy and the second is the electron-electron interaction, which accounts for momentum conservation and transfer by $\mathbf{q}$. $\mathcal{V}$ is the volume of the system. Since our system does not fix the number of electrons, we have a constraint on our system , namely the fact that the average number of particles is $N = \langle \Psi_{\mathrm{BCS}} | \hat{N} | \Psi_{\mathrm{BCS}} \rangle$, where $\hat{N} = \sum_{\mathbf{k},\sigma} \hat{c}^{\dagger}_{\mathbf{k},\sigma} \hat{c}_{\mathbf{k},\sigma}$. This is realised through introducing a Lagrange multiplier μ,

$$\begin{aligned} \hat{H}' &= \hat{H} - \mu \hat{N} \\ &= \sum_{\mathbf{k},\sigma} \xi_{\mathbf{k}} \hat{c}^{\dagger}_{\mathbf{k},\sigma} \hat{c}_{\mathbf{k},\sigma} + \frac{1}{2\mathcal{V}} \sum_{\mathbf{k},\mathbf{k}',\mathbf{q};\sigma,\sigma'} V_{\mathbf{k},\mathbf{k}',\mathbf{q};\sigma,\sigma'} \hat{c}^{\dagger}_{\mathbf{k}+\mathbf{q},\sigma} \hat{c}^{\dagger}_{\mathbf{k}'-\mathbf{q},\sigma'} \hat{c}_{\mathbf{k}',\sigma'} \hat{c}_{\mathbf{k},\sigma} = \hat{H}'_0 + \hat{H}_I, \end{aligned} \tag{2.15}$$

where $\xi_{\mathbf{k}} = \frac{\hbar^2 k^2}{2m} - \mu$ and μ is the chemical potential. To be able to proceed we have to make several assumptions. First, that the Landau-Fermi liquid picture is valid. In this case, the majority of all normal-state electron-electron interaction can be incorporated through the many-body corrected effective mass (which should not be confused with the effective mass in semiconductors arising from the band structure). There is also a contribution to the effective mass from the electron-phonon interaction, as long as we are limiting the energy to $\xi \lesssim \hbar\omega_D$, where $\hbar\omega_D$ is the Debye energy. Above this the effect is suppressed thanks to the lattice's inability to follow the electron's motion. Under these assumptions, we thus interpret the operators in (2.15) as creating and annihilating quasiparticles instead of regular particles, where quasiparticles are interpreted as electrons moving together with polarisation-correlation "clouds", which is the motion of the remaining particles getting out of the way. ξ is therefore the quasiparticle energy. This allows us to consider the electron-electron scattering as an effectively "weak" potential, since it now only contains components that not can be absorbed into the effective mass and therefore fewer interaction effects. Therefore, the residual electron-electron interaction is all what is left. When the indirect electron-phonon-electron interaction is added, the overall electron-electron interaction can become attractive for low energies.

Now, we focus only on the part of the interaction which are important for superconductivity. We keep only the attractive part leading to formation of Cooper pairs, i.e. replace $\mathbf{k}' \to -\mathbf{k}$ and $\mathbf{k} + \mathbf{q} \to \mathbf{k}'$ for opposite momenta, resulting in a "reduced" Hamiltonian:

$$\hat{H}'_R = \sum_{\mathbf{k},\sigma} \xi_{\mathbf{k}} \hat{c}^{\dagger}_{\mathbf{k},\sigma} \hat{c}_{\mathbf{k},\sigma} + \frac{1}{2\mathcal{V}} \sum_{\mathbf{k},\mathbf{k}'} V_{\mathbf{k},\mathbf{k}'} \hat{c}^{\dagger}_{\mathbf{k}',\uparrow} \hat{c}^{\dagger}_{-\mathbf{k}',\downarrow} \hat{c}_{-\mathbf{k},\downarrow} \hat{c}_{\mathbf{k},\uparrow} = \hat{H}'_0 + \hat{H}_{IR}. \tag{2.16}$$

The ground-state energy is

$$E' = \langle \Psi_{\mathrm{BCS}} | \hat{H}'_R | \Psi_{\mathrm{BCS}} \rangle , \tag{2.17}$$

which can be calculated by employing paring operators, defined as

$$\hat{b}^{\dagger}_{\mathbf{k}} = \hat{c}^{\dagger}_{\mathbf{k},\uparrow} \hat{c}^{\dagger}_{-\mathbf{k},\downarrow}, \tag{2.18}$$

$$\hat{b}_{\mathbf{k}} = \hat{c}_{-\mathbf{k},\downarrow} \hat{c}_{\mathbf{k},\uparrow}. \tag{2.19}$$

The rewritten Hamiltonian comes out

$$\hat{H}'_R = 2 \sum_{\mathbf{k}} \xi_{\mathbf{k}} \hat{b}^{\dagger}_{\mathbf{k}} \hat{b}_{\mathbf{k}} - \frac{1}{\mathcal{V}} \sum_{\mathbf{k},\mathbf{k}'} V_{\mathbf{k},\mathbf{k}'} \hat{b}^{\dagger}_{\mathbf{k}} \hat{b}_{\mathbf{k}'}, \tag{2.20}$$

and the BCS ground state as

$$|\Psi_{\text{BCS}}\rangle = \prod_{\mathbf{k}} \left(u_{\mathbf{k}} + v_{\mathbf{k}} \hat{b}^{\dagger}_{\mathbf{k}}\right) |\phi_0\rangle \,. \tag{2.21}$$

The expectation value for the interaction has terms on the form

$$\langle\phi_0| \left[... \left(u^*_{\mathbf{k}_i} + v^*_{\mathbf{k}_i} \hat{b}_{\mathbf{k}_i}\right) ... \left(u^*_{\mathbf{k}_j} + v^*_{\mathbf{k}_j} \hat{b}_{\mathbf{k}_j}\right) ...\right] V_{\mathbf{q},\mathbf{q}'} \hat{b}^{\dagger}_{\mathbf{q}} \hat{b}_{\mathbf{q}'} \left[\left(u_{\mathbf{k}'_i} + v_{\mathbf{k}'_i} \hat{b}^{\dagger}_{\mathbf{k}'_i}\right) ... \left(u_{\mathbf{k}'_j} + v_{\mathbf{k}'_j} \hat{b}^{\dagger}_{\mathbf{k}'_j}\right) ...\right] |\phi_0\rangle \,, \tag{2.22}$$

and the kinetic term is the same, just with the replacement $2\xi_{\mathbf{k}}\delta_{\mathbf{k},\mathbf{k}'}$ for $V_{\mathbf{k},\mathbf{k}'}$. Only terms with an even number of operators contribute and all $\hat{b}\,|\phi_0\rangle = 0$. We are left with a term which corresponds to the Hartree-Fock energy, that may be disregarded since $\xi_{\mathbf{k}}$ is the quasiparticle energy and is supposed to already include electron-electron interactions, and a term corresponding to the pairing energy,

$$\langle\Psi_{\text{BCS}}|\, \hat{H}'_{IR}\, |\Psi_{\text{BCS}}\rangle = \frac{1}{\mathcal{V}} \sum_{\mathbf{k},\mathbf{k}'} V_{\mathbf{k},\mathbf{k}'} u^*_{\mathbf{k}} v_{\mathbf{k}} u_{\mathbf{k}'} v^*_{\mathbf{k}'}. \tag{2.23}$$

The kinetic term becomes

$$\langle\Psi_{\text{BCS}}|\, \hat{H}'_0\, |\Psi_{\text{BCS}}\rangle = 2 \sum_{\mathbf{k}} |v_{\mathbf{k}}|^2 \xi_{\mathbf{k}}. \tag{2.24}$$

We need to minimise the ground-state energy, with respect to the normalisation condition (2.13) for it to be valid. A convenient choice of coefficients is

$$|u_{\mathbf{k}}| = \cos\theta_{\mathbf{k}}, \quad |v_{\mathbf{k}}| = \sin\theta_{\mathbf{k}}, \tag{2.25}$$

where we choose the phases to be real, resulting in

$$E' = E - \mu\overline{N} = 2 \sum_{\mathbf{k}} \xi_{\mathbf{k}} \sin^2\theta_{\mathbf{k}} + \frac{1}{4\mathcal{V}} \sum_{\mathbf{k},\mathbf{k}'} V_{\mathbf{k},\mathbf{k}'} \sin 2\theta_{\mathbf{k}} \sin 2\theta_{\mathbf{k}'}. \tag{2.26}$$

Minimisation with respect to $\theta_{\mathbf{k}}$ leaves

$$\xi_{\mathbf{k}} \tan 2\theta_{\mathbf{k}} = \Delta_{\mathbf{k}},$$

or

$$\sin 2\theta_{\mathbf{k}} = 2u_{\mathbf{k}} v_{\mathbf{k}} = \frac{\Delta_{\mathbf{k}}}{\epsilon_{\mathbf{k}}}, \tag{2.27}$$

where we have defined

$$\Delta_{\mathbf{k}} = -\frac{1}{\mathcal{V}} \sum_{\mathbf{k}'} V_{\mathbf{k},\mathbf{k}'} u_{\mathbf{k}'} v_{\mathbf{k}'} = -\frac{1}{2\mathcal{V}} \sum_{\mathbf{k}'} V_{\mathbf{k},\mathbf{k}'} \sin 2\theta_{\mathbf{k}'}, \tag{2.28}$$

which is called the "gap function" and

$$\epsilon_{\mathbf{k}} = \sqrt{\xi^2_{\mathbf{k}} + \Delta^2_{\mathbf{k}}}. \tag{2.29}$$

Now, adding a single electron in state $\mathbf{k}$ to the superconducting ground state will not put it in the superposition of zero and two particles from (2.12), and thus it does not take part in the superconductivity. Rather, it exists on the background of the superconducting

ground state and we therefore call it an excitation. It turns out that the energy of such excitations in state $\mathbf{k}$ is (2.29). The energy spectrum for excitations has a gap $\Delta_{\mathbf{k}}$, as illustrated in Figure 2.5, related to the energy gap discussed in 2.1.1, meaning that one cannot create excitations of arbitrary small energies and that the minimum energy of an excitation is $\Delta_{\mathbf{k}}$.

Let us have a closer look at the coefficients $u_{\mathbf{k}}$ and $v_{\mathbf{k}}$. Squaring (2.27) and inserting the normalisation condition will give

$$u_{\mathbf{k}}^2, v_{\mathbf{k}}^2 = \frac{1}{2}\left(1 \pm \frac{\xi_{\mathbf{k}}}{\epsilon_{\mathbf{k}}}\right). \tag{2.30}$$

Using the fact that for a non-superconducting, non-interacting Fermi gas material ($\Delta_{\mathbf{k}} = 0$) we must have $v^2 = 1$ and $u^2 = 0$ for $\xi_{\mathbf{k}} < 0$ and $v^2 = 0$ and $u^2 = 1$ for $\xi_{\mathbf{k}} > 0$. This fixes v^2 for the minus sign, so we have

$$u_{\mathbf{k}}^2 = \frac{1}{2}\left(1 + \frac{\xi_{\mathbf{k}}}{\epsilon_{\mathbf{k}}}\right), \quad v_{\mathbf{k}}^2 = \frac{1}{2}\left(1 - \frac{\xi_{\mathbf{k}}}{\epsilon_{\mathbf{k}}}\right). \tag{2.31}$$

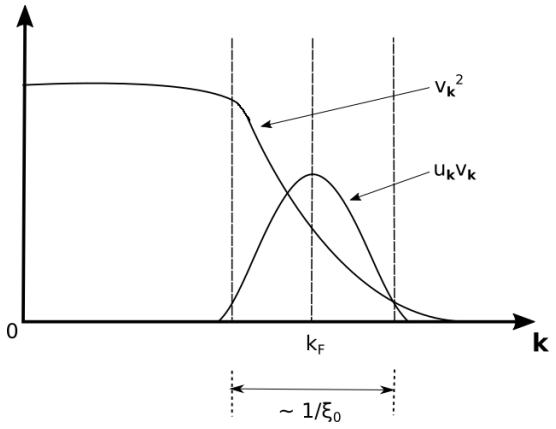

Figure 2.4: Illustration of the coherence factor $v_{\mathbf{k}}^2$ and the condensation amplitude $u_{\mathbf{k}}v_{\mathbf{k}}$ in the BCS ground state. Adapted from [41].

Note here that the condensation amplitude $u_{\mathbf{k}}v_{\mathbf{k}}$ and the coherence factor $v_{\mathbf{k}}^2$, as shown in Figure (2.4), are smeared out in the vicinity of the Fermi wavelength, showing how $u_{\mathbf{k}}$ and $v_{\mathbf{k}}$ are not step functions as in the case of a regular Fermi vacuum. This is a consequence of the pairing correlation, of width $\sim \xi_0^{-1}$, where ξ_0 is the Cooper-Pippard coherence length and is interpreted as the size of the Cooper pair, as mentioned earlier.

We can derive a more illuminating result for the gap function and other quantities if we employ the Cooper potential,

$$V_{\mathbf{k},\mathbf{k}'} = \begin{cases} -V & |\xi_{\mathbf{k}}|, |\xi_{\mathbf{k}'}| \leq \hbar\omega_D, \\ 0 & |\xi_{\mathbf{k}}|, |\xi_{\mathbf{k}'}| > \hbar\omega_D. \end{cases} \tag{2.32}$$

where $V > 0$ is the strength of the attractive, point-potential. The gap function then becomes, if the sum only contains terms of $\mathbf{k}'$ that satisfy $|\xi_{\mathbf{k}'}| \leq \hbar\omega_D$,

$$\begin{aligned}\Delta_{\mathbf{k}} =&\Delta = -\frac{1}{2\mathcal{V}}\sum_{\mathbf{k}'}(-V)\sin 2\theta_{\mathbf{k}'} = \frac{V}{2\mathcal{V}}\sum_{\mathbf{k}'}\frac{\Delta}{\sqrt{\xi_{\mathbf{k}'}^2+\Delta^2}}\\ =&\frac{V}{2}\int\frac{d^3\mathbf{k}}{(2\pi)^3}\frac{\Delta}{\sqrt{\xi_{\mathbf{k}'}^2+\Delta^2}} = V\mathcal{N}(0)\Delta\int_{-\hbar\omega_D}^{\hbar\omega_D}\frac{d\xi}{2\sqrt{\xi^2+\Delta^2}} \approx V\mathcal{N}(0)\Delta\ln\left(\frac{2\hbar\omega_D}{|\Delta|}\right),\end{aligned} \tag{2.33}$$

where we, for simplicity, have set Δ to be real. Here, we have used the sum-to-integral conversion $\frac{1}{\mathcal{V}}\sum_{\mathbf{k}} \to \int\frac{d^3\mathbf{k}}{(2\pi)^3}$ and changed the integration variables $\frac{d^3\mathbf{k}}{(2\pi)^3} \to \mathcal{N}(\xi)d\xi$, where $\mathcal{N}(\xi)$ is the density of states at energy ξ. We expect the main contribution to come from energies close to the Fermi energy, so we approximate $N(\xi) \approx N(0)$. Since $\hbar\omega_D/k_B \sim 300\text{K}$ and $|\Delta|/k_B \sim 10\text{K}$, the integral can be evaluated to the leading logarithmic approximation. All together leads to the approximation in (2.33), which we write as

$$|\Delta| = 2\hbar\omega_D e^{-1/\mathcal{N}(0)V}. \tag{2.34}$$

It should be noted that, in general, Δ can be a complex number and have any phase.

Insertion of the coherence factors into (2.26), converting the sums and calculating the resulting integrals with approximations of the form from earlier will give

$$E-\mu\overline{N} = E_0 - \frac{1}{2}\mathcal{N}(0)|\Delta|^2, \tag{2.35}$$

where $E_0 = 2\int_{-\mu}^{0}\mathcal{N}(\xi)\xi d\xi$, corresponding to the total ground-state energy. From this we find the total condensation energy in the BCS-model;

$$(E-\mu\overline{N}) - (E-\mu\overline{N})_{\Delta=0} = -\frac{1}{2}\mathcal{N}(0)|\Delta|^2. \tag{2.36}$$

To find the critical field H_C, we consider a superconducting slab of material brought reversibly from a position at infinity with zero applied magnetic field and to a position $\mathbf{r}$ in an applied magnetic field B, at constant temperature. The work done per unit volume of specimen is [18]

$$W = -\int_0^B \mathbf{M}\cdot d\mathbf{B} \tag{2.37}$$

$$\implies dF_S = -\mathbf{M}\cdot d\mathbf{B} = \frac{1}{4\pi}BdB, \tag{2.38}$$

where $\mathbf{M}$ is the magnetisation in the superconductor and F_S is the free energy of the superconductor. We have assumed perfect diamagnetism, i.e. Type I, which justifies neglecting the small susceptibility of a solid in the the normal state. Thus, the energy of the normal solid is independent of magnetic fields and we must have $F_N(B_C) = F_N(0)$. At the critical field, the normal state and the superconducting state coexist in equilibrium, i.e. $F_N(B_C) = F_S(B_C)$. Integrating (2.38), we have

$$F_S(B) - F_S(0) = \frac{B^2}{8\pi} \tag{2.39}$$

$$\implies F_S(0) - F_S(B_C) = F_S(0) - F_N(B_C) = F_S(0) - F_N(0) = -\frac{B_C^2}{8\pi}, \tag{2.40}$$

i.e. in Type I superconductors the critical field is a quantitative measure of the free energy difference between the superconducting state and the normal state at constant temperature. In CGS-units, we have $B_C = H_C$, so that by combining (2.36) and (2.40) we get

$$\frac{H_C^2}{8\pi}(T=0) = \frac{1}{2}\mathcal{N}(0)|\Delta|^2. \tag{2.41}$$

2.2 Bogoliubov-de Gennes equation

This section will go through the derivation of the Bogoliubov - deGennes (BdG) equation, a generalised mean field theory for solving problems in the BCS-theroy. Adapted from [41].

Let us start by looking at the electronic excitations of a superconductor. We call these excitations for *quasiparticles* (to distinguish between "real" particles and excitations), existing on the background of the superconducting ground state, as mentioned earlier. The energy of one quasiparticle is described in (2.29) and reads

$$\epsilon_{\mathbf{k}} = \sqrt{\xi_{\mathbf{k}}^2 + |\Delta|^2}. \tag{2.42}$$

This energy is the same if we want to add an electron of state $|\mathbf{k}\uparrow\rangle$ or remove an electron in state $|-\mathbf{k}\downarrow\rangle$.

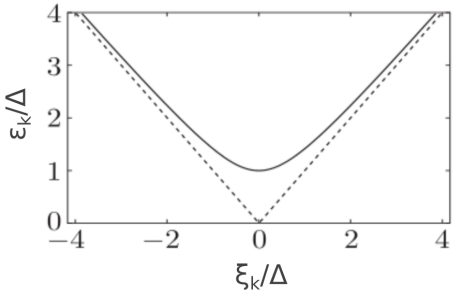

Figure 2.5: Quasiparticle spectrum in a superconductor. The dotted lines are $|\xi_{\mathbf{k}}|$ as it would appear in a non-interacting Fermi gas. Adapted from [11].

The exact nature of these quasiparticles is however not completely obvious at first sight. If one would try to explain them with regular creation and annihilation operators for electrons, one would run into trouble. For example, applying the annihilation operator $\hat{c}_{\mathbf{k}}$ to the ground state would not remove a quasiparticle and yield zero. Rather, it would "create" another quasiparticle by breaking up a Cooper pair. It actually turns out that the right operators for quasiparticles are linear combinations of single particle creation and annihilation operators,

$$\hat{\gamma}_{-\mathbf{k}\downarrow} = v_{\mathbf{k}}\hat{c}^\dagger_{\mathbf{k}\uparrow} + u_{\mathbf{k}}\hat{c}_{-\mathbf{k}\downarrow}, \tag{2.43}$$

$$\hat{\gamma}^\dagger_{-\mathbf{k}\downarrow} = v^*_{\mathbf{k}}\hat{c}_{\mathbf{k}\uparrow} + u^*_{\mathbf{k}}\hat{c}^\dagger_{-\mathbf{k}\downarrow}, \tag{2.44}$$

$$\hat{\gamma}^\dagger_{\mathbf{k}\uparrow} = u^*_{\mathbf{k}}\hat{c}^\dagger_{\mathbf{k}\uparrow} - v^*_{\mathbf{k}}\hat{c}_{-\mathbf{k}\downarrow}, \tag{2.45}$$

$$\hat{\gamma}_{\mathbf{k}\uparrow} = u_{\mathbf{k}}\hat{c}_{\mathbf{k}\uparrow} - v_{\mathbf{k}}\hat{c}^\dagger_{-\mathbf{k}\downarrow}, \tag{2.46}$$

so that, for example, $\hat{\gamma}^\dagger_{\mathbf{k}\uparrow}|\Psi_{\mathrm{BCS}}\rangle$ creates a quasiparticle and $\hat{\gamma}_{\mathbf{k}\uparrow}|\Psi_{\mathrm{BCS}}\rangle = 0$ (since the ground state contains no quasiparticles). These operators are called Bogoliubov operators, resulting from a canonical unitary transformation, and they satisfy the regular anticommutation relations. It should also be noted that in the absence of pairing correlations, i.e. $|\Delta| = 0$, we have

$$\hat{\gamma}^\dagger_{\mathbf{k}\uparrow} = \begin{cases} \hat{c}^\dagger_{\mathbf{k}\uparrow} & k > k_F, \\ -\hat{c}_{-\mathbf{k}\downarrow} & k < k_F, \end{cases} \qquad \hat{\gamma}^\dagger_{-\mathbf{k}\downarrow} = \begin{cases} \hat{c}^\dagger_{-\mathbf{k}\downarrow} & k > k_F, \\ \hat{c}_{\mathbf{k}\uparrow} & k < k_F. \end{cases} \tag{2.47}$$

The interpretation for $\hat{\gamma}^\dagger_{\mathbf{k}\uparrow}$ is as follows: To create an electron excitation $|\mathbf{k}\uparrow\rangle$ for $k > k_F$, we just add an electron of the same quantum numbers. However, for creating an excitation for $k < k_F$, we need to destroy an existing electron state. Removing an electron in the state $|-\mathbf{k}\downarrow\rangle$ corresponds to creating a hole-like excitation with momentum $\mathbf{k}$ and spin $\uparrow$. The sign difference between the $\hat{c}$'s in (2.47) reflects both an arbitrary phase convention and the fact that we have restricted the pairing to singlet states. The second γ is interpreted the same way.

Digression: Holes

Here, we do a quick digression to discuss the concept of *holes* in electronic structures.

A hole can be interpreted as a vacancy of an orbital in an otherwise filled band [18]. In semiconductor physics they are often thought of as the absence of an electron. It is a mathematical trick, introduced because it is often more convenient to count "absence of electron" than the rest of a typically almost filled valence band. They do, however, have physical properties, like

$$\mathbf{k}_h = -\mathbf{k}_e. \tag{2.48}$$

This fact is explained as follows: the total wavevector in filled bands has to be zero, $\sum_{\mathbf{k}} \mathbf{k} = 0$, where we sum over all states in the first Brillouin zone. An electron with $\mathbf{k}_e$ excited to the conduction band thus leaves behind a wavevector in the valence band, $-\mathbf{k}_e$, which we then ascribe to the hole. Of course, total momentum for the entire system is unchanged, the electron wavevector still exists in the conduction band. By the same logic, the charge left behind after an electron is excited away from the valence band is $+e$, and therefore we ascribe a charge $q_h = e$ to holes.

Back to Bogoliubov operators

For $|\Delta| \neq 0$, the operators $\hat{c}^\dagger_{\mathbf{k}\uparrow}$ (electron-like) and $\hat{c}_{-\mathbf{k}\downarrow}$ (hole-like) become mixed, we have a superposition of electron- and hole-states. This is a reflection of how we have correlations from the pairing interaction. Note that all the above was done for the ground state, i.e. $T = 0$. Temperature dependence is easily incorporated into the Bogoliubov operators, by noting that in our mean-field theory the fermion-quasiparticles do not interact, so $\langle\hat{\gamma}^\dagger_{\mathbf{k}\sigma}\hat{\gamma}_{\mathbf{k}\sigma}\rangle = f_{\mathbf{k}\sigma}$ and $\langle\hat{\gamma}_{\mathbf{k}\sigma}\hat{\gamma}^\dagger_{\mathbf{k}\sigma}\rangle = 1 - f_{\mathbf{k}\sigma}$, where $f_{\mathbf{k}\sigma}$ is the normal ideal Fermi-gas occupation factor, $f_{\mathbf{k}\sigma} = 1/(e^{\epsilon_{\mathbf{k}}/k_B T} + 1)$.

Nonuniform systems, e.g. with boundaries or scattering centres, require a generalisation of the microscopic pairing theory. The most accurate approach to this would be a many-body Green's function method. However, we will follow a different approach, namely Bogoliubov's self-consistent field method, which is accurate enough for many situations. We write the Hamiltonian of the system as

$$\hat{H} = \int d^3r \hat{\psi}^\dagger_\alpha(\mathbf{r}) \left[-\frac{\hbar^2}{2m} \left(\nabla - \frac{ie}{\hbar c}\mathbf{A} \right)^2 \delta_{\alpha\beta} + U^{(1)}_{\alpha\beta}(\mathbf{r}) \right] \hat{\psi}_\beta(\mathbf{r}) \tag{2.49}$$

$$+\frac{1}{2} \int d^3r \int d^3r' \hat{\psi}^\dagger_\delta(\mathbf{r}) \hat{\psi}^\dagger_\gamma(\mathbf{r}') U^{(2)}_{\delta\gamma;\alpha\beta}(\mathbf{r},\mathbf{r}') \hat{\psi}_\alpha(\mathbf{r}') \hat{\psi}_\beta(\mathbf{r}) - \mu\hat{N}, \tag{2.50}$$

where Greek letters denote spin indices and summation convention is implied. $\hat{N} = \int d^3r \hat{\psi}^\dagger_\alpha(\mathbf{r})\hat{\psi}_\alpha(\mathbf{r})$ is the number operator and $\hat{\psi}_\alpha(\mathbf{r})$ and $\hat{\psi}^\dagger_\alpha(\mathbf{r})$ are the usual field operators, which annihilate and create, respectively, a particle of spin α at point $\mathbf{r}$.

The term involving $\mathbf{A}$ accounts for the magnetic action on the orbital motion. Ignoring magnetic coupling to the spin (and various relativistic effects), we write the one-electron potential as $U^{(1)}_{\alpha\beta} = U^{(1)}\delta_{\alpha\beta}$. Assuming no spin-dependence in the two-particle interaction, we have $U^{(2)}_{\delta\gamma;\alpha\beta} = U^{(2)}\delta_{\alpha\gamma}\delta_{\delta\beta}$. We further assume contact potential, $U^{(2)}(\mathbf{r},\mathbf{r}') = -V\delta^{(3)}(\mathbf{r},\mathbf{r}')$. To get approximate solutions to this many-body problem, one defines an effective, mean-field Hamiltonian which minimises the total free energy, and reads

$$\hat{H}_{\text{eff}} = \int d^3r \hat{\psi}^\dagger_\alpha(\mathbf{r}) \mathcal{H}_0 \hat{\psi}_\alpha(\mathbf{r}) + \hat{\psi}^\dagger_\alpha(\mathbf{r}) U(\mathbf{r}) \hat{\psi}_\alpha(\mathbf{r}) \tag{2.51}$$

$$+\Delta(\mathbf{r})\hat{\psi}^\dagger_\uparrow(\mathbf{r})\hat{\psi}^\dagger_\downarrow(\mathbf{r}) + \Delta^*(\mathbf{r})\hat{\psi}_\downarrow(\mathbf{r})\hat{\psi}_\uparrow(\mathbf{r}), \tag{2.52}$$

where $\mathcal{H}_0 = -\frac{\hbar^2}{2m}\left(\nabla - \frac{ie}{\hbar c}\mathbf{A}\right)^2 - \mu$. U is now the (real) mean, one-particle potential and Δ is often referred to as the (complex) coupling potential. For a nonsuperconducting material the field operators could be expanded in terms of a complete set of eigenfunctions, such as the eigenfunctions of $\mathcal{H}_0\phi_n = \xi_n\phi_n$, so that

$$\hat{\psi}_\alpha(\mathbf{r}) = \sum_n \phi_n(\mathbf{r})\hat{c}_{n\alpha}. \tag{2.53}$$

For a uniform superconductor, it would be enough to find an expression for $\hat{c}$ with (2.46) and insert it into (2.53) for the two spin states. For a nonuniform superconductor, however, we need two sets of eigenfunctions $u_n(\mathbf{r})$ and $v_n(\mathbf{r})$, so we write the generalised Bogoliubov transformations as

$$\hat{\psi}_\uparrow(\mathbf{r}) = \sum_n \left[u_n(\mathbf{r})\hat{\gamma}_{n\uparrow} - v^*_n(\mathbf{r})\hat{\gamma}^\dagger_{n\downarrow} \right], \quad \hat{\psi}_\downarrow(\mathbf{r}) = \sum_n \left[u_n(\mathbf{r})\hat{\gamma}_{n\downarrow} + v^*_n(\mathbf{r})\hat{\gamma}^\dagger_{n\uparrow} \right]. \tag{2.54}$$

These operators can in some cases actually result in a lower free energy (and thus a more accurate solution). We therefore develop a set of equations for the new functions u_n and v_n. Thus, we demand that the effective Hamiltonian is diagonalisable in $\hat{\gamma}$, i.e.

$$E_{\text{eff}} = E_{gS} + \sum_{n,\alpha} \epsilon_n \hat{\gamma}^\dagger_{n\alpha}\hat{\gamma}_{n\alpha}, \tag{2.55}$$

where E_{gS} is the superconducting ground-state energy and ϵ_n is the energy of the excitation in state n. This is satisfied if the commutators between the Hamiltonian and the operators are sensible. First,

$$\left[\hat{H}_{\text{eff}}, \hat{\psi}_\uparrow(\mathbf{r})\right] = -\left[\mathcal{H}_0 + U(\mathbf{r})\right]\hat{\psi}_\uparrow(\mathbf{r}) - \Delta(\mathbf{r})\hat{\psi}_\downarrow^\dagger(\mathbf{r}), \tag{2.56}$$

$$\left[\hat{H}_{\text{eff}}, \hat{\psi}_\downarrow(\mathbf{r})\right] = -\left[\mathcal{H}_0 + U(\mathbf{r})\right]\hat{\psi}_\downarrow(\mathbf{r}) + \Delta(\mathbf{r})\hat{\psi}_\uparrow^\dagger(\mathbf{r}), \tag{2.57}$$

Inserting (2.54) leaves one set of commutation relations. Another set could be found by directly introducing (2.54) and then evaluate the resulting operators with $\left[\hat{H}_{\text{eff}}, \hat{\gamma}_{n\alpha}\right] = -\epsilon_n\hat{\gamma}_{n\alpha}$ and $\left[\hat{H}_{\text{eff}}, \hat{\gamma}_{n\alpha}\right]^\dagger = \epsilon_n\hat{\gamma}_{n\alpha}^\dagger$. Comparing the terms of $\hat{\gamma}$ and $\hat{\gamma}^\dagger$ in the two sets of equations yields a provision for (2.55), which in matrix form reads

$$\begin{pmatrix} \left[\mathcal{H}_0 + U(\mathbf{r})\right] & \Delta(\mathbf{r}) \\ \Delta^*(\mathbf{r}) & -\left[\mathcal{H}_0^* + U(\mathbf{r})\right] \end{pmatrix} \begin{pmatrix} u_n(\mathbf{r}) \\ v_n(\mathbf{r}) \end{pmatrix} = \epsilon_n \begin{pmatrix} u_n(\mathbf{r}) \\ v_n(\mathbf{r}) \end{pmatrix}. \tag{2.58}$$

Here $u_n(\mathbf{r})$ and $v_n(\mathbf{r})$ are eigenfunctions of electron and hole excitations, respectively, often presented in a spinor representation $\psi = \begin{pmatrix} u(\mathbf{r}) \\ v(\mathbf{r}) \end{pmatrix}$, and ϵ_n is the eigenenergy. The effective mean field potentials are found by choosing them such that the effective Hamiltonian is as close to the true Hamiltonian as possible. This means that the statistical averaged energy $\langle\hat{H}_{\text{eff}}\rangle$ has the same minimum as $\langle\hat{H}\rangle$ for the same wavefunction. With the Cooper potential we have

$$U(\mathbf{r}) = -V\langle\hat{\psi}_\uparrow^\dagger(\mathbf{r})\hat{\psi}_\uparrow(\mathbf{r})\rangle = -V\langle\hat{\psi}_\downarrow^\dagger(\mathbf{r})\hat{\psi}_\downarrow(\mathbf{r})\rangle = -V\sum_n \left[|u_n(\mathbf{r})|^2 f_n + |v_n(\mathbf{r})|^2(1-f_n)\right], \tag{2.59}$$

$$\Delta(\mathbf{r}) = -V\langle\hat{\psi}_\downarrow(\mathbf{r})\hat{\psi}_\uparrow(\mathbf{r})\rangle = V\langle\hat{\psi}_\uparrow(\mathbf{r})\hat{\psi}_\uparrow(\mathbf{r})\rangle = V\sum_n (1-2f_n)\, u_n(\mathbf{r})v_n^*(\mathbf{r}). \tag{2.60}$$

Equation (2.60) (when $T = 0$) is the gap function as found in Section 2.1.3.

When including spin in the potentials, the most important realisation is that we will end up with four equations, for u_1, u_2, v_1 and v_2, where $1, 2 = \uparrow, \downarrow$. The pair potential is now of the form

$$\Delta(\mathbf{r}) = \frac{V}{2}\rho_{\alpha\beta}\langle\hat{\psi}_\alpha(\mathbf{r})\hat{\psi}_\beta(\mathbf{r})\rangle, \tag{2.61}$$

where we have the operator $\hat{\rho} = i\sigma_y$, σ_y being the second Pauli matrix. We won't go through the derivation of the spin-dependent equations, it follows more or less the same procedure outlined above, just with $n \to N = (n, \nu)$, $\nu = 1, 2$ for spin up and down. The spin-generalised form of (2.58) is

$$\epsilon u_\alpha(\mathbf{r}) = \left[\frac{\hbar^2}{2m}\left(\nabla - \frac{ie}{\hbar c}\mathbf{A}\right)^2 - \mu\right] u_\alpha(\mathbf{r}) + U_{\alpha\beta}(\mathbf{r})u_\beta(\mathbf{r}) + \Delta(\mathbf{r})\rho_{\alpha\beta}v_\beta(\mathbf{r}) \tag{2.62}$$

$$-\epsilon v_\beta(\mathbf{r}) = \left[\frac{\hbar^2}{2m}\left(\nabla + \frac{ie}{\hbar c}\mathbf{A}\right)^2 - \mu\right] v_\alpha(\mathbf{r}) + U_{\alpha\beta}^*(\mathbf{r})v_\beta(\mathbf{r}) + \Delta^*(\mathbf{r})\rho_{\alpha\beta}u_\beta(\mathbf{r}) \tag{2.63}$$

Here one can clearly see how the pairing potential couples electrons with spin up (down) to holes with spin down (up). In the end, we have the total *Bogoliubov-de Gennes (BdG) Hamiltonian* [54]

$$\mathcal{H} = \begin{pmatrix} \hat{H} - \mu & \hat{\Delta} \\ \hat{\Delta}^\dagger & -(\hat{H}^* - \mu) \end{pmatrix}, \tag{2.64}$$

where $\hat{H}$ is the regular Hamiltonian describing the system and $\hat{\Delta} = \Delta\hat{\rho}$. Thus, the *Bogoliubov - de Gennes equation* reads

$$\boxed{\mathcal{H}\Psi = E\Psi}, \tag{2.65}$$

where Ψ is a spinor representation of the wavevectors. If $\mathcal{H}$ has the form of (2.64), $\Psi = (u_\uparrow, u_\downarrow, v_\uparrow, v_\downarrow)^T$ will be our spinor.

There is another way to write this equation, so that $\hat{\Delta}$ becomes diagonal. This is achieved with a reorientation of the basis, so that we have

$$\begin{pmatrix} \hat{H} - \mu & \hat{\Delta} \\ \hat{\Delta}^* & -(\mathcal{T}\hat{H}\mathcal{T}^\dagger - \mu) \end{pmatrix} \Psi' = E\Psi', \tag{2.66}$$

where $\Psi' = (u_\uparrow, u_\downarrow, v_\downarrow, -v_\uparrow)^T$. $\hat{\Delta}$ now becomes $\hat{\Delta} = \hat{1}\Delta(\mathbf{r})$, where $\hat{1}$ is the identity matrix. $\mathcal{T}$ is the time-reversal operator and reads $\mathcal{T} = -i\sigma_y K$, where K is the complex conjugate operator, i.e. $Kf = f^*$. This operator flips momentum and spin, for example $\mathcal{T}\hat{\mathbf{p}}\mathcal{T}^\dagger = -\hat{\mathbf{p}}$ and $\mathcal{T}\boldsymbol{\sigma}\mathcal{T}^\dagger = -\boldsymbol{\sigma}$.

2.3 Andreev Scattering

As mentioned in Chapter 1, the behaviour around normal material-superconductor (NS) interfaces allows for more exotic reflections than normal interfaces. As described, an electron incident from the normal (N) region can cause the injection of a Cooper pair into the superconductor (S) and the reflection of a hole back into the N-region. Or an incident hole can "annihilate" a Cooper pair at the interface, causing the reflection of an electron back into the N-region. This type of scattering is called *Andreev scattering*, or *Andreev reflection* [33] and is the origin of the proximity effect. This section, adapted from [35], will give a more thorough qualitative explanation for Andreev reflection before a quantitative derivation will be given in Section 3.2.

Imagine a piece of normal material brought into contact with a superconductor. Quasiparticles in the superconductor can only exist at an energy higher than the superconducting gap $|\Delta|$ when measured from the Fermi level. An electron from the N-region with energy $E > |\Delta|$ can enter the superconductor, where it is converted into a quasiparticle. However, if the electron has lower energy than $|\Delta|$, "normal" transfer of charge cannot occur. If a hole is reflected back, a charge deficit of $2e$ arises, which implies that an object of charge $2e$ has been added to the superconductor. The same is of course true for the opposite situation, hole to electron. This object is of course a Cooper pair, and charge transfer can occur over the NS-interface even for electrons with $E < |\Delta|$, see Figure 2.6. This means that normal current from the N-region can be converted to supercurrent in the superconductor. This process conserves energy (as it has to) and the momentum of the hole is $\hbar k_h = \hbar k_e - 2E/v_F$. If $E << \mu$, k_e, k_h and k_F are all more or less the same, yet $v_h = \hbar^{-1}\partial E/\partial k_h$, which is opposite from that of the incoming electron. This means that holes with $k_h > 0$ actually move in the opposite direction of electrons with $k_e > 0$. This point will become important in the details of the derivation of the Andreev reflection coefficient.

Andreev reflected electrons and holes will acquire a phase shift which depends on the superconducting energy gap $|\Delta|$. If we write the pairing potential as$\Delta = |\Delta|e^{i\phi}$, where $|\Delta|$ is the energy gap, we can anticipate a result which will be derived in Section 3.2, and the phase shift will look like

$$r_A = e^{-i\arccos\left(\frac{E}{|\Delta|}\right)}e^{\pm i\phi}. \tag{2.67}$$

The minus (plus) sign refers to electron to hole (hole to electron) reflection. We call r_A the Andreev reflection coefficient to distinguish it from the normal reflection which can occur at any interface. However, the Andreev reflection can dominate for energies much smaller than μ, which will become apparent in Section 3.2.

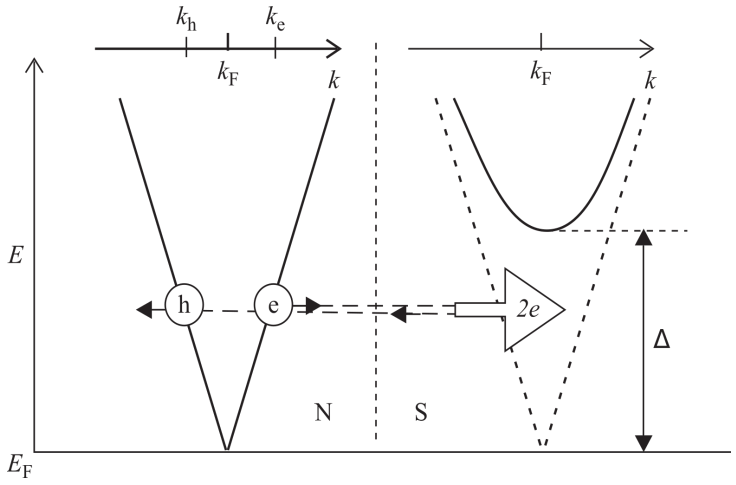

Figure 2.6: Schematic illustration of the Andreev reflection. Electron with momentum $\hbar k_e$ reflected back as a hole with momentum $\hbar k_h$. Figure adapted from [35]

Lastly, it is worth noting that Andreev reflection is special in the following sense: When particles are specularly (normally) reflected from a planar NN-interface, only the velocity component normal to the interface changes sign, the in-plane component stays the same, see Figure 2.7(a). When incident on a NS-interface, all velocity components change sign, i.e. the direction is completely reversed, see Figure 2.7(b).

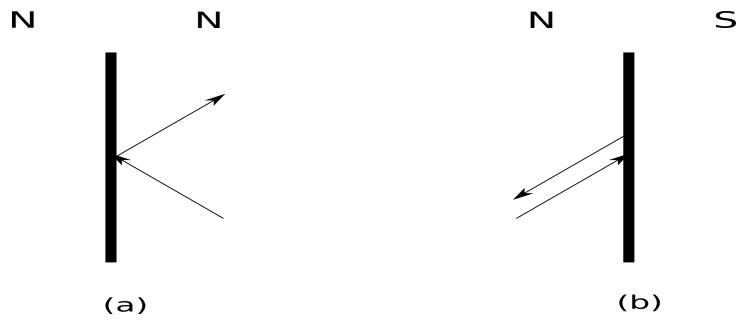

Figure 2.7: Illustration of (a) specular (normal) reflection and (b) Andreev reflection.

2.4 SNS-junction

This section will cover the essentials for a superconductor-normal material-superconductor (SNS) junction. Section 2.4.1 will cover the setup of such a junction and the Andreev bound states which mediate the supercurrent through the junction. Section 2.4.2 will describe the Josephson effect, the sin-relation for the supercurrent and the extended SNS-junction, which exhibits a Fraunhofer pattern in the critical current.

2.4.1 SNS-junction

SNS-junctions, also known as Josephson junctions, are two superconductors coupled by a normal material, where the critical supercurrent in the junction is much smaller than in the bulk superconductor [41]. This normal material can be an insulating barrier, a normal metal, a semiconductor, a nanostructure or a physical constriction that weakens the superconductivity at the point of contact. We call it a normal material, in the sense that it is a material that is usually non-superconducting, i.e. normally conducting. In general the superconductors can be different, as is indicated in Figure 2.8 through the difference in the superconducting pairing potential for the left (L) and the right (R) superconductor, relative to the normal region. The phase difference is of the utmost importance for understanding the effects of current through such junctions.

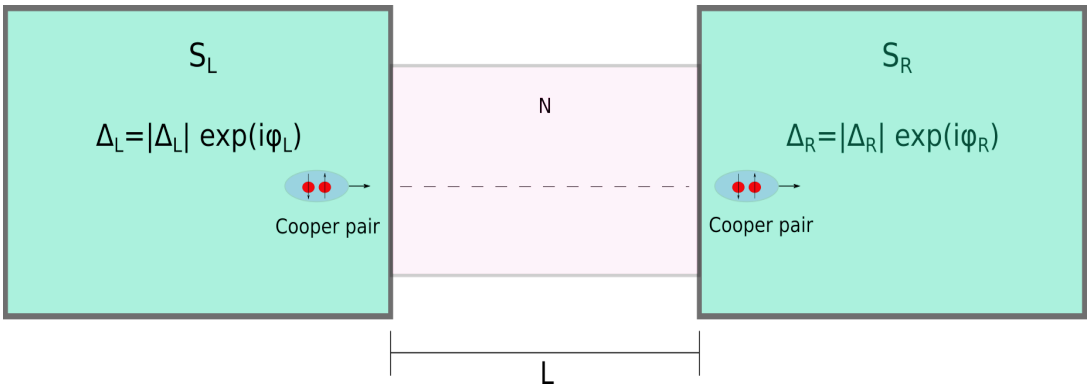

Figure 2.8: Illustration of a SNS-junction, indicating the two superconductors, L and R, with their respective pairing potentials. Transmission of a Cooper pair from the left SC to the right SC is indicated.

Such junctions have been around for a long time. The effect where a supercurrent flows through the junction, also known as the Josephson effect, was first predicted theoretically in 1962 by B.D. Josephson [36].

Andreev Bound States

Consider a SNS-junction with two identical superconductors except for the phase of Δ, which differ by $\Delta\phi = \phi = \phi_L - \phi_R$. An electron with energy less than $|\Delta|$ will experience Andreev reflection trying to get into either of the superconductors. The reflected hole experiences the same, it is converted back as an electron. Thus, in the semiclassical picture, the electron/hole performs a confined motion by bouncing back and forth in a localised area, coherently coupling electrons and holes, which corresponds to the existence

of a bound state. For low energies will this bound state have discrete energy levels around the Fermi level within the superconducting energy gap. These bound states are also known as *Andreev bound states* [35], or Andreev levels. The Andreev levels can mediate the supercurrent in the junction. The supercurrent is in general derived from [46]

$$I_S(\phi) = (2e/\hbar)\partial F/\partial\phi. \tag{2.68}$$

The general supercurrent of the Josephson effect, when calculated from the free energy found in [55], is made up of three parts [56]

$$\begin{aligned} I &= I_S(\phi) = I_1 + I_2 + I_3, \\ I_1 &= -\frac{2e}{\hbar}\sum_n \tanh\left(\frac{E_n}{2k_BT}\right)\frac{dE_n}{d\phi}, \qquad (2.69) \\ I_2 &= -\frac{2e}{\hbar}2k_BT\int_{|\Delta|}^{\infty} dE \ln\left(2\cosh\left(\frac{E}{2k_BT}\right)\right)\frac{\partial\rho}{\partial\phi}, \qquad (2.70) \\ I_3 &= \frac{2e}{\hbar}\frac{d}{d\phi}\int d\mathbf{r}|\Delta|^2/|g|. \qquad (2.71) \end{aligned}$$

Here E_n is the quasiparticle spectrum, ρ is the density of states and g is the interaction constant of the BSC-theory. I_1 is a sum over the discrete energy spectrum, i.e. $E_n \in (0, |\Delta|)$, corresponding to the Andreev bound states discussed above. I_2 is an integral over the continuous spectrum, i.e. $E_n \in (|\Delta|, \infty)$ and I_3 vanishes for a ϕ-independent $|\Delta|$. We want to focus on the discrete spectrum, which has the strongest dependence on ϕ, and for the case where $|\Delta|$ is independent of ϕ, meaning we disregard (2.70) and (2.71) and only keep (2.69). If $|E_n|/k_BT >> 1$, i.e. very low temperatures, will $\tanh(E_n/k_BT) \to \pm 1$, depending on the sign of E_n. Thus, the supercurrent I_S reduces to

$$I_S(\phi) = \frac{e}{\hbar}\sum_n{}' \frac{dE_n}{d\phi}, \tag{2.72}$$

where the $'$ is to remind us that the sum is taken over all negative Andreev levels, $E_n < 0$ [57]. The critical current is simply $I_C = \max_\phi I_S(\phi)$. Notice how there is a factor 2 difference between (2.69) and (2.72). This is because I_1, I_2 and I_3 is based on a spinless basis, while (2.72) is what one should use if spin is included in the basis.

2.4.2 Ginzburg-Landau approach to the Josephson Effect

Here we want to derive the Josephson effect by employing Ginzburg-Landau theory, as presented in 2.1.2. We do this even though we have already presented the Josephson effect in the previous section. However, we now want to illustrate Ginzburg-Landau theory in practice and thereby develop a more thorough understanding of the Josephson effect. Adapted from [58].

Recall Equation (2.9),

$$\xi^2 f''(x) + f(x) - f^3(x) = 0, \tag{2.73}$$

where $f(x) = \sqrt{\frac{\beta}{|\alpha|}}\psi$. We consider the same setup as above, where we have set two bulk superconductors to fill $x < 0$ and $x > L$. If we assume the superconductors to be uniform and identical in every aspect except for a relative phase difference $\Delta\phi$, we can write

$$f(x) = \begin{cases} 1 & x < 0, \\ e^{i\Delta\phi} & x > L. \end{cases} \tag{2.74}$$

For the normal material, we have to solve (2.73) for the boundary conditions $f(0) = 1$ and $f(L) = e^{i\Delta\phi}$. If we assume that the length of the junction is much smaller than the coherence length for the electrons, i.e. $L << \xi$, will the first term in (2.73) dominate, unless $\Delta\phi = 0$ and we have a trivial solution, so that it is sufficient to solve $f''(x) = 0$. This has the solution

$$f(x) = \frac{e^{i\Delta\phi}}{L}x + \frac{L-x}{L}. \tag{2.75}$$

One could think of this as "leakage" of wavefunctions into the normal material. Setting $\mathbf{A} = 0$, the second GL-equation reads

$$j(x) = -i\frac{e^*\hbar}{2m^*}\left(\psi^*(x)\psi'(x) - \phi(x)(\psi'(x))^*\right). \tag{2.76}$$

Insertion of (2.75) into (2.76) gives the current density

$$j_S = j(x) = \frac{e^*\hbar|\alpha|}{m^*L\beta}\sin(\Delta\phi) = j_c\sin(\Delta\phi). \tag{2.77}$$

The current is just the integration of j_S over the cross-sectional area of the normal material. Since j_S is independent of position this is just

$$I_S = I_C\sin(\Delta\phi), \tag{2.78}$$

where $I_C = \frac{e^*\hbar|\alpha|A}{m^*L\beta}$ is the critical current supported by the junction, and A the cross-sectional area. We see that I_S depends on the phase difference between the two superconductors with a sin-behaviour. We have here assumed no electrical fields in the junction, resulting in a time-independent current density through the junction, only sustained by the phase difference. This is called *the DC Josephson effect*. If a DC voltage V is applied across the junction, the phase ϕ is modified to $\phi \to \phi(t) = \phi_0 - \frac{e^*}{\hbar}Vt$, where ϕ_0 is the original phase difference. This is called for *the AC Jospehson effect*.

The extended SNS-junction

Just as the phase in the AC Josephson effect is affected by the electric potential, so can the magnetic potential $\mathbf{A}$ affect the phase. For a pure gauge field, where only $\mathbf{A}$ is affecting the electrons, the phase change is shifted to include a position-dependent part. The gauge-invariant phase difference is given by

$$\phi \to \phi(\mathbf{r}) = \phi_0 + \frac{2\pi}{\Phi_0}\int_1^2 \mathbf{A}\cdot d\mathbf{l}, \tag{2.79}$$

where $\Phi_0 = hc/2e$ is the (superconducting) flux quantum and 1 and 2 refers to the two superconductors. For a single planar Josephson junction, as shown in Figure 2.9, penetrated by a magnetic field in the y-direction,

$$A = \begin{cases} -Hxe^{-(z-a/2)/\lambda_L} & a/2 < z, \\ -Hx & -a/2 < z < a/2, \\ -Hxe^{(z+a/2)/\lambda_L} & z < -a/2, \end{cases} \tag{2.80}$$

a characteristic pattern for the critical current as a function of the magnetic flux Φ appears, as mentioned in Chapter 1. Let us show this.

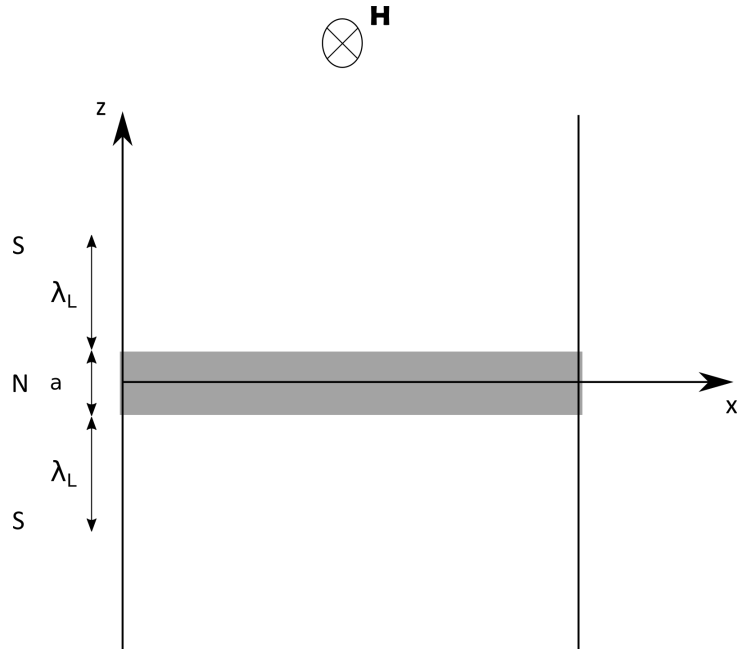

Figure 2.9: Illustration of an extended SNS-junction with the magnetic field **H** in the y-direction. The extension of the junction in the z-direction, a and the London penetration length λ_L are also indicated. Adopted from [41]

The phase difference acquired when crossing the junction, starting at $z = -\infty$ and going to $z = \infty$ is

$$\Delta\phi(x) = \phi_0 + \frac{2\pi}{\Phi_0}\int_{-\infty}^{\infty} A dz, \tag{2.81}$$

where

$$\begin{aligned}\int_{-\infty}^{\infty} A dz =& - Hx\left(\int_{-\infty}^{-a/2} e^{(z+a/2)/\lambda_L} dz + \int_{-a/2}^{a/2} dz + \int_{a/2}^{\infty} e^{-(z-a/2)/\lambda_L} dz\right) \\ =& - Hx\left(\left(\frac{a}{2} - \left(-\frac{a}{2}\right)\right) + e^{a/2\lambda_L}\lambda_L\left(e^{-a/2\lambda_L} - e^{-\infty} - \left(e^{-\infty} - e^{-a/2\lambda_L}\right)\right)\right) \\ =& - Hx\left(a + 2\lambda_L\right).\end{aligned} \tag{2.82}$$

We can find the current though a rectangular junction with sides L_x and L_y by integrating (2.77) with (2.81) for the phase difference over the rectangular area. We do this by setting $\alpha = \frac{2\pi H(a+2\lambda_L)}{\Phi_0}$ for convenience and preforming the integral in two dimensions.

$$
\begin{aligned}
I = &\int_{-L_y/2}^{L_y/2}\int_{-L_x/2}^{L_x/2} j_x \quad dxdy = j_C L_y \int_{-L_x/2}^{L_x/2} \sin(\Delta\phi(x))dx \\
=&j_C L_y \int_{-L_x/2}^{L_x/2} \sin(-\alpha x + \phi_0) = j_C L_y \frac{L_x}{L_x}\left(\frac{2}{\alpha}\sin\left(\frac{\alpha L_x}{2}\right)\sin(\phi_0)\right) \\
=&I_{C0}\frac{\sin\left(\pi\frac{\Phi}{\Phi_0}\right)}{\pi\frac{\Phi}{\Phi_0}}\sin(\phi_0),
\end{aligned}
\tag{2.83}
$$

where $I_{C0} = j_C L_x L_y$ and $\Phi = H(a+2\lambda_L)L_x$ is the magnetic flux penetrating the junction (and the tiny area into the superconductors, thereby $2\lambda_L$). The critical current now has the form

$$
I_C = I_{C0}|\sin(\pi\Phi/\Phi_0)/\pi\Phi/\Phi_0|, \tag{2.84}
$$

which demonstrates the Fraunhofer pattern $(\sin(x)/x)$, earlier described, in the critical current for rectangular junctions, see Figure 2.10.

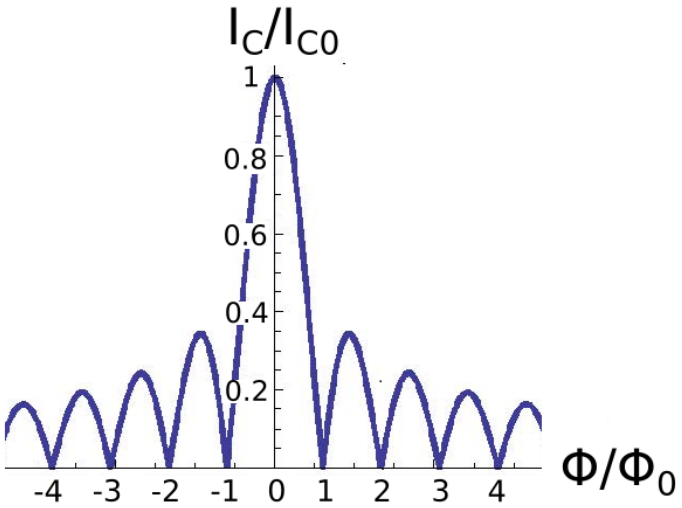

Figure 2.10: Illustration of the normalised Fraunhofer pattern in the critical current plotted as a function of the magnetic flux Φ.

2.5 Spin-Orbit-Interaction

This section will introduce the effect called Spin-Orbit Interaction (SOI), or spin-orbit coupling, and will mainly be adopted from [59].

SOI is an interaction between the spin and the orbital angular momentum of a particle. It is a relativistic effect usually conceptualised in two ways: symmetry-independent SOI, which exists in all crystals and stems from SOI in atomic orbitals, and symmetry-dependent SOI, which exists only in crystals without inversion symmetry. The symmetry-independent SOI is comparably much smaller than the symmetry-dependent one, and can

therefore be neglected for many systems. Asymmetry features prominently in semiconductor heterostructures, therefore justifying a short overview of this type of SOI in this section. The effect arises from an expansion of the Dirac equation to second order in $\frac{1}{c}$. This second order expansion is the most important correction to the non-relativistic Schrodinger-Pauli equation (which includes the Zeeman interaction). The full expansion, with $B \neq 0$, reads

$$\left\{\frac{\hat{\mathbf{p}}^2}{2m}+V+\frac{e\hbar}{2m}\boldsymbol{\sigma}\cdot\mathbf{B}-\frac{e\hbar}{4m^2c^2}\boldsymbol{\sigma}\cdot(\hat{\mathbf{p}}\times\mathbf{E})-\frac{e\hbar^2}{8m^2c^2}\nabla\cdot\mathbf{E}-\frac{\hat{\mathbf{p}}^4}{8m^3c^2}-\frac{e\hbar\hat{\mathbf{p}}^2}{4m^3c^2}\boldsymbol{\sigma}\cdot\mathbf{B}-\frac{e^2\hbar^2B^2}{8m^3c^2}\right\}\psi = E\psi. \tag{2.85}$$

We have, from the left, the non-relativistic kinetic energy, the potential term, the Zeeman term, **SOI**, the Darwin term (introduces a small energy shift) and higher order corrections to both the kinetic energy and the Zeeman term. Here m is the free electron mass, $\hbar$ is Planck's constant, c is the speed of light, $\boldsymbol{\sigma}$ is the Pauli spin vector, $\hat{\mathbf{p}}$ is the momentum operator, e is the elementary charge, $\mathbf{E}$ is the electric field and B is the magnetic field. The Hamiltonian for SOI, with the electric field $\mathbf{E} = \frac{1}{e}\nabla V$ and spin $\mathbf{S} = \frac{\hbar}{2}\boldsymbol{\sigma}$, then reads

$$\hat{H}_{\text{SO}} = -\frac{e\hbar}{4m^2c^2}\boldsymbol{\sigma}\cdot(\hat{\mathbf{p}}\times\mathbf{E}) = -\frac{1}{2m^2c^2}\mathbf{S}\cdot(\hat{\mathbf{p}}\times\nabla V). \tag{2.86}$$

For an atom with spherically symmetric $V(r)$, we can use that the orbital angular momentum is $\hat{\mathbf{L}} = \mathbf{r}\times\hat{\mathbf{p}}$ to get

$$H_{\text{SO}} = -\frac{1}{2m^2c^2}\mathbf{S}\cdot(\hat{\mathbf{p}}\times\frac{dV}{dr}\hat{r}) = \frac{1}{2m^2c^2}\frac{1}{r}\frac{dV}{dr}\mathbf{S}\cdot\hat{\mathbf{L}} = \lambda_{\text{SO}}\mathbf{S}\cdot\hat{\mathbf{L}}. \tag{2.87}$$

This explains the terminology "spin-orbit", even though the concept is more general, whenever a charged particle moves in an electric field there will be interaction between the spin and the momentum.

A different way to interpret this is to consider the electron in its rest frame. By doing a Lorentz transformation from the reference frame of the electron moving with $\mathbf{v}$ to the electron rest frame, as described in Figure 2.11, the electric field spawns an effective magnetic field,

$$\mathbf{B}_{\text{eff}} = -\frac{1}{2}\mathbf{v}\times\frac{\boldsymbol{\epsilon}}{c^2}, \tag{2.88}$$

where the fraction 1/2 is from the Thomas precession. Precession here means a change in the orientation of the rotation axis for a rotating object [60].

In this frame, this effective field couples to the spin through the Zeeman effect, yielding

$$H_{\text{SO}} = \frac{1}{2}g\mu_B\mathbf{B}_{\text{eff}}(\mathbf{k})\cdot\boldsymbol{\sigma}, \tag{2.89}$$

where g is the gyromagnetic factor and μ_B is the Bohr magneton. In the absence of an external magnetic field, time reversal symmetry requires $\mathbf{B}_{\text{eff}}(-\mathbf{k}) = -\mathbf{B}_{\text{eff}}(\mathbf{k})$, which one can see from the fact that the time reversal symmetry operator $\mathcal{T}$ flips the wave vector $\mathbf{k}\to-\mathbf{k}$, time $t\to-t$ and the spin $\boldsymbol{\sigma}\to-\boldsymbol{\sigma}$. Inversion symmetry in space requires $\mathbf{B}_{\text{eff}}(-\mathbf{k}) = \mathbf{B}_{\text{eff}}(\mathbf{k})$. These in combination would imply $\mathbf{B}_{\text{eff}}(\mathbf{k}) = 0$. Thus, for a three-dimensional system, $\mathbf{B}_{\text{eff}}(\mathbf{k})$ would only be present with a broken inversion symmetry. Examples are inversion asymmetry in, for example, 3D-crystals or asymmetry in the confinement potential for a 2D-systems. These different sources of asymmetry are called

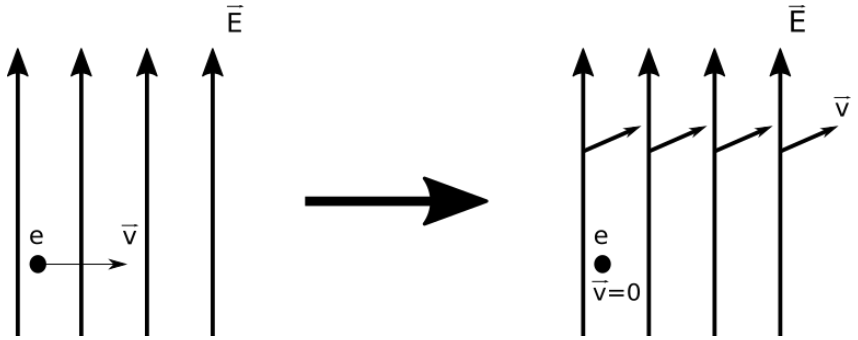

Figure 2.11: Illustration of electron in movement and in rest frame in the presence of an electric field **E**.

bulk inversion asymmetry (BIA) and structural inversion asymmetry (SIA), respectively. Unlike, for example, diamond structures like Si and Ge, zinc-blende structures, like GaAs and InAs, have BIA, leading to the so-called Dresselhaus SOI. To the lowest order in k, the SOI in the bulk is described by

$$H_D = \gamma(\sigma_x k_x(k_y^2 - k_z^2) + \sigma_y k_y(k_z^2 - k_x^2) + \sigma_z k_z(k_x^2 - k_y^2)), \tag{2.90}$$

where σ_i and k_i are components of the Pauli spin vector and wavevector, respectively. γ is a material constant with values $\gamma \approx 27$ eVÅ^3 for both GaAs and InAs [61]. For the case of a quasi-2D electron gas hosted by such a semiconductor, we can integrate out the z-dependence of (2.90) by replacing k_z and k_z^2 with their expectation values. $\langle k_z \rangle$ will have to be zero, since the electrons are confined in the xy-plane and do not have average movement in the z-direction. $\langle k_z^2 \rangle$, on the other hand, has a non-zero value. One can see this by realising $\langle k_z^2 \rangle$ will be part of the energy expectation value, which is non-zero from the uncertainty principle. We then get

$$H_D = \beta(\sigma_y k_y - \sigma_x k_x) + \gamma k_x k_y(\sigma_x k_y - \sigma_y k_x), \tag{2.91}$$

where $\beta = \gamma\langle k_z^2 \rangle$, which roughly equals $\frac{\gamma\pi^2}{d^2}$ [61], where d is the width of the confinement. For strong confinement, i.e. close to a real 2D-systems, the BIA can be accounted for by only using the first term, linear in k.

If the confinement potential in the growth direction of the heterostructure is not symmetric, i.e. there is SIA, we have another coupling term. This is the so-called Rashba term, which to the lowest order in **k** and **E** is written as

$$H_R = \Lambda \boldsymbol{\sigma} \cdot \mathbf{k} \times \mathbf{E} = -\Lambda |\mathbf{E}| \boldsymbol{\sigma} \cdot \hat{z} \times \mathbf{k} = \alpha(\sigma_x k_y - \sigma_y k_x), \tag{2.92}$$

with $\mathbf{E} = (0, 0, |\mathbf{E}|)$ and where Λ is a material-specific constant. The parameters α and β describe the strength of the Rashba and Dresselhaus SOI, respectively. β is a comparatively easy-to-find material constant, while α has attracted a lot of research interest, being much more difficult to predict.

As an ending remark, we note on how SOI can have a spin splitting effect on the energy bands, even for zero magnetic field. This can be because of both BIA and SIA, as well as contributions from the atomic core to the SOI.

3 — Andreev Reflection and 1D SNS-junctions

This chapter will focus on understanding and using the Andreev reflection, as well as introducing the concept of a ballistic 1D nanowire (NW). Section 3.1 will present our assumptions and describe the system we are investigating, which is a 1D NW sandwiched between two superconductors, i.e. a SNS-junction. Section 3.2 will employ wavefunctions and the BdG-formalism to derive the Andreev reflection coefficients at the NS-interfaces. We will additionally show how to employ these results to derive the supercurrent through the junction and discover the sinus-form of the supercurrent. Section 3.3 will repeat the same calculations, but now including electron spin and a finite Zeeman effect in each part of the junction. It will also illustrate how electrons with spin up couples to holes with spin down and vice versa, and how this follows naturally from the BdG-equation. The SOI will be introduced in Section 3.4 and a method of combining it with the magnetic field is developed, resulting in an equation for the energy levels. At the end, Section 3.4.3 will present the result of this equation and a way to probe for effects from magnetic fields and SOI. The understanding of NW's and Andreev reflection will serve as a basis for an expansion into a 2D-system, which will be the theme of the next chapter.

3.1 Assumptions and system description

The system that will be considered in this chapter is a SNS-junction at zero temperature. Typical normal materials for use in experiments are insulators or semiconductors. Here, we will treat the NW as a purely 1D object, which supports a single transport mode. In experiments, however, they are usually realised as quasi-1D objects. [62]. We will further assume complete ballistic behaviour, i.e. impurity-free wires. This means that the size of the normal region (N-region) L, as shown in Figure 3.1, is smaller than the electronic mean free path, l_e, $L \ll l_e$. The ballistic behaviour, together with the 1D NW's, imply that we can safely disregard angle-dependence in the trajectories of the electrons and only focus on one direction, which we choose to be the x-direction. Thus, electrons will follow well-defined trajectories.

We will have to make a few assumptions about the superconductors. The first assumption is that the superconducting (SC) components (S_L and S_R) are identical, meaning the gap function Δ and critical temperature T_C are equal, $|\Delta_L| = |\Delta_R|$ and $T_{CL} = T_{CR}$. Here L and R refers to the left superconductor and the right superconductor, respectively, with respect to the N-region. However, we keep a phase difference between the two gap functions. If we also, for simplicity, assume that Δ changes abruptly at the interfaces, we can write it as a function of position,

$$\Delta(x) = \begin{cases} |\Delta|e^{i\phi_L} & x < 0, \\ 0 & 0 < x < L, \\ |\Delta|e^{i\phi_R} & x > L, \end{cases} \tag{3.1}$$

where ϕ_L and ϕ_R indicates the phase of the left and right superconductors, respectively.

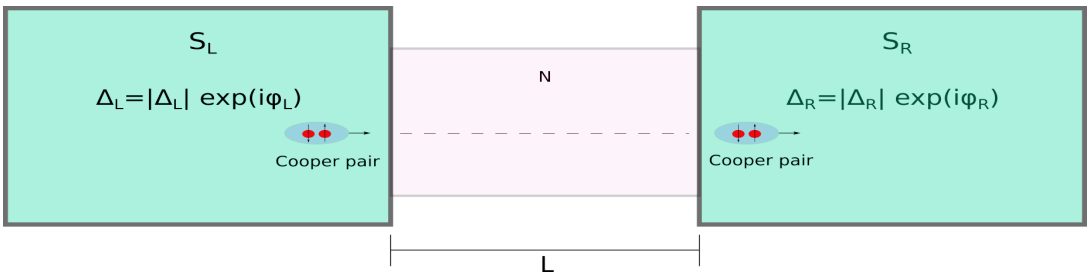

Figure 3.1: Illustration of a SNS-junction, indicating the two superconductors, L and R, with their respective pairing potentials. Transmission of a Cooper pair from the left SC to the right SC is indicated.

Throughout this thesis, we will focus on bound states in the subgap regimé, $E < |\Delta|$, where we further assume that the Fermi energy (or chemical potential, μ) is by far the largest energy value in the system (i.e. $\mu >> E, |\Delta|$). This is the semiclassical approximation, where the Fermi wavelength λ_F of the electrons is the smallest length scale in the problem. States with these energies cannot propagate in the superconductor, so excitations travelling in the N-region towards a NS-interface are therefore Andreev-reflected back. These excitations are then localised in the N-region and form Andreev bound states, with discrete energy levels E_n mediated by the Andreev reflections. We could, of course, also calculate for $E > |\Delta|$, i.e. the unbound solutions. However, states with these energies do not have as strong dependence on the phase difference between the superconductors as the bound states, and will thus not contribute as strongly to the Josephson current. In fact, in the short-junction limit, the continuous spectrum from the unbound solutions will not contribute to the supercurrent at all [56].

If the N-region were to be filled with a semiconductor, an useful modelling of the band structure would be to simplify the band structures by modelling the behaviour of a free particle, but with an effective mass m^*. This effective mass represents the interaction between the particle and the crystal potential, in such a way that we can interpret the particle as moving freely, but with an enhanced or diminished mass. We will use throughout the rest of this thesis m for the mass. However, because of what we just noted above, our result is also valid for solids with band structure, if we were to change m to m^*.

3.2 No fields

This section will focus on the SNS-junction with no external fields. We will start off by considering the general solutions of the BdG-Hamiltonian (2.65) in the normal and the superconducting regions separately in Section 3.2.1. In Section 3.2.2 we will match the wavefunctions and their derivatives across the NS-interfaces to derive the Andreev

reflection coefficients, which represent the phase acquired by an electron reflected into a hole and vice versa. In Section 3.2.3, these coefficients will be used to find the energy levels of the SNS-junction and the resulting supercurrent.

3.2.1 Solutions to the BdG-equation

The Hamiltonian for this system is that of a free particle, $\hat{H} = \frac{\hat{\mathbf{p}}^2}{2m} = -\frac{\hbar^2}{2m}\frac{\partial^2}{\partial x^2}$, everywhere. The BdG-equation (2.65) then becomes

$$\begin{pmatrix} -\frac{\hbar^2}{2m}\frac{\partial^2}{\partial x^2} - \mu & \Delta \\ \Delta^* & \frac{\hbar^2}{2m}\frac{\partial^2}{\partial x^2} + \mu, \end{pmatrix} \Psi = E\Psi. \tag{3.2}$$

Let us start with a wavefunction "deep" in the N-region. It has to be a superposition of electron and hole excitation types, travelling in one direction. So, given an excitation travelling to the right, we have [63]

$$\Psi(x) = Ae^{ik_e x}\begin{pmatrix}1\\0\end{pmatrix} + Be^{-ik_h x}\begin{pmatrix}0\\1\end{pmatrix}, \tag{3.3}$$

written in a spinor representation $\begin{pmatrix}u\\v\end{pmatrix}$, where u and v corresponds to particles and holes, respectively. We have suppressed spin components, since when there are no fields, spin up and down will act in the same way. Notice how the hole state has a negative sign with the wavenumber even though it travels in the positive direction. This is because wavevectors for holes have opposite sign compared to electrons, which count in the positive direction, as explained in Section 2.2. Inserting our expression for Ψ into (3.2) will give us the wavenumber k_e and k_h for the electron and hole in the N-region, respectively. Remembering that $\Delta(x) = 0$ in the N-region yields

$$k_e^2 = \frac{2m}{\hbar^2}(\mu + E), \quad k_h^2 = \frac{2m}{\hbar^2}(\mu - E). \tag{3.4}$$

We stress again, for electrons we define the positive solution as travelling from left to right and negative solution as right to left. The opposite is true for holes, as already noted. Now, the wavefunctions in the superconducting region (SC-region) can be written in a general form

$$\Psi(x) = \sum_n e^{i\lambda_n x}\begin{pmatrix}u_n\\v_n\end{pmatrix}. \tag{3.5}$$

Insertion into (3.2) leaves

$$\begin{pmatrix} \frac{\hbar^2\lambda_n^2}{2m} - \mu - E & \Delta \\ \Delta^* & -\frac{\hbar^2\lambda_n^2}{2m} + \mu - E \end{pmatrix}\begin{pmatrix}u_n\\v_n\end{pmatrix} = \hat{M}\begin{pmatrix}u_n\\v_n\end{pmatrix} = 0, \tag{3.6}$$

for a specific n. Non-trivial solutions for a matrix system like (3.6) are guaranteed if the determinant of the system matrix (e.g. M) is zero. Thus, we can require that $\det\left(\hat{M}\right) = 0$, which gives us

$$\lambda_n^2 = \frac{2m}{\hbar^2}(\mu \pm i\sqrt{|\Delta|^2 - E^2}). \tag{3.7}$$

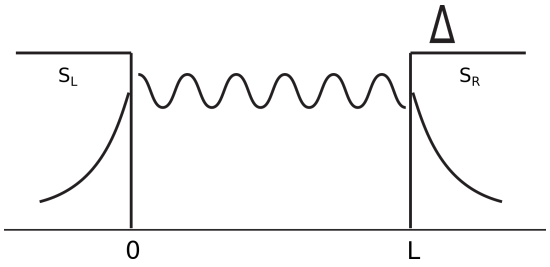

Figure 3.2: Illustration of the wavefunctions in a SNS-junction, with the evanescent wavefunctions in the superconductors indicated.

Now, we need the waves in the SC-region to attenuate exponentially, since we do not allow for solutions in the superconductors, as illustrated in Figure 3.2.
From (3.7), we observe the following behaviour for Ψ_{SC}:

$$\begin{cases} +\lambda_+ & \text{decays for } x > 0, \\ -\lambda_- & \text{decays for } x > 0, \\ -\lambda_+ & \text{decays for } x < 0, \\ +\lambda_- & \text{decays for } x < 0. \end{cases} \tag{3.8}$$

Here, n has become $\pm$ and $\pm\lambda$ refers to the positive or negative solutions. Thus, we have two wavevectors for each superconductor that will make the waves evanescent, and therefore specific wavefunctions for each superconductor, $\Psi_{SCL}(x)$ for $x < 0$ and $\Psi_{SCR}(x)$ for $x > 0$.

3.2.2 Andreev reflection coefficients

We now want to investigate and derive the Andreev reflection coefficient for electrons to holes, r_{he}. Starting out with an electron incident on the left NS-interface from the N-region, as in Figure 3.3, we write the wavefunction to the right of the interface as a superposition of incident and reflected parts,

$$\Psi_N(x) = e^{-ik_e x}\begin{pmatrix}1\\0\end{pmatrix} + \begin{pmatrix} r_{ee}e^{ik_e x} \\ r_{he}e^{-ik_h x}\end{pmatrix}, \tag{3.9}$$

where the first and second part is the incident and reflected part, respectively. r_{ee} and r_{he} is the reflection coefficient for normal reflection (electron to electron) and Andreev reflection (electron to hole), respectively.
The wavefuction to the left of the interface will be of the form

$$\Psi_{SCL}(x) = e^{-i\lambda_+ x}\begin{pmatrix}u_+\\v_+\end{pmatrix} + e^{i\lambda_- x}\begin{pmatrix}u_-\\v_-\end{pmatrix}. \tag{3.10}$$

The relations between the coefficients $u_\pm$ and $v_\pm$ can be found by insertion of (3.10) into (3.6), and reads

$$v_\pm = \frac{|\Delta|e^{-i\phi_L}}{E \pm i\sqrt{|\Delta|^2 - E^2}}u_\pm. \tag{3.11}$$

For convenience, we define $\gamma = \frac{|\Delta|}{E+i\sqrt{|\Delta|^2-E^2}}$, so that we can write

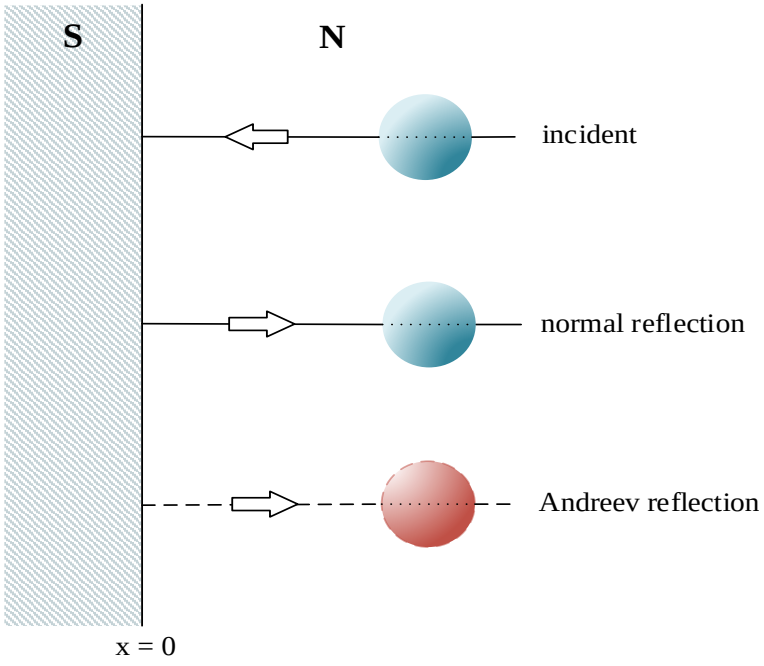

Figure 3.3: Illustration of an electron incident on the left NS-interface ($x = 0$). Normal reflection with probability $|r_{ee}|^2$ and Andreev reflection with probability $|r_{he}|^2$.

$$\begin{aligned}\Psi_{SCL}(x) &= u_+ e^{-i\phi_L} e^{-i\lambda_+ x} \begin{pmatrix} e^{i\phi_L} \\ \gamma \end{pmatrix} + u_- e^{-i\phi_L} e^{i\lambda_- x} \begin{pmatrix} e^{i\phi_L} \\ \gamma^* \end{pmatrix} \\ &= A e^{-i\lambda_+ x} \begin{pmatrix} e^{i\phi_L} \\ \gamma \end{pmatrix} + B e^{i\lambda_- x} \begin{pmatrix} e^{i\phi_L} \\ \gamma^* \end{pmatrix},\end{aligned} \tag{3.12}$$

where we have defined $A = u_+ e^{-i\phi_L}$ and $B = u_- e^{-i\phi_L}$. Employing the continuity conditions for wavefunctions at the interfaces, for Ψ_N and Ψ_{SC1}, we end up with a system of equations [64],

$$\begin{pmatrix} A e^{i\phi_L} + B e^{i\phi_L} \\ A\gamma + B\gamma^* \end{pmatrix} = \begin{pmatrix} 1 + r_{ee} \\ r_{he} \end{pmatrix}. \tag{3.13}$$

It is worth noting that, since $\Delta(x)$ changes abruptly at the interfaces, we should not directly match derivatives at the interfaces, but rather use [64]

$$\lim_{\epsilon \to 0} \int_{\epsilon^-}^{\epsilon^+} (H - E)\psi(x) dx = 0. \tag{3.14}$$

In this case, (3.14) reduces to just matching derivatives, however, it is worth to keep in mind as a general note. We thus get

$$\begin{pmatrix} -\lambda_+ A e^{i\phi_L} + \lambda_- B e^{i\phi_L} \\ -\lambda_+ A\gamma + \lambda_- B\gamma^* \end{pmatrix} = \begin{pmatrix} -k_e + k_e r_{ee} \\ -k_h r_{he} \end{pmatrix}. \tag{3.15}$$

Therefore, we have four equations, (3.13) and (3.15), and four unknown coefficients, A, B, r_{ee}, r_{he}. Solving the equations and expanding the coefficients in series of $\frac{1}{\mu}$, allows us to neglect all higher orders than the first one and we end up with

$$A = \frac{1}{4}\frac{(4i\sqrt{|\Delta|^2 - E^2}\mu + 4E\mu + |\Delta|^2)e^{-i\phi_L} + 4\mu(E + i\sqrt{|\Delta|^2 - E^2})\mathcal{O}\left(\frac{1}{\mu^2}\right)}{(E + i\sqrt{|\Delta|^2 - E^2})\mu}, \tag{3.16}$$

$$B = \frac{1}{4}\frac{-i\sqrt{|\Delta|^2 - E^2}e^{-i\phi_L} + Ee^{-i\phi_L} + 4\mu\mathcal{O}\left(\frac{1}{\mu^2}\right)}{\mu}, \tag{3.17}$$

$$r_{ee} = \frac{1}{2}\frac{2\mu(E + i\sqrt{|\Delta|^2 - E^2})\mathcal{O}\left(\frac{1}{\mu^2}\right) + |\Delta|^2}{(E + i\sqrt{|\Delta|^2 - E^2})\mu}, \tag{3.18}$$

and

$$r_{he} = \frac{1}{2}\frac{|\Delta|(E + 2\mu)(E + i\sqrt{|\Delta|^2 - E^2})e^{-i\phi_L} + 4\mu\left(iE\sqrt{|\Delta|^2 - E^2} + E^2 - \frac{|\Delta|^2|}{2}\right)\mathcal{O}\left(\frac{1}{\mu^2}\right)}{(E + i\sqrt{|\Delta|^2 - E^2})^2\mu}. \tag{3.19}$$

This was possible because $\mu \gg E, |\Delta|$ ("the semiclassical approximation"). However, we can find even simpler forms for r_{ee} and r_{he}. This means that if the chemical potential is by far the largest energy scale in the system, we have

$$r_{ee} = 0, \quad r_{he} = \gamma e^{-i\phi_L}, \tag{3.20}$$

i.e. the normal reflection is completely absent and all we are left with is the Andreev reflection. Thence, the electron is transformed completely into a Cooper pair at the interface and reflects a hole. Here it is appropriate to find a more suitable form of γ. First, we note that

$$e^{\pm i\arccos(x)} = x \pm i\sqrt{1 - x^2}.$$

Then, we rewrite γ so that we have

$$\gamma^{-1} = \frac{E + i\sqrt{|\Delta|^2 - E^2}}{|\Delta|} = \frac{E}{|\Delta|} + i\sqrt{1 - \frac{E^2}{|\Delta|^2}} = e^{i\arccos\left(\frac{E}{|\Delta|}\right)}, \tag{3.21}$$

and we get

$$\gamma = e^{-i\arccos\left(\frac{E}{|\Delta|}\right)} \tag{3.22}$$

Thus, the Andreev reflection coefficient on the left interface becomes

$$r_{he} = e^{-i\arccos\left(\frac{E}{|\Delta|}\right)}e^{-i\phi_L} \tag{3.23}$$

We can do the same for the right interface. The set-up will be exactly the same, just with different signs for the wavevectors, since the electrons and holes are travelling in the opposite directions, and Ψ_{SC2} as the wavefunction for the superconductor. The result is exactly the same, just with $L \to R$. It is here worth to note that we have a free choice of

coordinate system. This means that, when calculating for the right interface, we can also place this interface at $x = 0$. It is only after we define two interfaces relative to each other that we need two fixed coordinates. For incoming holes, the set-up is again the same, just with the first equation of (3.6) to find an expression for $u_\pm$ expressed via $v_\pm$, and we end up with $r_{eh} = \gamma e^{+i\phi_{L/R}}$, i.e. hole to electron. The Andreev reflection coefficients for the four different situations, incoming electron/hole and L/R interface, are subsequently

$$\boxed{r_{he} = e^{-i\arccos\left(\frac{E}{|\Delta|}\right)} e^{-i\phi_{L/R}}, \quad r_{eh} = e^{-i\arccos\left(\frac{E}{|\Delta|}\right)} e^{+i\phi_{L/R}}}. \tag{3.24}$$

This result is extremely important for our calculations of the currents in SNS-junctions, so we again stress the notation; r_{he} is the reflection *from* electrons *to* holes, r_{eh} is the reflection *from* holes *to* electrons.

3.2.3 Energy levels and supercurrent

Now that we have found the Andreev reflection coefficients we can start to construct a localised state in the SNS-junction. Assuming that $E < |\Delta|$, a particle moving to the left through the N-region will be Andreev reflected back from the NS-interface at $x = 0$ as a hole. This reflection will be total as long as we keep our assumption of large μ. The hole will then move back through the N-region to the right NS-interface at $x = L$, where it will be Andreev reflected back as an electron. This will then move back again to the left and so on. The situation is shown in Figure 3.4. It will thus be a bound state localised in the N-region, which we refer to as an Andreev bound state.

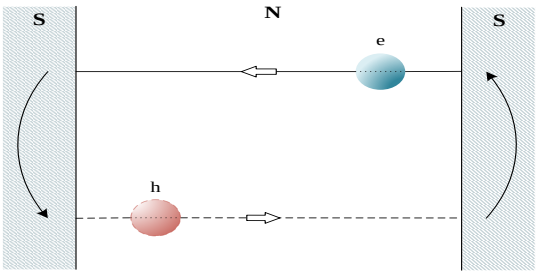

Figure 3.4: Conceptual illustration of the electron path considered. An electron travels to the left, is Andreev reflected back as a hole, travels back again and is Andreev reflected back again as an electron.

The wavefunction in the N-region now has to read

$$\Psi_N(x) = C \begin{pmatrix} e^{-ik_e x} \\ r_{he} e^{-ik_h x} \end{pmatrix} = \begin{pmatrix} f_e(x) \\ f_h(x) \end{pmatrix}, \tag{3.25}$$

due to the Andreev reflection at the left interface, where C is a normalisation constant. At $x = L$, the two amplitudes in the wavefunction are related as

$$r_{eh} = \frac{f_e(L)}{f_h(L)}, \tag{3.26}$$

due to Andreev reflection at the right NS-interface. We so get

$$e^{-2i\arccos\left(\frac{E}{|\Delta|}\right)}e^{i\phi_R}e^{-i\phi_L} = e^{-i(k_e-k_h)L} \quad \Rightarrow \quad e^{-2i\arccos\left(\frac{E}{|\Delta|}\right)}e^{-i\phi}e^{i(k_e-k_h)L} = 1 = e^{2\pi in}, \tag{3.27}$$

where $n \in \mathbb{Z}$. $\phi \equiv \Delta\phi = \phi_L - \phi_R$ is the phase-difference between the two superconductors. This is an example of the Bohr-Sommerfeld quantisation condition, namely that if the bound state corresponds to a closed quasiparticle trajectory, then the total phase accumulated during one cycle must be a multiple of 2π. In order to evaluate $k_e - k_h$, we again linearise assuming large μ, leaving $k_e - k_h = \sqrt{\frac{2m}{\hbar^2\mu}}E = \frac{2E}{\hbar v_F}$, where $v_F = \sqrt{\frac{2\mu}{m}}$, which is the Fermi velocity in the N-region. For electrons travelling from the left to the right, we have the same equations, just with $L \to R$ for r_{eh} and $R \to L$ for r_{eh} meaning $\phi \to -\phi$. Thus, the resulting bound state energies become

$$E_n^{\pm} = \frac{\hbar v_F}{L}\left[(\pi n + \arccos\left(\frac{E}{|\Delta|}\right) \mp \frac{\phi}{2})\right], \tag{3.28}$$

where the upper sign corresponds to electrons moving from the left to the right and the lower sign to excitations from the right to the left. If we now concentrate on the short-junction limit, we can assume $\frac{2E}{\hbar v_F}L \to 0$. The energy can then be written out explicitly as

$$E = \pm|\Delta|\cos\left(\frac{\phi}{2}\right). \tag{3.29}$$

In addition, equation (2.72) will give us the supercurrent through the 1D NW, i.e.

$$I_S(\phi) = \frac{e}{\hbar}{\sum_n}' \frac{dE_n}{d\phi}, \tag{3.30}$$

where the apostrophe is to remind us that the sum is taken over all negative Andreev levels, $E_n < 0$.

The energy levels, or the Andreev levels, constitute the Andreev spectrum and is presented in Figure 3.5 *a*). The supercurrent is presented in Figure 3.5 *b*). This is in agreement with the zero temperature cases from the litterature [65].

We end this section by noting that our system possesses spin degeneracy. Thus, the supercurrent we calculated here is actually only half of what it should be.

3.3 Magnetic field

This section will focus on the SNS-junction with a magnetic field $\mathbf{B}$, where we choose the z-direction along this magnetic field. We will start off with a short discussion on the effects of $\mathbf{B}$. The BdG-Hamiltonian will so be written out in detail. In Section 3.3.2, we will derive the Andreev reflection coefficients, and explicitly show how spin up and spin down down are connected, before we use these coefficients in Section 3.3.3 to find the energy levels of the SNS-junction and the supercurrent that can be maintained.

3.3.1 BdG-equation

With the introduction of a magnetic field, $\mathbf{B}$, there will be some new changes in our description of the system. For example, in general, a magnetic field will introduce a shift

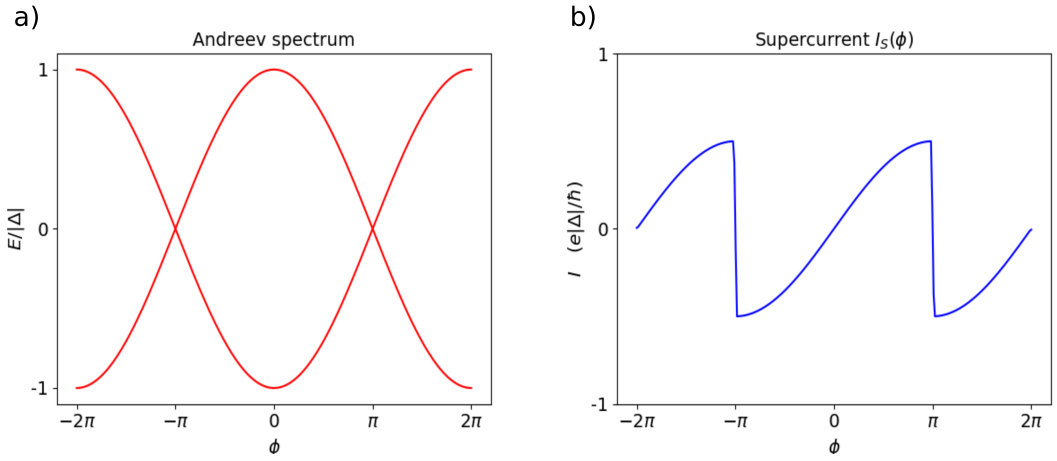

Figure 3.5: Analytical solution for a) the Andreev spectrum in a 1D NW as a function of ϕ and b) the resulting supercurrent for an intervall $[-2\pi, 2\pi]$ with no fields.

in the momentum operator $\hat{\mathbf{p}}$, from $\hat{\mathbf{p}} = \frac{\hbar}{i}\nabla$ to $\hat{\mathbf{p}} = \frac{\hbar}{i}\nabla - q\mathbf{A}$, where $\mathbf{A}$ is the magnetic potential. However, to simplify, we will neglect this magnetic potential shift. This means that we do not care about the magnetic action on the particle trajectory, which is justified for a 1D NW. Up until now spin has been disregarded since it had no effect on the result, apart from a factor of 2 in the supercurrent. This fact will change due to the introduction of $\mathbf{B}$, as particles with different spin will behave differently according to their spin orientation. We choose a basis such that our spinor becomes four-dimensional, spin up and down for electrons and spin down and up for holes, $\{\Psi_\uparrow^\dagger, \Psi_\downarrow^\dagger, \Psi_\downarrow, -\Psi_\uparrow\}$. The spinor thus reads $\psi = \left(u_\uparrow, u_\downarrow, v_\downarrow, -v_\uparrow\right)^T$. $u_\uparrow$ ($u_\downarrow$) and $v_\uparrow$ ($v_\downarrow$) corresponds to electrons with spin up (down) and holes with spin up (down), respectively. The spin quantisation axis is chosen along the magnetic field, i.e. the z-direction.

The spin effect is felt by the particles through a pure quantum mechanic phenomenon called the Zeeman effect, with Hamiltonian

$$\hat{H}_Z = \frac{1}{2} g \mu_B \mathbf{B} \cdot \boldsymbol{\sigma}. \tag{3.31}$$

Here, g is the gyromagnetic factor, or just g-factor, $\mu_B = \frac{e\hbar}{2m}$ is the Bohr magneton, e is the elementary charge, $\mathbf{B}$ is the external magnetic field and $\boldsymbol{\sigma} = (\sigma_x, \sigma_y, \sigma_z)$ is the Pauli spin vector. The g-factor is, in general, material dependent, so we choose g to be position dependent, i.e.

$$g(x) = \begin{cases} g_N & \text{for } 0 < x < L, \\ g_S & \text{otherwise.} \end{cases}$$

It is worth noting that the normal materials often are made of materials with large g-factor. In this way they have a strong Zeeman effect while preserving the superconductivity, i.e. the magnetic field does not surpass the critical magnetic field. We have the following position dependent expression for the Zeeman part of the Hamiltonian,

$$H_Z = E_Z(x)\sigma_z, \tag{3.32}$$

where $E_Z(x) = \frac{|\mathbf{B}|\mu_B}{2} g(x)$.

With our choice of basis, our BdG-equation will be (2.66), as described in Section 2.2. The time-reversal operator changes the expression for H_Z, by setting $\boldsymbol{\sigma} \to -\boldsymbol{\sigma}$, so that we have

$$\begin{aligned}\mathcal{H} &= \begin{pmatrix} H_0 + H_Z - \mu & \Delta \\ \Delta^* & -(H_0 - H_Z - \mu) \end{pmatrix} \\ &= \begin{pmatrix} \frac{\hat{\mathbf{p}}_x^2}{2m} + E_Z(x) - \mu & 0 & \Delta(x) & 0 \\ 0 & \frac{\hat{\mathbf{p}}_x^2}{2m} - E_Z(x) - \mu & 0 & \Delta(x) \\ \Delta^*(x) & 0 & -\frac{\hat{\mathbf{p}}_x^2}{2m} + E_Z(x) + \mu & 0 \\ 0 & \Delta^*(x) & 0 & -\frac{\hat{\mathbf{p}}_x^2}{2m} - E_Z(x) + \mu \end{pmatrix}.\end{aligned} \tag{3.33}$$

Δ is the same as before. This Hamiltonian will decouple in our basis, as it can be seen if we set $(\mathcal{H} - E)\psi = 0$ with ψ written in our spinor representation from earlier. We will then have two decoupled systems of equations,

$$\begin{pmatrix} \frac{\hat{\mathbf{p}}_x^2}{2m} + E_Z(x) - \mu - E & \Delta(x) \\ \Delta^*(x) & -\frac{\hat{\mathbf{p}}_x^2}{2m} + E_Z(x) + \mu - E \end{pmatrix} \begin{pmatrix} u_\uparrow \\ v_\downarrow \end{pmatrix} = 0, \tag{3.34}$$

and

$$\begin{pmatrix} \frac{\hat{\mathbf{p}}_x^2}{2m} - E_Z(x) - \mu - E & \Delta(x) \\ \Delta^*(x) & -\frac{\hat{\mathbf{p}}_x^2}{2m} - E_Z(x) + \mu - E \end{pmatrix} \begin{pmatrix} u_\downarrow \\ -v_\uparrow \end{pmatrix} = 0. \tag{3.35}$$

These systems couple an electron with spin up to a hole with spin down (equation (3.34)) and an electron with spin down to a hole with spin up (equation (3.35)). We see that the Andreev reflection follows naturally from the BdG-equation, both in the case without spin (just electron to hole) and with spin (e.g. electron with spin up to hole with spin down).

3.3.2 Andreev reflection coefficients

Let us start out by investigating the reflection from the left NS-interface for a left-moving electron. As illustrated in Figure 3.6, we see that it can either be normally reflected or Andreev reflected into a hole with opposite spin.

As before, write the wavefunction "deep" in the N-region as

$$\Psi_N(x) = Ae^{-ik_{e\uparrow}x} \begin{pmatrix} 1 \\ 0 \end{pmatrix} + Be^{ik_{h\downarrow}x} \begin{pmatrix} 0 \\ 1 \end{pmatrix}, \tag{3.36}$$

expressed in a spinor representation $\begin{pmatrix} u_\uparrow \\ v_\downarrow \end{pmatrix}$. The insertion of (3.36) into the corresponding decoupled BdG-equation, (3.34), gives us

$$k_{e\uparrow}^2 = \frac{2m}{\hbar^2}\left[\mu + (E - E_{Z,N})\right], \quad k_{h\downarrow}^2 = \frac{2m}{\hbar^2}\left[\mu - (E - E_{Z,N})\right], \tag{3.37}$$

where $E_{Z,N} = \frac{g_N \mu_B B}{2}$ and $B = |\mathbf{B}|$. Let us write the wavefunction in the SC's as we did before, namely $\Psi = \sum_n e^{i\lambda_n}\psi_n$. Insertion into (3.34) and the condition for a non-trivial solution for the matrix-equation will give

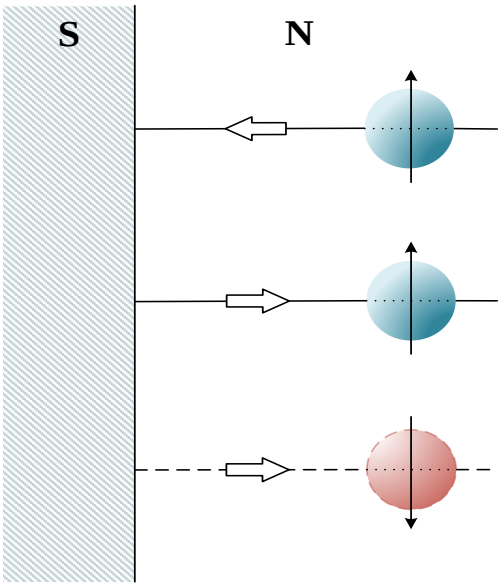

Figure 3.6: Illustration of an electron with spin up incident on the left NS-interface ($x = 0$). Normal reflection with probability $|r_{ee}^{\uparrow\uparrow}|^2$ and Andreev reflection into a hole with opposite spin with probability $|r_{he}^{\downarrow\uparrow}|^2$.

$$\lambda_{n,1}^2 = \frac{2m}{\hbar^2}\left[\mu \pm i\sqrt{|\Delta|^2 - (E - E_{Z,S})^2}\right], \tag{3.38}$$

where $n = \pm$ and $E_{Z,S} = \frac{g_S \mu_B B}{2}$. We label this with 1 for the first of the two decoupled BdG-equations. Equation (3.35) gives us

$$\lambda_{n,2}^2 = \frac{2m}{\hbar^2}\left[\mu \pm i\sqrt{|\Delta|^2 - (E + E_{Z,S})^2}\right]. \tag{3.39}$$

If we assume that $|\Delta| > E \pm E_{Z,S}$, the wavefunctions in the SC's will have the same evanescent behaviour as before. Thus, if we focus on the electron spin up and hole spin down, we write the wavefunction in the left SC as

$$\Psi_{SCL} = e^{-i\lambda_{+,1}x}\begin{pmatrix} u_{+,\uparrow} \\ v_{+,\downarrow} \end{pmatrix} + e^{i\lambda_{-,1}x}\begin{pmatrix} u_{-,\uparrow} \\ v_{-,\downarrow} \end{pmatrix}. \tag{3.40}$$

Proceeding as in Section 3.2.2, we insert (3.40) into (3.34) to find a correlation between the coefficients. We end up with

$$\Psi_{SCL} = Ae^{-i\lambda_{+,1}x}\begin{pmatrix} e^{i\phi_L} \\ \alpha \end{pmatrix} + Be^{i\lambda_{-,1}x}\begin{pmatrix} e^{i\phi_L} \\ \alpha^* \end{pmatrix}, \tag{3.41}$$

where $\alpha = \frac{|\Delta|}{(E-E_{Z,S})+i\sqrt{|\Delta|^2-(E-E_{Z,S})^2}}$. The wavefunction to the right of the left interface is

$$\Psi_N = e^{-ik_{e\uparrow}x}\begin{pmatrix} 1 \\ 0 \end{pmatrix} + \begin{pmatrix} r_{ee}^{\uparrow\uparrow}e^{ik_{e\uparrow}x} \\ r_{he}^{\downarrow\uparrow}e^{-k_{h\downarrow}x} \end{pmatrix}, \tag{3.42}$$

Again, we proceed as in Section 3.2.2. Connecting the wavefunctions at the interface with continuity conditions, solving the subsequent equations and expanding in series of $\frac{1}{\mu}$ will, in the end, give us

$$\begin{aligned}A =&\frac{1}{4}\frac{1}{\mu(E-E_{Z,S}+i\sqrt{|\Delta|^2-(E-E_{Z,S})^2})}\Bigg(\\&\left(i(4\mu-E_{Z,N}+E_{Z,S})e^{-i\phi_L}+4i\mu\mathcal{O}\left(\frac{1}{\mu^2}\right)\right)\sqrt{|\Delta|^2-(E-E_{Z,S})^2}\\&+(-E_{Z,S}^2+(E-4\mu+E_{Z,N})E_{Z,S}+4E\mu-EE_{Z,N}+|\Delta|^2)e^{-i\phi_L}+4\mu(E-E_{Z,S})\mathcal{O}\left(\frac{1}{\mu^2}\right)\Bigg),\end{aligned} \tag{3.43}$$

$$\begin{aligned}B =&\frac{1}{4}\frac{1}{\mu(E-E_{Z,S}+i\sqrt{|\Delta|^2-(E-E_{Z,S})^2})}\Bigg(\\&\left(i(E_{Z,N}-E_{Z,S})e^{-i\phi_L}+4i\mu\mathcal{O}\left(\frac{1}{\mu^2}\right)\right)\sqrt{|\Delta|^2-(E-E_{Z,S})^2}\\&+(-E_{Z,S}^2+(E+E_{Z,N})E_{Z,S}-EE_{Z,N}+|\Delta|^2)e^{-i\phi_L}+4\mu(E-E_{Z,S})\mathcal{O}\left(\frac{1}{\mu^2}\right)\Bigg),\end{aligned} \tag{3.44}$$

$$\begin{aligned}r_{ee}^{\uparrow\uparrow} =&\frac{1}{2}\frac{1}{\mu(E-E_{Z,S}+i\sqrt{|\Delta|^2-(E-E_{Z,S})^2})}\Bigg(\\&2\left(i\sqrt{|\Delta|^2-(E-E_{Z,S})^2}+E-E_{Z,S}\right)\mu\mathcal{O}\left(\frac{1}{\mu^2}\right)-E_{Z,S}^2+(E+E_{Z,N})E_{Z,S}-EE_{Z,N}+|\Delta|^2\Bigg),\end{aligned} \tag{3.45}$$

and

$$\begin{aligned}r_{he}^{\downarrow\uparrow} =&\frac{1}{2}\frac{1}{\mu\left(E-E_{Z,S}+i\sqrt{|\Delta|^2-(E-E_{Z,S})^2}\right)^2}\Bigg(\\&\left(i|\Delta|(E+2\mu-E_{Z,N})e^{-i\phi_L}+4i\mu(E-E_{Z,S})\mathcal{O}\left(\frac{1}{\mu^2}\right)\right)\sqrt{|\Delta|^2-(E-E_{Z,S})^2}\\&+|\Delta|(E-E_{Z,S})(E+2\mu-E_{Z,N})e^{-i\phi_L}+4\mu\left(-\frac{|\Delta|^2}{2}+(E-E_{Z,S})^2\right)\mathcal{O}\left(\frac{1}{\mu^2}\right)\Bigg).\end{aligned} \tag{3.46}$$

We see that the reflection coefficients reduce to

$$r_{ee}^{\uparrow\uparrow}=0,\quad r_{he}^{\downarrow\uparrow}=\alpha e^{-i\phi_L}=e^{-i\arccos\left(\frac{E-E_{Z,S}}{|\Delta|}\right)}e^{-i\phi_L}, \tag{3.47}$$

i.e. we have complete Andreev reflection if μ is the by far the largest energy value, as we had before.

Let us also quickly investigate an incident electron with spin down on the left interface. Again, write the wavefunction "deep" in the N-region as

$$\Psi(x) = Ae^{-ik_{e\downarrow}x}\begin{pmatrix}1\\0\end{pmatrix} + Be^{ik_{h\uparrow}x}\begin{pmatrix}0\\1\end{pmatrix}, \tag{3.48}$$

expressed in a spinor representation $\begin{pmatrix}u_\downarrow\\-v_\uparrow\end{pmatrix}$. This gives

$$k_{e\downarrow}^2 = \frac{2m}{\hbar^2}\left[\mu + (E + E_{Z,N})\right], \quad k_{h\uparrow}^2 = \frac{2m}{\hbar^2}\left[\mu - (E + E_{Z,N})\right]. \tag{3.49}$$

The wavefunction in the SC-region is

$$\Psi_{SCL} = Ae^{-i\lambda_{+,2}x}\begin{pmatrix}-e^{i\phi_L}\\\beta\end{pmatrix} + Be^{i\lambda_{-,2}x}\begin{pmatrix}-e^{i\phi_L}\\\beta^*\end{pmatrix}, \tag{3.50}$$

where $\beta = \frac{|\Delta|}{(E+E_{Z,S})+i\sqrt{|\Delta|^2-(E+E_{Z,S})^2}}$. Solving as before leaves

$$r_{ee}^{\downarrow\downarrow} = 0, \quad r_{he}^{\uparrow\downarrow} = \beta e^{-i\phi_L} = e^{-i\arccos\left(\frac{E+E_{Z,S}}{|\Delta|}\right)}e^{-i\phi_L}. \tag{3.51}$$

We can do the same calculations for incident holes, following the derivation outlined above, and in total we have

$$\boxed{r_{he}^{\downarrow\uparrow} = e^{-i\arccos\left(\frac{E-E_{Z,S}}{|\Delta|}\right)}e^{-i\phi_{L/R}}, \quad r_{he}^{\uparrow\downarrow} = e^{-i\arccos\left(\frac{E+E_{Z,S}}{|\Delta|}\right)}e^{-i\phi_{L/R}},} \tag{3.52}$$

and

$$\boxed{r_{eh}^{\uparrow\downarrow} = e^{-i\arccos\left(\frac{E-E_{Z,S}}{|\Delta|}\right)}e^{i\phi_{L/R}}, \quad r_{eh}^{\downarrow\uparrow} = e^{-i\arccos\left(\frac{E+E_{Z,S}}{|\Delta|}\right)}e^{i\phi_{L/R}}.} \tag{3.53}$$

If we would assume bulk superconducting contacts instead of one-dimensional wires, one expects them to expel all magnetic fields in principle. In this case, we could consider the situation where the Zeeman splitting inside the SC's vanishes, $E_{Z,S} = 0$, and we retrieve (3.24).

3.3.3 Energy levels and supercurrent

To find the bound state energies, we follow the same procedure as before. For an electron with spin up, we have

$$\frac{f_e^\uparrow(L)}{f_h^\downarrow(L)} = r_{eh}^{\uparrow\downarrow} \Rightarrow 2\pi n = 2\frac{E - E_{Z,N}}{\hbar v_F}L - 2\arccos\left(\frac{E - E_{Z,S}}{|\Delta|}\right) \mp \phi, \tag{3.54}$$

where $n \in \mathbb{Z}$. For an electron with spin down, we have a similar expression,

$$\frac{f_e^\downarrow(L)}{f_h^\uparrow(L)} = r_{eh}^{\downarrow\uparrow} \Rightarrow 2\pi n = 2\frac{E + E_{Z,N}}{\hbar v_F}L - 2\arccos\left(\frac{E + E_{Z,S}}{|\Delta|}\right) \mp \phi, \tag{3.55}$$

where $-\phi$ and $+\phi$ refers to left- and right-moving, respectively. We assume bulk superconductors, in which we have $E_{Z,S} = 0$, so that the energy can be written as

$$\pi n = \frac{E\{\pm\}E_Z}{\hbar v_F}L - \arccos\left(\frac{E}{|\Delta|}\right) \mp \phi/2, \tag{3.56}$$

where the energy split from the Zeeman effect is expressed through $E_Z = E_{Z,N}$. The curly parentheses is supposed to indicate that the $\mp E_Z$ belongs to both signs for ϕ. If we further assume the short junction limit, so that $\frac{EL}{\hbar v_F} \to 0$, we are left with

$$E = \pm|\Delta| \cos\left(\phi\{\pm\}\epsilon_Z\right), \tag{3.57}$$

where $\epsilon_Z = \frac{E_Z L}{\hbar v_F}$ is a magnetic field parameter. The Zeeman term is allowed to remain, because $E_Z L$ can be large due to a potentially very large g-factor.

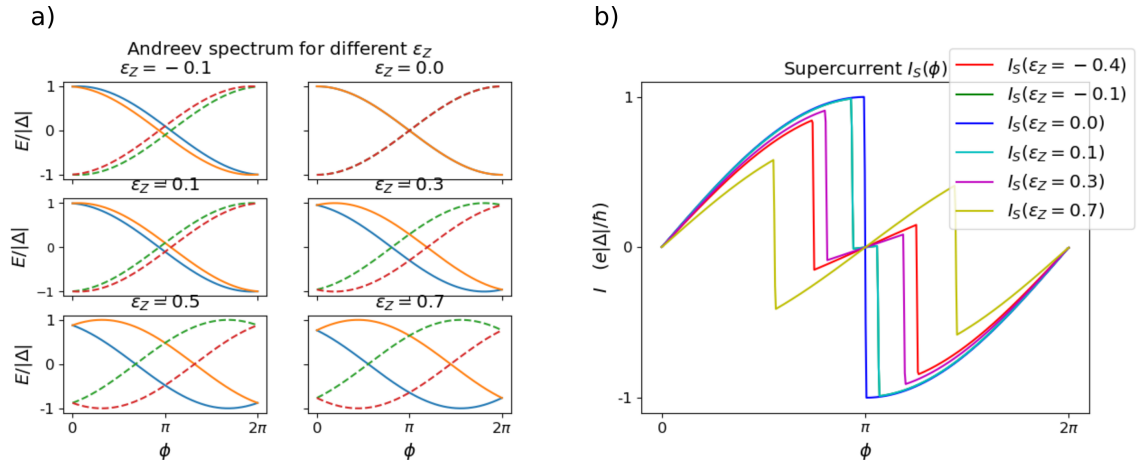

Figure 3.7: a) Analytical solution for the Andreev spectrum in a 1D NW as a function of ϕ. The magnetic field parameter ϵ_Z is indicated. Solid line is the positive cosine-solution, broken is the negative solution. b) Supercurrent through the junction for different ϵ_Z.

Figure 3.7 a) shows the Andreev spectrum for six different values of ϵ_Z. When $\epsilon_Z = 0$ we recover the result of Section 3.2. However, when $\epsilon_Z \neq 0$, we observe the Zeeman effect, where the energy bands are split according to spin orientation. Notice how an oppositely oriented magnetic field changes which spin that increases or decreases in value. Increasing the magnetic field results in oscillations of the bands. Figure 3.7 b) shows the resulting supercurrent, or Josephson current, through the junction. At zero magnetic field, we recover the current from Section 3.2, yet the absolute value of the current here is not the same as in Section 3.2. This is a consequence of accounting for spin and spin degeneracy in this section. The energy levels are double degenerated when no fields are applied, so, when disregarding spin, we end up with half of the actual value for the current. Finally, when the magnetic field is applied over the junction, we observe two kinks (or abrupt changes) in the supercurrent, instead of only one like in Section 3.2.3, both symmetric around $\phi = \pi$, which is a consequence of lifting the spin degeneracy.

3.4 Magnetic field and Spin-Orbit Interaction

This section will focus on the SNS-junction with a magnetic field **B** and spin orbit interaction (SOI), as introduced in 2.5. We will start off by describing the elements of the BdG-Hamiltonian, before we simplify the BdG-equation for our situation, in Section 3.4.1. In Section 3.4.2, we will derive transmission coefficients for transmission across the junction, where the spins are mixed as a consequence of the effective magnetic-SO field. Further, we will solve for the energy of the Andreev bound state in the junction. Section 3.4.3 will present the energy levels and the supercurrent, displayed in a convenient way so that we can entangle the combined effects of the SOI and the magnetic field. We base our approach on [57].

3.4.1 BdG-Hamiltonian

In this section, we want to investigate the Hamiltonain for a 1D NW when we have both magnetic field and SOI, which we let be present only in the N-region. We will also continue to neglect the vector potential shift in the momentum operator. The SOI-terms will be simplified to the lowest order in $\mathbf{k}$ and can be written in a general form as

$$\hat{H}_{\text{SOI}} = k_x \boldsymbol{\alpha} \cdot \boldsymbol{\sigma}, \tag{3.58}$$

where $\boldsymbol{\alpha}$ is the SO-field and, since we only have movement in the x-direction, we focus only on the $k_x = \frac{\hat{p}_x}{\hbar}$-term. We are interested in the combined effects of spin-orbit and magnetic field, so we introduce a general magnetic field $\mathbf{B}$, with the same Zeeman Hamiltonian as introduced in Section 3.3. Choosing the same basis as in Section 3.3, we have

$$\begin{pmatrix} \hat{H} & \Delta \\ \Delta^* & -\mathcal{T}\hat{H}\mathcal{T}^\dagger \end{pmatrix}, \tag{3.59}$$

where

$$\hat{H} = \hat{H}_0 + \hat{H}_Z + \hat{H}_{\text{SOI}} = \left(\frac{\hat{p_x}^2}{2m} - \mu \right) \hat{1} + \left(\frac{1}{2} g \mu_B \mathbf{B} + \frac{\hat{p_x}}{\hbar} \boldsymbol{\alpha} \right) \cdot \boldsymbol{\sigma}. \tag{3.60}$$

Here, we assume that $\mathbf{B}$ and $\boldsymbol{\alpha}$ equal zero outside of the N-region. Following the procedure outlined in [66, 67], in which we are interested in the energy spectrum in a range of energies of order $|\Delta|$ around the Fermi level μ, we can simplify this Hamiltonian. We set $\Psi = e^{\pm i k_F x}(\psi_e^\pm, \psi_h^\pm)^T$, where $\psi_e^\pm$ and $\psi_h^\pm$ are envelope functions. The positive (negative) sign refers to excitation movement in the right-going (left-going) direction for electrons and the left-going (right-going) direction for holes. k_F is the Fermi wavenumber. Since we are interested in the spectrum around μ, we can safely assume that the envelope functions $\psi_{e(h)}^{(\pm)}$ vary over length scales much larger than k_F^{-1}. Inserting Ψ into $\mathcal{H}\Psi = E\Psi$ and expanding in powers of k_F^{-1} allows us to neglect all terms except for the first order. This last step is equivalent to neglecting quickly oscillating terms proportional to $e^{\pm i k_F x}$. With this, $\hat{H}$ becomes

$$\hat{H} = \mp i\hbar v_F \frac{\partial}{\partial x} \hat{1} + \left(\frac{1}{2} g \mu_B \mathbf{B} \pm k_F \boldsymbol{\alpha} \right) \cdot \boldsymbol{\sigma}. \tag{3.61}$$

Keeping in mind that the time-reversal operation flips the momentum and spin operators, we have to write

$$-\mathcal{T}\hat{H}\mathcal{T}^\dagger = \pm i\hbar v_F \frac{\partial}{\partial x} \hat{1} + \left(\frac{1}{2} g \mu_B \mathbf{B} \mp k_F \boldsymbol{\alpha} \right) \cdot \boldsymbol{\sigma}. \tag{3.62}$$

Now, we can define effective fields, containing the magnetic field and the SO-field, in such a way that

$$\mathbf{B}_e^\pm = \frac{1}{2} g \mu_B \mathbf{B} \pm k_F \boldsymbol{\alpha}, \quad \mathbf{B}_h^\pm = \frac{1}{2} g \mu_B \mathbf{B} \mp k_F \boldsymbol{\alpha}. \tag{3.63}$$

In total, we have

$$\mathcal{H} = \begin{pmatrix} \mp i\hbar v_F \frac{\partial}{\partial x} + \mathbf{B}_e^\pm \cdot \boldsymbol{\sigma} & \Delta \\ \Delta^* & \pm i\hbar v_F \frac{\partial}{\partial x} + \mathbf{B}_h^\pm \cdot \boldsymbol{\sigma} \end{pmatrix}, \tag{3.64}$$

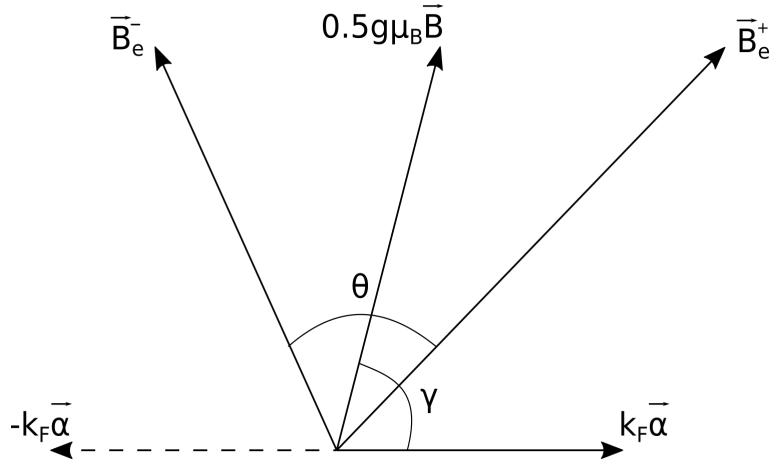

Figure 3.8: Illustration of the magnetic field $\mathbf{B}$, the SO-field $\boldsymbol{\alpha}$ and the resulting effective fields. θ and γ are the angles between the effective fields and $\mathbf{B}$ and $\boldsymbol{\alpha}$, respectively.

Note how $B_e^+ = B_h^-$ and $B_e^- = B_h^+$.

There are two angles defining our system, as shown in Figure 3.8. γ is the angle between the magnetic field and the SO-field, and can be changed to investigate different orientations of $\mathbf{B}$, and θ is the angle between the effective fields. We can find an expression for θ by preforming a dot product between $\mathbf{B}_e^+$ and $\mathbf{B}_e^-$, i.e.

$$\cos(\theta) = \frac{\mathbf{B}_e^+ \cdot \mathbf{B}_e^-}{|\mathbf{B}_e^+||\mathbf{B}_e^-|} = \frac{b_B^2 - b_{\text{SOI}}^2}{\sqrt{(b_B^2 + b_{\text{SOI}}^2)^2 - 4b_B^2 b_{\text{SOI}}^2 \cos^2(\gamma)}}, \tag{3.65}$$

where we have defined

$$b_B = \frac{g\mu_B|\mathbf{B}|L}{2\hbar v_F}, \quad b_{\text{SOI}} = \frac{k_F|\boldsymbol{\alpha}|L}{\hbar v_F}. \tag{3.66}$$

These are dimensionless parameters allowing us to easily distinguish between the effects of the SOI and the magnetic field. They describe the number of precessions the spin experiences while travelling across the junction, caused by SOI (b_{SOI}) and magnetic field (b_B). Thus, we have three parameters (b_B, b_{SOI}, γ) which we can use to probe the NW for the effects of magnetic field and SOI.

3.4.2 Andreev bound state

In this section, we want to find an expression for the energies of the Andreev bound state. We will do so by finding transmission matrices for the N-region in the junction, where the elements are the phases acquired by the electrons and holes when traversing the junction. Combining this with matrices representing the Andreev reflection at the two interfaces allows us to set up a system of equations for a bound state like the one described in Section 3.2.3. The Hamiltonian in the N-region looks like

$$\mathcal{H}_N = \begin{pmatrix} \mp i\hbar v_F \frac{\partial}{\partial x} + \mathbf{B_e}^{(\pm)} \cdot \boldsymbol{\sigma} & 0 \\ 0 & \pm i\hbar v_F \frac{\partial}{\partial x} + \mathbf{B_h}^{(\pm)} \cdot \boldsymbol{\sigma} \end{pmatrix}. \tag{3.67}$$

To find the elements of the transmission matrices, we will follow the procedure presented in [57]. We will show it consistently for a right-moving electron and extrapolate the other

results from that.

The BdG-equation in the N-region reads $\mathcal{H}_N\Psi = E\Psi$, where $\Psi = (\psi_{e,\uparrow}, \psi_{e,\downarrow}, \psi_{h,\downarrow}, -\psi_{h,\uparrow})^T$. The transmission matrix for right-moving (R←L) electron part has to connect the wavefunctions at $x = 0$ and $x = L$,

$$\begin{pmatrix} \psi_{e,\uparrow}^{(+)}(L) \\ \psi_{e,\downarrow}^{(+)}(L) \end{pmatrix} = t_{RL}^{e} \begin{pmatrix} \psi_{e,\uparrow}^{(+)}(0) \\ \psi_{e,\downarrow}^{(+)}(0) \end{pmatrix}. \tag{3.68}$$

The wavefunction $\psi_e^{(+)}(x) = \begin{pmatrix} \psi_{e,\uparrow}^{(+)}(x) \\ \psi_{e,\downarrow}^{(+)}(x) \end{pmatrix}$ satisfies

$$\partial_x \psi_e^{(+)} = i\frac{E - \mathbf{B}_e^+ \cdot \boldsymbol{\sigma}}{\hbar v_F}\psi_e^{(+)} \equiv \hat{f}\psi_e^{(+)}. \tag{3.69}$$

$\hat{f}$ is a 2×2-matrix in spin-space. We write it in a different form with a unitary operation $\hat{S}$, $\hat{S}^\dagger \hat{f} \hat{S} = \mathrm{diag}(\lambda_+, \lambda_-)$, where λ_+ and λ_- are the eigenvectors for spin up and down, respectively. If we define $u_e^{(+)} = \hat{S}^\dagger \psi_e^{(+)}$, will (3.69) become

$$\partial_x u_e^{(+)} = \hat{S}^\dagger \hat{f} \hat{S} (\hat{S}^\dagger \psi_e^{(+)}) = \begin{pmatrix} \lambda_+ & 0 \\ 0 & \lambda_- \end{pmatrix} u_e^{(+)}. \tag{3.70}$$

This equation can be solved for the two spin-components of $u_e^{(+)}$, giving $u_{e,\uparrow}^{(+)}(x) = Ce^{\lambda_+ x}$, $u_{e,\downarrow}^{(+)}(x) = De^{\lambda_- x}$, where $C, D = u_{e,\uparrow}^{(+)}(0), u_{e,\downarrow}^{(+)}(0)$. We get

$$\begin{aligned} \begin{pmatrix} \psi_{e,\uparrow}^{(+)}(x) \\ \psi_{e,\downarrow}^{(+)}(x) \end{pmatrix} = \hat{S} \begin{pmatrix} e^{\lambda_+ x} & 0 \\ 0 & e^{\lambda_- x} \end{pmatrix} \begin{pmatrix} u_{e,\uparrow}^{(+)}(0) \\ u_{e,\downarrow}^{(+)}(0) \end{pmatrix} &= \hat{S} \begin{pmatrix} e^{\lambda_+ x} & 0 \\ 0 & e^{\lambda_- x} \end{pmatrix} \hat{S}^\dagger \begin{pmatrix} \psi_{e,\uparrow}^{(+)}(0) \\ \psi_{e,\downarrow}^{(+)}(0) \end{pmatrix} \\ &= e^{\hat{f}x} \begin{pmatrix} \psi_{e,\uparrow}^{(+)}(0) \\ \psi_{e,\downarrow}^{(+)}(0) \end{pmatrix}. \end{aligned} \tag{3.71}$$

Comparison between (3.71) at $x = L$ and (3.68) gives

$$\hat{t}_{RL}^{e} = e^{i\frac{E - \mathbf{B}_e^+ \cdot \boldsymbol{\sigma}}{\hbar v_F} L}. \tag{3.72}$$

This derivation can be done for all the transmission matrices. Remember that $\psi(0) = \hat{t}_{LR}\psi(L)$ and that the signs for holes refer to the opposite situations than for electrons. All this leaves us with

$$\hat{t}_{LR}^{e} = e^{i\frac{E - \mathbf{B}_e^- \cdot \boldsymbol{\sigma}}{\hbar v_F} L}, \tag{3.73}$$

for the left-moving electron part and

$$\hat{t}_{RL}^{h} = e^{i\frac{E - \mathbf{B}_h^{(-)} \cdot \boldsymbol{\sigma}}{\hbar v_F} L}, \tag{3.74}$$

$$\hat{t}_{LR}^{h} = e^{i\frac{E - \mathbf{B}_h^{(+)} \cdot \boldsymbol{\sigma}}{\hbar v_F} L}, \tag{3.75}$$

for the hole parts.

As we are free to define our quantisation axis for the spin, we make a choice and define it along the effective field $\mathbf{B}_e^+$. Since we are also free to define our coordinate system, we

can align the quantisation axis with the z-direction, i.e. $\mathbf{B}_e^+ \cdot \boldsymbol{\sigma} = |\mathbf{B}_e^+|\sigma_z$. Furthermore, we are free to define the xz-plane such that $\mathbf{B}_e^+$ and $\mathbf{B}_e^-$ lie in the same plane. This means we can write

$$\mathbf{B}_e^- = |\mathbf{B}_e^-|(\sin(\theta)\hat{x} + \cos(\theta)\hat{z}), \tag{3.76}$$

where $|\mathbf{B}_e^\pm| = \sqrt{\mathbf{B}_e^\pm \cdot \mathbf{B}_e^\pm}$. We simplify the exponentials in the $\hat{t}$'s by defining $\theta_{e/h}^{(\pm)} = \frac{\left|\mathbf{B}_{e/h}^{(\pm)}\right| L}{\hbar v_F}$. With our earlier observation about the effective fields, we have $\theta_e^+ = \theta_h^- = \theta_+$ and $\theta_e^- = \theta_h^+ = \theta_-$, where

$$\theta_\pm = \sqrt{b_B^2 \pm 2 b_B b_{\mathrm{SOI}} \cos(\gamma) + b_{\mathrm{SOI}}^2}. \tag{3.77}$$

In total

$$\hat{t}_{RL}^e = \hat{t}_{RL}^h = e^{i\epsilon} e^{-i\theta_+ \sigma_z}, \quad \hat{t}_{LR}^e = \hat{t}_{LR}^h = e^{i\epsilon} e^{-i\boldsymbol{\theta}_- \cdot \boldsymbol{\sigma}}, \tag{3.78}$$

where $\epsilon = EL/\hbar v_F$. Matrix exponentials for Pauli matrices can be expressed in a convenient way, namely

$$e^{ia(\mathbf{n}\cdot\boldsymbol{\sigma})} = \hat{1}\cos(a) + i(\mathbf{n}\cdot\boldsymbol{\sigma})\sin(a), \tag{3.79}$$

which means that we can write all the $\hat{t}$'s as 2×2-matrices., i.e.

$$\hat{t}_{LR}^{e,h} = e^{i\epsilon} \begin{pmatrix} \cos(\theta_-) - i\sin(\theta_-)\cos(\theta) & -i\sin(\theta_-)\sin(\theta) \\ -i\sin(\theta_-)\sin(\theta) & \cos(\theta_-) + i\sin(\theta_-)\cos(\theta) \end{pmatrix}, \tag{3.80}$$

and

$$\hat{t}_{RL}^{e,h} = e^{i\epsilon} \begin{pmatrix} e^{-i\theta_+} & 0 \\ 0 & e^{i\theta_+} \end{pmatrix}. \tag{3.81}$$

We can combine this into transmission matrices for the right-moving situation (RL) and the left-moving situation (LR),

$$\hat{T}_{RL} = \begin{pmatrix} \hat{t}_{RL}^e & 0 \\ 0 & \hat{t}_{RL}^h \end{pmatrix}, \quad \hat{T}_{LR} = \begin{pmatrix} \hat{t}_{LR}^e & 0 \\ 0 & \hat{t}_{LR}^h \end{pmatrix}. \tag{3.82}$$

These transmission matrices represent the phase accumulated by a particle moving ballisticly across a junction of length L. $\hat{t}_{LR}^{e,h}$ mixes the spins, since it is not diagonal. The spin mixing is present due to not all of the effective fields aligning with the spin quantisation axis. In contrast, the Andreev reflection matrix connects the spin up electron to spin down hole and vice versa. The matrix reads

$$\hat{A}_{R/L} = e^{-i\arccos\left(\frac{E}{|\Delta|}\right)} \begin{pmatrix} 0 & 0 & e^{i\phi_{R/L}} & 0 \\ 0 & 0 & 0 & e^{i\phi_{R/L}} \\ e^{-i\phi_{R/L}} & 0 & 0 & 0 \\ 0 & e^{-i\phi_{R/L}} & 0 & 0 \end{pmatrix}, \tag{3.83}$$

where L/R refers to the the left/right NS-interface.

The bound state for a given situation exists if a state returns to its initial state after one round in the SNS-junction. We represent both of the situations described in Section 3.2.3 with

$$\Psi = \hat{A}_L \hat{T}_{LR} \hat{A}_R \hat{T}_{RL} \Psi, \tag{3.84}$$

which yields the quantisation condition

$$\det\left(1 - \hat{A}_L \hat{T}_{LR} \hat{A}_R \hat{T}_{RL}\right) = 0. \tag{3.85}$$

This equation is equivalent to the BdG-equation and decouples into the right-moving electron and left-moving electron situation. This reduces to

$$\begin{aligned}\left(i\sin(\theta_-)\cos(\theta) - \cos(\theta_-)\right) e^{-i\theta_+} e^{i(\kappa\pm\phi)} + \left(-i\sin(\theta_-)\cos(\theta) - \cos(\theta_-)\right) e^{i\theta_+} e^{i(\kappa\pm\phi)} \\ + e^{2i(\kappa\pm\phi)} + 1 = 0\end{aligned} \tag{3.86}$$

where $\kappa = 2\left(\frac{EL}{\hbar v_F} - \arccos\left(\frac{E}{|\Delta|}\right)\right)$. Solving (3.86) results in

$$\frac{EL}{\hbar v_F} - \arccos\left(\frac{E}{|\Delta|}\right) = \pi n\{\pm\}\frac{1}{2}\arccos(\lambda) \mp \frac{\phi}{2}, \tag{3.87}$$

where

$$\lambda = \cos(\theta_+)\cos(\theta_-) - \cos(\theta)\sin(\theta_+)\sin(\theta_-), \tag{3.88}$$

and $n \in \mathbb{Z}$ and $\{\pm\}$ means that the $\pm$ in front of the arccos belongs to each of the signs in front of ϕ. The upper sign of ϕ refers to the rightmoving situation and the lower sign to the leftmoving situation. We also see that the effects of the magnetic field and SOI are combined by the single parameter λ. In the short-junction limit, we get

$$E = \pm|\Delta|\cos\left(\frac{\phi}{2}\{\pm\}\frac{1}{2}\arccos(\lambda)\right). \tag{3.89}$$

3.4.3 Energy levels and supercurrent

In this section, we want to investigate the effects of SOI and magnetic fields in combination on the NW. We focus on the short short-junction limit, so that we may present the analytical solutions of (3.89).

To check our approach to the combination of magnetic field and SOI, we set b_{SOI} to zero. Plotting for several magnetic field strengths, we reproduce the result from Section 3.3, as seen in Figure 3.9.

Let us so turn to the combination of magnetic fields and SOI. Figure 3.10 presents the supercurrent as a function of ϕ for different magnetic field strengths, with several values of the SO-field strength and the orientation of the magnetic field, γ. We present here three different cases for the SO-field strength, $b_{\text{SOI}} = 1$ (weak SOI-regimé), $b_{\text{SOI}} = 4$ (intermediate SOI-regimé) and $b_{\text{SOI}} = 9$ (strong SOI-regimé). For each regimé, we have three values of γ to exemplify the effects of the interplay between magnetic fields and SOI.

Investigation of Figure 3.10 reveals that we will retrieve the no-fields case from Section 3.2 for all values of b_{SOI} when $\mathbf{B} = 0$. This fact is at first confusing, since SOI is supposed to have the effect of spin splitting the energy bands, even in the absence of magnetic fields. However, this is not the case for the Andreev bound states of SNS-junctions in the short-junction limit [68]. Simply stated, during one "cycle" in the SNS-junction, which

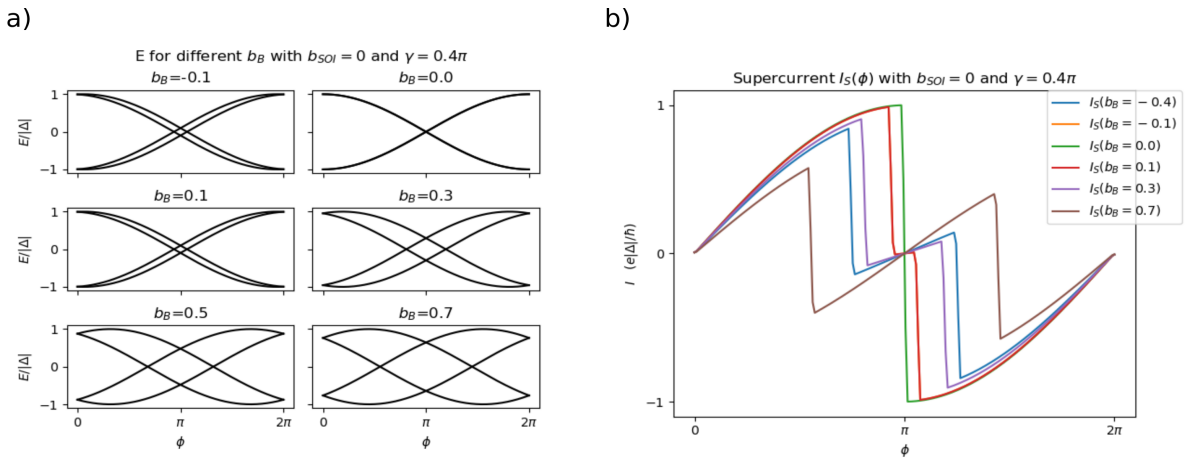

Figure 3.9: Analytical solution of a) the Andreev spectrum in a 1D NW and b) the supercurrent for different magnetic field strengths b_B, with $b_{\text{SOI}} = 0$ and $\gamma = 0.4\pi$.

constitutes a bound state, two electrons will be transported from one side of the junction to the other, i.e. a Cooper pair will have been transferred from one superconductor to the other. The electrons will have opposite $\mathbf{k}$ and spin (since one of them is a hole). This means that they feel the same SOI-induced energy shift and thus no relative phase difference develops between the two. We can conclude from this that the effect of SOI is first important when in combination with a magnetic field.

For simplicity, let us call the different supercurrents for different b_B for lines. We observe an oscillatory behaviour in the lines for changing γ. When γ goes from 0 to $\pi/2$, the lines will become more and more centred around $\phi = \pi$. The effect is not so clear in Figure 3.10 a)-c), but becomes clearer for stronger SO-fields, as seen in d)-i). Very large b_{SOI} will centre all the lines on the no-fields case. From $\gamma = \pi/2$ to π, the lines will relax back out to the original position for $\gamma = 0$. In the same intervals, we observe an increase and then a decrease, respectively, in the maximum (and minimum) values of the lines, as the kinks in the lines move towards $\phi = \pi$. This means that the slope of the lines between the two kinks becomes less steep around $\gamma = \pi/2$ than for lower or higher γ. We observe the same type of oscillatory behaviour for $\gamma \in [\pi, 2\pi]$.

We can explain the tendency of the lines to drift towards the no-fields case at $\gamma = \pi/2$ by considering how this angle changes the effective fields. At γ equal to $\pi/2$, we have $\mathbf{B} \perp \boldsymbol{\alpha}$, so that the effective fields are closely mirrored around $\mathbf{B}$. If b_{SOI} is close in value to b_B, θ_+ and θ_- will vary enough for the lines not become very similar, as seen in Figure 3.10 a)-c). However, when b_{SOI} becomes larger compared to b_B, θ_+ and θ_- will become more and more close in value, i.e. the phase acquired from the different effective fields will start to cancel each other out. In the strong SOI-regimé, the effective fields will almost completely cancel the effect of each other (at $\gamma = \pi/2$), and we are back to the no-fields case.

For the case when γ is small, we see that we have a supercurrent strongly resembling that of Figure 3.9, with no SOI. This is because when the SO-field and the magnetic field almost align, the spin quantisation direction will be more or less in the same direction as the magnetic field, and we have in effect just the Zeeman effect from earlier.

We end this chapter with a short discussion on the anomalous Josephson current. As introduced in Chapter 1, the interplay between SOI and magnetic fields can cause

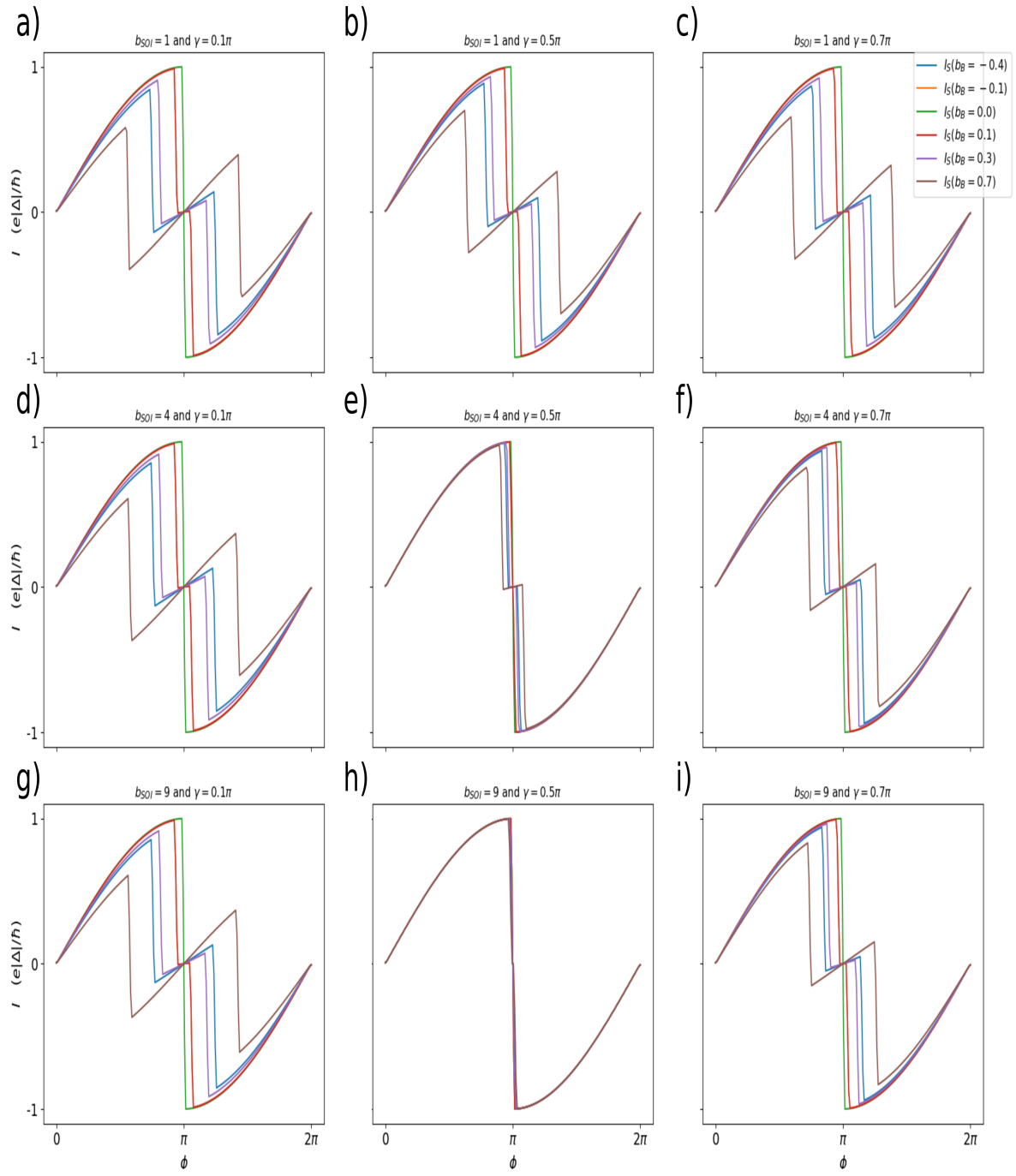

Figure 3.10: Analytical solution the supercurrent in 1D NW with magnetic field and SO-field for different magnetic field strengths b_B. The variables are $b_{\text{SOI}} = 1$ for a) $\gamma = 0.1\pi$, b) $\gamma = 0.5\pi$ and c) $\gamma = 0.7\pi$, $b_{\text{SOI}} = 4$ for d) $\gamma = 0.1\pi$, e) $\gamma = 0.5\pi$ and f) $\gamma = 0.7\pi$ and $b_{\text{SOI}} = 9$ for g) $\gamma = 0.1\pi$, h) $\gamma = 0.5\pi$ and i) $\gamma = 0.7\pi$.

a supercurrent to exist at zero phase difference, $I_S(\phi = 0) \neq 0$, called the anomalous Josephson effect. Our model fails to produce such currents, as was expected. [57] did not find an anomalous supercurrent, which the authors attributed to the fact that SOI is caused by spin-dependent channel mixing. However, let us do a quick overview for possible reasons for the absence of the anomalous supercurrent, as there can be several. First, the semiclassical approximation and the absence of certain symmetries can be a

cause for not obtaining the anomalous supercurrent [38, 40]. Furthermore, the current was predicted when the length of the junction was larger or comparable to the coherence length in the system. For example, a anomalous supercurrent has been derived for long junction with a single conductance channel [69]. However, as shown in [67, 70], the anomalous supercurrent can also be obtained in short-junction limit NW's with SOI and magnetic fields. This was the case with more than one conduction channel for the single scatterer model, but also for a single conductance channel with more than one scatterer. Thus, we attribute the absence of an anomalous Josephson current in our NW to the fact that we considered a single conduction channel in a ballistic NW.

4 — Toy model for a disordered 2D SNS-junction

This chapter will develop a simple toy model to study a two-dimensional disordered SNS-junction. As discussed in Chapter 1, such SNS-junctions can exhibit asymmetries in the critical current as a function of the perpendicular magnetic field. The spatial asymmetries introduced in the system by disorder is believed to play an important role for this asymmetrical critical current [47]. For example, a strong disorder can lead to many preferred paths across the N-region, which all come with different dynamical phase, different phase acquired from the magnetic potential, SOI-induced spin rotation, etc. We want to create the simplest situation to mimic this effect of disorder. This will be done by allowing for two possible paths across the N-region, where the paths are split by a beamsplitter. We locate the beamsplitters at the NS-interfaces to simulate disorder, as shown in Figure 4.1. For this reason, we have enclosed magnetic flux in the area encompassed by the two paths and thus an Aharonov-Bohm (AB) effect. The formalism for beamsplitters, scattering matrix theory, and the formalism for transfer matrices are introduced in Section 4.1, and are adopted from [61]. We will employ this formalism to find the general transmission and reflection coefficients for the N-region with two paths in Section 4.2. We will look at both symmetric (probability) injection and asymmetric injection into the two paths. In Section 4.3, we will find expressions for these coefficients for a few specific cases. Andreev reflection will be introduced in Section 4.4 in a procedure to find the Andreev levels, the supercurrent I_S and the critical current I_C.

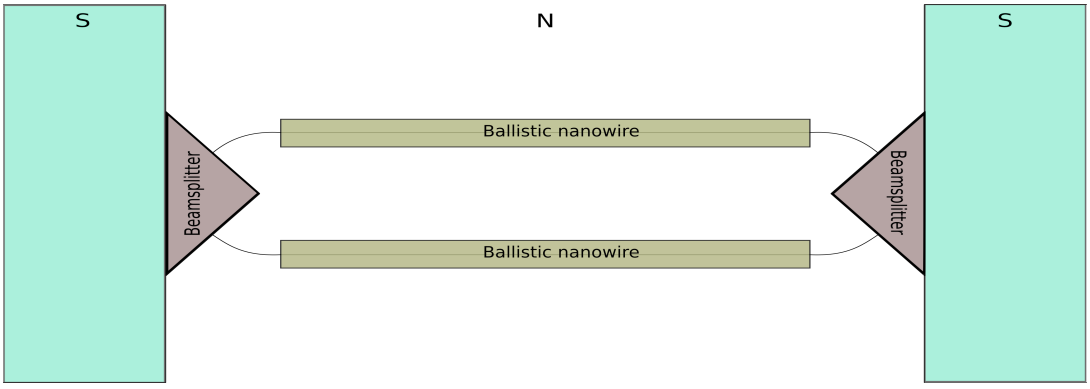

Figure 4.1: Illustration of two paths across the N-region. Rectangular boxes represent the ballistic NW's in the N-region and the triangles represent the beamsplitters located at the NS-interfaces.

4.1 Scattering matrix formalism

This section will cover the formalism and method of scattering matrix theory for beamsplitters and the formalism for transfer matrices. The scattering matrix is used to relate the outgoing and incoming waves on a beamsplitter. Our approach to the scattering matrix was first introduced by Shapiro [71] in relation to Cayley trees and further developed by Büttiker et. al. [72] in their work on quantum rings. The Büttiker formalism is able to represent leads coupled to the ring (shown by filled triangles in Figure 4.2), varying from complete coupling (completely transparent beamsplitter) to no coupling at all (decoupled ring from leads).

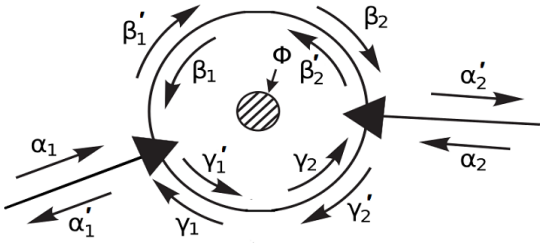

Figure 4.2: Illustration of leads coupled to a quantum ring (at beamsplitters ◀). Primed (unprimed) greek letters represent wave amplitudes of outgoing (incoming) waves. Φ is the enclosed flux. Adapted from [61].

We want to have a relation between the outgoing amplitudes of the wavefunctions (represented by primed greek letters in Figure 4.2) and incoming amplitudes (unprimed). This is done by relating them via a scattering matrix $\hat{S}$,

$$\boldsymbol{\alpha'} = \hat{S}\boldsymbol{\alpha}. \tag{4.1}$$

Here $\boldsymbol{\alpha} = (\alpha, \beta, \gamma)$. In Figure 4.2, we have three outgoing $(\alpha', \beta', \gamma')$ wave amplitudes and three incoming (α, β, γ) amplitudes, making $\hat{S}$ a 3×3-matrix. The β's and γ's are for the two paths, or arms, in the N-region, while the α's are for the leads coupling the two arms to the NS-interfaces. Current conservation and time-reversal symmetry imply that $\hat{S}$ is unitary and that $\hat{S}^{-1} = \hat{S}^*$, respectively, so that $\hat{S}$ in general depends on only five independent parameters [72]. Here, it is worth noting that we assume time-reversal symmetry even in the presence of a magnetic field penetrating the junction. We justify this by continuation of our assumption of completely 1D NW's, meaning the magnetic potential can be neglected in the arms. We also neglect magnetic effects in the beamsplitters.

4.1.1 Symmetric injection

We focus first on the case where $\hat{S}$ is symmetric with respect to the two arms, i.e. the transmission probability from the lead into each of the two arms is considered equal. With this assumption, we reduce the number of independent parameters to three. By further assuming that S is real, we can write $\hat{S}$ as

$$\hat{S} = \begin{pmatrix} -(a+b) & \sqrt{\epsilon} & \sqrt{\epsilon} \\ \sqrt{\epsilon} & a & b \\ \sqrt{\epsilon} & b & a \end{pmatrix}. \tag{4.2}$$

The diagonal elements represent the reflection coefficients from one arm or lead to itself. The off-diagonal elements represent transmission from one arm or lead into another. Unitarity of $\hat{S}$ leads to the following relations:

$$(-(a+b))^2 + \sqrt{\epsilon}^2 + \sqrt{\epsilon}^2 = 1, \quad \sqrt{\epsilon}^2 + a^2 + b^2 = 1, \quad 2ab + \epsilon = 0. \tag{4.3}$$

This simplifies to

$$(a+b)^2 + 2\epsilon = 1, \quad a^2 + b^2 + \epsilon = 1, \quad 2ab + \epsilon = 0, \tag{4.4}$$

which have four solutions,

$$(a_1)_\pm = \pm\frac{1}{2}\left(\sqrt{1-2\epsilon} - 1\right), (b_1)_\pm = \pm\frac{1}{2}\left(\sqrt{1-2\epsilon} + 1\right), \tag{4.5}$$

and

$$(a_2)_\pm = \pm\frac{1}{2}\left(\sqrt{1-2\epsilon} + 1\right), (b_2)_\pm = \pm\frac{1}{2}\left(\sqrt{1-2\epsilon} - 1\right). \tag{4.6}$$

ϵ represents here the coupling parameter between the lead and the arms, describing the (equal) probability for transmission into the arms. A completely transparent beamsplitter gives $\epsilon = 1/2$ and the lead is strongly coupled to the arms. On the other hand, if $\epsilon = 0$, all electrons from the lead are completely reflected and we have no coupling at all. Consider a wave incoming on the beamsplitter. It will be reflected back with probability $|a+b|^2 = 1-2\epsilon$ and is transmitted into each of the two arms with probability ϵ. If $\epsilon = 0$, all electrons are reflected back, the ring is decoupled from the lead and the transmission probability from one arm to the other is $|b|^2 = 1$. If $\epsilon = 0.5$ we have a complete coupling between the lead and the ring and all electrons incoming on the beamsplitter are transmitted through.

We choose to continue working with the first set of solutions, meaning we set $a_1 = a$ and $b_1 = b$. With this choice we have

$$b - a = \pm 1, \quad b + a = \pm\sqrt{1-2\epsilon}, \quad b^2 - a^2 = \sqrt{1-2\epsilon}. \tag{4.7}$$

If we further choose the positive solutions, we write $\hat{S}$ as

$$\begin{pmatrix} -\sqrt{1-2\epsilon} & \sqrt{\epsilon} & \sqrt{\epsilon} \\ \sqrt{\epsilon} & \frac{1}{2}\left(\sqrt{1-2\epsilon} - 1\right) & \frac{1}{2}\left(\sqrt{1-2\epsilon} + 1\right) \\ \sqrt{\epsilon} & \frac{1}{2}\left(\sqrt{1-2\epsilon} + 1\right) & \frac{1}{2}\left(\sqrt{1-2\epsilon} - 1\right) \end{pmatrix}. \tag{4.8}$$

Thus, $\hat{S}$ depends on a single independent parameter, $0 < \epsilon < 1/2$.

4.1.2 Asymmetric injection

Here, we want to focus on asymmetric probability injection into the two arms. We will model this by allowing for a favouring of one of the arms over the other by a parameter β. As before, we require $\hat{S}$ to be unitary and $\hat{S}^* = \hat{S}^{-1}$, making it symmetric, and we continue to assume it real for simplicity. We write

$$\hat{S} = \begin{pmatrix} a & b & c \\ b & d & e \\ c & e & f \end{pmatrix}. \tag{4.9}$$

Note that the a in this matrix is not the same as the one in Section 4.1.1. a here plays the role of the coupling parameter, as ϵ did before. Unitarity of $\hat{S}$ leads to the following relations:

$$a^2 + b^2 + c^2 = 1, \tag{4.10}$$
$$b^2 + d^2 + e^2 = 1, \tag{4.11}$$
$$c^2 + e^2 + f^2 = 1, \tag{4.12}$$

and

$$ab + bd + ce = 0, \tag{4.13}$$
$$ac + be + cf = 0, \tag{4.14}$$
$$bc + de + ef = 0. \tag{4.15}$$

We introduce the asymmetry between the two arms by setting $b = \beta c$. β is thus the asymmetric probability injection parameter, i.e. β decides the ratio of probability for e.g. transmission into one arm from the lead compared to the other arm. $\beta = 1$ means equivalent transmission probability, as in Section 4.1.1. $\beta > 1$ means that the upper arm is preferred. Now, we want to express b, d, e and f as functions of β and a. From (4.10), (4.13) and (4.14) we have

$$b = \pm\frac{\beta\sqrt{1-a^2}}{\mu}, \tag{4.16}$$
$$e = -\beta(a + d), \tag{4.17}$$
$$f = a(\beta^2 - 1) + \beta^2 d, \tag{4.18}$$

respectively, where $\mu = \sqrt{\beta^2 + 1}$. Insertion of (4.16) and (4.17) into (4.11) give us

$$d = \frac{\pm 1 - \beta^2 a}{\mu^2}, \tag{4.19}$$

which gives (4.17) and (4.18) as functions of β and a. In total we have

$$b = \beta\nu_\pm, \quad c = \nu_\pm, \quad d = \eta_\pm - a, \quad e = -\beta\eta_\pm, \quad f = \xi_\pm, \tag{4.20}$$

where

$$\eta_\pm = \frac{a \pm 1}{\mu^2}, \quad \nu_\pm = \pm\frac{\sqrt{1-a^2}}{\mu}, \quad \xi_\pm = \frac{\pm\beta^2 - a}{\mu^2}. \tag{4.21}$$

Note how the signs for $\nu_\pm$ are independent from those of $\eta_\pm$ and $\xi_\pm$ (which are the same). This means that we have four different valid versions of $\hat{S}$, as we did for the symmetric injection-case. However, since we made a choice for which parameters to be used in the

symmetric injection-case, we do the same here. Therefore, for this $\hat{S}$ to coincide with the symmetric injection-case when we let $\beta = 1$, as in (4.8), we choose the parameters ν_+, η_- and ξ_-. Thus, our $\hat{S}$ will be the same as for the positive solutions of a_1 and b_1 from 4.1.1. Suppressing the subscripts we write

$$\hat{S} = \begin{pmatrix} a & \beta\nu & \nu \\ \beta\nu & \eta - a & -\beta\eta \\ \nu & -\beta\eta & \xi \end{pmatrix}. \tag{4.22}$$

We see that $a^2 = 1 - 2\epsilon$, which shows us the relationship between a and the coupling parameter ϵ. $a = 0$ corresponds to perfect coupling between lead and ring, while $a = -1$ corresponds to no coupling at all, since then $a = -\sqrt{1 - 2\epsilon}$. If we set $\beta = 1$ and we insert this a into (4.22), we end up back to the symmetric case of (4.8).

As an ending note, notice how the asymmetry in (4.22) implies that the probability for transmission from one lead into the arms is fixed by $|\beta\nu|^2$ for the upper arm, both when incoming from the left and when incoming from the right, as shown in Figure 4.3.

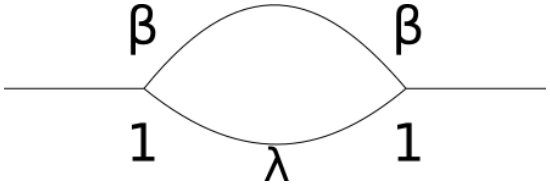

Figure 4.3: Illustration of the upper and lower arm and the probability injection ratio β between them, which is the same for the right and the left beamsplitters. λ indicates the asymmetry in the arm lengths. $\lambda < 1$ means the upper arm is longer than the lower arm.

4.1.3 Transfer matrix

The transfer matrix method is a mathematical method for the analysis of wave propagation in 1D systems, for quantum particles, such as electrons and holes and electromagnetic, acoustic and elastic waves. In order to represent scattering on a potential, one can connect the incoming wave amplitudes to the outgoing amplitudes with a scattering matrix like $\hat{S}$ [73],

$$\begin{pmatrix} \beta_{out} \\ \tilde{\beta}_{out} \end{pmatrix} = \hat{s} \begin{pmatrix} \beta_{in} \\ \tilde{\beta}_{in} \end{pmatrix}. \tag{4.23}$$

However, another way to connect the amplitudes is by relating the ones at the right to the ones at the left,

$$\hat{t} \begin{pmatrix} \beta_{in} \\ \beta_{out} \end{pmatrix} = \begin{pmatrix} \tilde{\beta}_{out} \\ \tilde{\beta}_{in} \end{pmatrix}, \tag{4.24}$$

where

$$\hat{t} = \begin{pmatrix} \frac{1}{t^*} & -\frac{r^*}{t^*} \\ -\frac{r}{t} & \frac{1}{t} \end{pmatrix}. \tag{4.25}$$

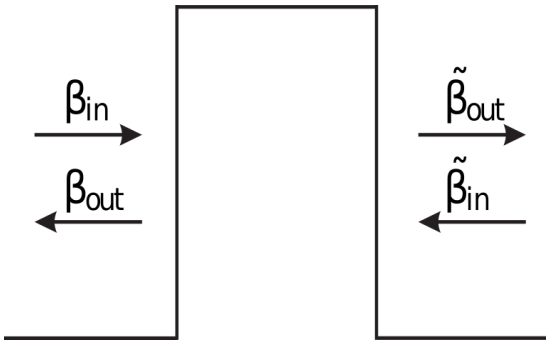

Figure 4.4: Illustration of wave amplitudes on the left side and on the right side (marked by tilde) of a potential barrier (could also be a well). Illustration adapted from [61].

t and r are the transmission and reflection coefficients, respectively, for the potential. The matrix $\hat{t}$ is called the transfer matrix. If relating the left amplitudes to the right amplitudes, we use $\hat{t}'$ in such a way that

$$\begin{pmatrix} \beta_{out} \\ \beta_{in} \end{pmatrix} = \hat{t}' \begin{pmatrix} \tilde{\beta}_{in} \\ \tilde{\beta}_{out} \end{pmatrix}. \tag{4.26}$$

The elements of $\hat{t}$ are

$$t = \sqrt{T_s} e^{i\chi}, \quad r = e^{-i\frac{\pi}{2}} \sqrt{R_s} e^{i\chi} e^{i\chi_a}, \tag{4.27}$$

where T_s and R_s are the transmission and reflection probability for the particle, χ is the phase change in the transmitted wave and χ_a is a possible additional phase difference between the transmitted and reflected amplitudes. In the case of a symmetric potential, the length the reflected particle traverses inside the potential (twice the penetration depth) will be equal to the length the transmitted particle travels to traverse the potential, and thus no additional phase difference is acquired between the reflected and transmitted parts of the wavefunction, i.e. $\chi_a = 0$. Lastly, it should be noted that in the case of current-conservation, time-reversal symmetry and a symmetric potential ($\chi_a = 0$), we will have $\hat{t} = \hat{t}'$.

Transfer matrix approach to the no fields-case

Let us here try to use this formalism to reproduce the result from Section 3.2. We have a ballistic wire, so we can set the part of the wavefunction travelling to the right in Figure 4.4 as the electron part and the part travelling left as the hole part. Thus, we have the total transmission matrix from right-to-left (LR) and left-to-right (RL) as

$$\hat{t}_{LR} = \hat{t}_{RL} = \begin{pmatrix} e^{ik_e L} & 0 \\ 0 & e^{-ik_h L} \end{pmatrix}. \tag{4.28}$$

Here, $k_e = \sqrt{\frac{2m}{\hbar^2}(\mu + E)}$ and $k_h = \sqrt{\frac{2m}{\hbar^2}(\mu - E)}$. For the Andreev reflection we have

$$\hat{A}_{R/L} = e^{-i \arccos\left(\frac{E}{|\Delta|}\right)} \begin{pmatrix} 0 & e^{i\phi_{R/L}} \\ e^{-i\phi_{R/L}} & 0 \end{pmatrix}. \tag{4.29}$$

The localisation condition, from the description given in Section 3.2.3, will be

$$\det\left(\hat{1} - \hat{A}_R \hat{t}_{RL} \hat{A}_L \hat{t}_{LR}\right) = 0. \tag{4.30}$$

Solving this equation gives

$$2\arccos\left(\frac{E}{|\Delta|}\right) - (k_e - k_h)L = (\phi_L - \phi_R) + 2\pi n, \tag{4.31}$$

which is the same result as we achieved in Chapter 3.

4.2 Transmission and reflection coefficients

This Section will derive the transmission and reflection coefficients through the N-region when we have two possible paths, or arms, both for the symmetric (probability) injection and for the asymmetric injection. The N-region is illustrated in Figure 4.5. We will base our approach on the method of [61] and allow for a perpendicular magnetic field enclosed by the two arms. The arms will be modelled as 1D NW's, which we investigated in Chapter 3. A significant difference from the 1D case, however, is that we now have the possibility of quantum interference effects, like constructive and destructive interference and the AB-effect, where the magnetic flux enclosed in the ring will induce phase shifts in the two arms.

Possible effects like local scattering, Zeeman effect, SOI, etc. would all have to be considered only in the two arms and not in the beamsplitters [1]. Thus, the induced phase shifts will, in general, depend on the length of the two arms, so that we denote them by 1 for the upper arm and 2 for the lower one, e.g. θ_1 and θ_2 are the AB-phases, for the upper and lower arm, respectively. The AB phase shifts will always satisfy $\theta_1 + \theta_2 = 2\pi\Phi/\Phi_0$, where Φ is the enclosed magnetic flux and $\Phi_0 = h/e$ is the flux quantum. It should be mentioned that the final result should depend on Φ, not θ_1 or θ_2 alone, as Φ has physical meaning while the individual phases do not.

Note that, even though the beamsplitters are completely transparent, we can still have reflection on the "ring". This is because the waves have the possibility of travelling all the way around the ring and then exiting the same way as they entered, thus effectively be reflected even though direct reflection on the beamsplitter is not present.

4.2.1 Symmetric injection

In this section, we will find expressions for the transmission and reflection coefficients for the N-region. The derivation will, for completeness, be done for both solutions of a and b ($\pm$), even though we will choose the positive solution in the end.

We start out by finding relations for the two symmetric beamsplitters, or junctions. For the right junction we have

$$\alpha_2' = -(a+b)\alpha_2 + \sqrt{\epsilon}\beta_2 + \sqrt{\epsilon}\gamma_2, \tag{4.32}$$
$$\beta_2' = \sqrt{\epsilon}\alpha_2 + a\beta_2 + b\gamma_2, \tag{4.33}$$
$$\gamma_2' = \sqrt{\epsilon}\alpha_2 + b\beta_2 + a\gamma_2. \tag{4.34}$$

[1] This thesis will not consider these spin-dependent effects.

Solving this for γ_2' and γ_2 expressed with β_2' and β_2 gives

$$\begin{pmatrix}\gamma_2'\\ \gamma_2\end{pmatrix} = \hat{t}_j \begin{pmatrix}\beta_2\\ \beta_2'\end{pmatrix} + \hat{t}_\alpha \alpha_2. \tag{4.35}$$

Here,

$$\hat{t}_j = \frac{1}{b}\begin{pmatrix} b^2-a^2 & a\\ -a & 1\end{pmatrix} = \frac{1}{b}\begin{pmatrix}\sqrt{1-2\epsilon} & a\\ -a & 1\end{pmatrix} = \frac{1}{b}\hat{l}_j, \tag{4.36}$$

where $\hat{l}_j$ will be useful later, and

$$\hat{t}_\alpha = \frac{\sqrt{\epsilon}}{b}\begin{pmatrix} b-a\\ -1\end{pmatrix} = \frac{\sqrt{\epsilon}}{b}\begin{pmatrix}\pm 1\\ -1\end{pmatrix}. \tag{4.37}$$

We emphasize that $\hat{t}_j$ is a 2×2-matrix, while $\hat{t}_\alpha$ is a 2×1-vector. The left junction gives

$$\alpha_1' = -(a+b)\alpha_1 + \sqrt{\epsilon}\beta_1 + \sqrt{\epsilon}\gamma_1, \tag{4.38}$$
$$\beta_1' = \sqrt{\epsilon}\alpha_1 + a\beta_1 + b\gamma_1, \tag{4.39}$$
$$\gamma_1' = \sqrt{\epsilon}\alpha_1 + b\beta_1 + a\gamma_1, \tag{4.40}$$

which again gives

$$\begin{pmatrix}\beta_1'\\ \beta_1\end{pmatrix} = \hat{t}_j \begin{pmatrix}\gamma_1\\ \gamma_1'\end{pmatrix} + \hat{t}_\alpha \alpha_1. \tag{4.41}$$

These equations symbolise the amplitudes that are transmitted from one arm into the other, taking into account that they can also be supplied by the leads.

If we were to introduce spin and assume no spin-mixing or spin effects in the beamsplitters, all elements of the scattering matrices become diagonal two-dimensional matrices (with the old element now on the diagonal), $a \to \begin{pmatrix} a & 0\\ 0 & a\end{pmatrix}$ [74].

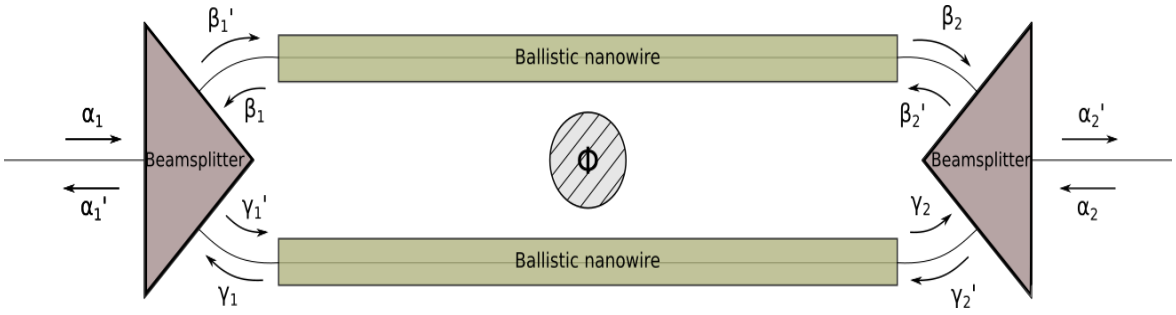

Figure 4.5: Illustration of two paths across the N-region, enclosing a magnetic flux Φ. Incoming (unprimed) and outgoing (primed) waves indicated.

With (4.32), (4.33) and (4.38), (4.39), we can find expressions for α_1' as a function of $\alpha_1, \beta_1, \beta_1'$ and α_2' as functions of and $\alpha_2, \beta_2, \beta_2'$, respectively. However, we want to express α_1' and α_2' as functions of α_1 and α_2 only. The next step is therefore to connect the two sides of the N-region and use this to connect the waves all the way through the two arms

in a concise way. With these comments in mind, we set up relations for the amplitudes as seen in Figure 4.5 in the upper and lower arms. For the upper arm, we have

$$\begin{pmatrix}\beta_2\\ \beta_2'\end{pmatrix} = e^{-i\theta_1}\hat{t}_1 \begin{pmatrix}\beta_1'\\ \beta_1\end{pmatrix}, \tag{4.42}$$

going from left to right in a clockwise sense. In the lower arm we have

$$\begin{pmatrix}\gamma_1\\ \gamma_1'\end{pmatrix} = e^{-i\theta_2}\hat{t}_2' \begin{pmatrix}\gamma_2'\\ \gamma_2\end{pmatrix}, \tag{4.43}$$

going from right to left in a clockwise sense. Note that the AB-phases are both taken in a positive counterclockwise sense and that $\hat{t}_1$ and $\hat{t}_2'$ are numbered differently (1,2) The transfer matrices are in general different, depending on which potentials are present in which arm and the lengths of the two arms.

Starting out with $\begin{pmatrix}\beta_1'\\ \beta_1\end{pmatrix}$, we can for example write

$$\begin{pmatrix}\beta_1'\\ \beta_1\end{pmatrix} = \hat{t}_j \begin{pmatrix}\gamma_1\\ \gamma_1'\end{pmatrix} + \hat{t}_\alpha \alpha_1 = \hat{t}_j \left(e^{-i\theta_2}\hat{t}_2' \begin{pmatrix}\gamma_2'\\ \gamma_2\end{pmatrix}\right) + \hat{t}_\alpha \alpha_1. \tag{4.44}$$

Here, we have first employed (4.41) and so (4.43). Following this procedure around the ring back to $\begin{pmatrix}\beta_1'\\ \beta_1\end{pmatrix}$, employing (4.35) and (4.42) at the necessary steps, we will in effect have followed the N-region in a clockwise sense. We end up with

$$\hat{\Pi}^* \begin{pmatrix}\beta_1'\\ \beta_1\end{pmatrix} = -\hat{t}_\alpha \alpha_1 - \hat{\Pi}_\alpha \alpha_2, \tag{4.45}$$

where

$$\hat{\Pi}^* = e^{-i(\theta_1+\theta_2)}\hat{t}_j\hat{t}_2'\hat{t}_j\hat{t}_1 - \hat{1} \tag{4.46}$$

and

$$\hat{\Pi}_\alpha = e^{-i\theta_2}\hat{t}_j\hat{t}_2'\hat{t}_\alpha. \tag{4.47}$$

* is used as a denotation, not as the complex conjugate operator. To find α_2', use (4.32) and (4.33) to get an expression with $(\beta_2, \beta_2')^T$,

$$\alpha_2' = -\left(a + b + \frac{\epsilon}{b}\right)\alpha_2 + \frac{\sqrt{\epsilon}}{b}(\pm 1, 1)\begin{pmatrix}\beta_2\\ \beta_2'\end{pmatrix}. \tag{4.48}$$

Insert (4.42) and $\hat{1} = \hat{\Pi}^{*-1}\hat{\Pi}^*$ to get

$$\alpha_2' = -\left(a + b + \frac{\epsilon}{b}\right)\alpha_2 + \frac{\sqrt{\epsilon}}{b}(\pm 1, 1)\left(e^{-i\theta_1}\hat{t}_1\hat{\Pi}^{*-1}\hat{\Pi}^* \begin{pmatrix}\beta_1'\\ \beta_1\end{pmatrix}\right). \tag{4.49}$$

Lastly, to have α_2' as a function of only α_1 and α_2, insert (4.45) and (4.7) to get

$$\alpha_2' = -\frac{\epsilon}{b^2}e^{-i\theta_1}h_1^*\alpha_1 - \left(a + b + \frac{\epsilon}{b} + \frac{\epsilon}{b^2}e^{-i(\theta_1+\theta_2)}h_2^*\right)\alpha_2, \tag{4.50}$$

where

$$h_1^* = (\pm 1, 1)\hat{t}_1\hat{\Pi}^{*-1}\begin{pmatrix}\pm 1\\ -1\end{pmatrix} \tag{4.51}$$

and

$$h_2^* = (\pm 1, 1)\hat{t}_1\hat{\Pi}^{*-1}\hat{t}_j\hat{t}'_2\begin{pmatrix}\pm 1\\ -1\end{pmatrix}. \tag{4.52}$$

If we take $\alpha_1 = 1$ and $\alpha_2 = 0$, will α'_2 be the same expression as in [61].

The same can be done for α'_1 and we end up with

$$\alpha'_1 = -\left(a + b + \frac{\epsilon}{b} + \frac{\epsilon}{b^2}m_1^*\right)\alpha_1 - \frac{\epsilon}{b^2}e^{-i\theta_2}m_2^*\alpha_2 \tag{4.53}$$

where

$$m_1^* = (1, \pm 1)\hat{\Pi}^{*-1}\begin{pmatrix}\pm 1\\ -1\end{pmatrix} \tag{4.54}$$

and

$$m_2^* = (1, \pm 1)\hat{\Pi}^{*-1}\hat{t}_j\hat{t}'_2\begin{pmatrix}\pm 1\\ -1\end{pmatrix}. \tag{4.55}$$

The forms of these coefficients are all correct, but they are not in the most convenient form. To simplify the expressions, we see first that $a + b + \epsilon/b = z$, where we defined $z = \pm 1$, and we write $\theta_1 + \theta_2 \equiv \theta_B = 2\pi\Phi/\Phi_0$. Furthermore, we note that $\hat{\Pi}^*$ is a 2×2-matrix, as a consequence of only one conduction channel and the one-dimensionality of our nanowire, so that we can write $\hat{\Pi}^{*-1}$ in a much more preferred way. We have

$$\hat{\Pi}^* = e^{-i\theta_B}\frac{1}{b^2}\hat{l}_j\hat{t}'_2\hat{l}_j\hat{t}_1 - \hat{1} = \frac{1}{b^2}\left(e^{-i\theta_B}\hat{l}_j\hat{t}'_2\hat{l}_j\hat{t}_1 - b^2\hat{1}\right) = \frac{1}{b^2}\hat{\Pi}, \tag{4.56}$$

so that we have

$$\hat{\Pi}^{*-1} = \frac{b^2}{\det\left(\hat{\Pi}\right)}\hat{M}, \quad \text{where} \quad \hat{M} = \begin{pmatrix}\Pi_{22} & -\Pi_{12}\\ -\Pi_{21} & \Pi_{11}\end{pmatrix}, \tag{4.57}$$

where Π_{ij}, $i, j = 1, 2$, are the elements $\hat{\Pi}$. We rewrite the amplitudes coming out on the left, α'_1, and on the right, α'_2, with new coefficients

$$\alpha'_1 = m_1\alpha_1 + m_2\alpha_2, \quad \alpha'_2 = h_1\alpha_1 + h_2\alpha_2. \tag{4.58}$$

These coefficients are expressed in a more convenient way for further use, so we list them here.

$$m_1 = -z - \frac{\epsilon}{\det\left(\hat{\Pi}\right)}\begin{pmatrix}1 & z\end{pmatrix}\hat{M}\begin{pmatrix}z\\ -1\end{pmatrix}, \tag{4.59}$$

$$m_2 = -\frac{\epsilon e^{-i(\theta_2)}}{\det\left(\hat{\Pi}\right)b}\begin{pmatrix}1 & z\end{pmatrix}\hat{M}\hat{l}_j\hat{t}'_2\begin{pmatrix}z\\ -1\end{pmatrix}, \tag{4.60}$$

$$h_1 = -\frac{\epsilon e^{-i(\theta_1)}}{\det\left(\hat{\Pi}\right)}\begin{pmatrix}z & 1\end{pmatrix}\hat{t}_1\hat{M}\begin{pmatrix}z\\ -1\end{pmatrix}, \tag{4.61}$$

and

$$h_2 = -z - \frac{\epsilon e^{-i\theta_B}}{\det\left(\hat{\Pi}\right)b}\begin{pmatrix}z & 1\end{pmatrix}\hat{t}_1\hat{M}\hat{l}_j\hat{t}'_2\begin{pmatrix}z\\ -1\end{pmatrix}. \tag{4.62}$$

Now, we want to have the transmission and reflection coefficients both when incoming from the left and when incoming from the right. We sum this up with the following,

$$\begin{aligned} r_{LL} =&\alpha_1'(\alpha_1 = 1, \alpha_2 = 0), \qquad t_{RL} = \alpha_2'(\alpha_1 = 1, \alpha_2 = 0), \\ r_{RR} =&\alpha_2'(\alpha_1 = 0, \alpha_2 = 1), \qquad t_{LR} = \alpha_1'(\alpha_1 = 0, \alpha_2 = 1), \end{aligned} \tag{4.63}$$

where r_{LL} and r_{RR} are the reflection coefficients for the ring at the left (L) and right(R) side, respectively, and t_{RL} and t_{LR} are the transmission coefficients for the ring from left to right (LR) and right to left (LR), respectively. If we return to our choice of sign as defined in (4.8), we sum all of this up with

$$\begin{pmatrix} \alpha_1' \\ \alpha_2' \end{pmatrix} = \hat{s} \begin{pmatrix} \alpha_1 \\ \alpha_2 \end{pmatrix}, \tag{4.64}$$

where

$$\begin{aligned} \hat{s} &= \begin{pmatrix} m_1 & m_2 \\ h_1 & h_2 \end{pmatrix} = \begin{pmatrix} r_{LL} & t_{LR} \\ t_{RL} & r_{RR} \end{pmatrix} \\ &= \begin{pmatrix} -1 - \frac{\epsilon}{\det(\hat{\Pi})} \begin{pmatrix} 1 & 1 \end{pmatrix} \hat{M} \begin{pmatrix} 1 \\ -1 \end{pmatrix} & -\frac{\epsilon e^{-i(\theta_2)}}{\det(\hat{\Pi}) b} \begin{pmatrix} 1 & 1 \end{pmatrix} \hat{M} \hat{l}_j \hat{t}_2' \begin{pmatrix} 1 \\ -1 \end{pmatrix} \\ -\frac{\epsilon e^{-i(\theta_1)}}{\det(\hat{\Pi})} \begin{pmatrix} 1 & 1 \end{pmatrix} \hat{t}_1 \hat{M} \begin{pmatrix} 1 \\ -1 \end{pmatrix} & -1 - \frac{\epsilon e^{-i\theta_B}}{\det(\hat{\Pi}) b} \begin{pmatrix} 1 & 1 \end{pmatrix} \hat{t}_1 \hat{M} \hat{l}_j \hat{t}_2' \begin{pmatrix} 1 \\ -1 \end{pmatrix} \end{pmatrix} \end{aligned} \tag{4.65}$$

As a final note, all of these coefficients are general for symmetric injection and our choice of $\hat{S}$. Possible effects like local scattering, Zeeman effect, SOI, etc. will all have to be considered only in the two arms, i.e. the effects are incorporated by the matrices $\hat{t}_1$ and $\hat{t}_2'$. Thus, specifying $\hat{t}_1$ and $\hat{t}_2'$ corresponds to defining the ingredients of our junction.

4.2.2 Asymmetric injection

This section will present the result of the asymmetric injection case. The derivation follows the same procedure as in Section 4.2.1. We start out by finding relations for the junctions, with the elements of (4.9). For the right junction, we have

$$\begin{pmatrix} \gamma_2' \\ \gamma_2 \end{pmatrix} = \hat{t}_{\alpha R} \alpha_2 + \hat{t}_{jR} \begin{pmatrix} \beta_2 \\ \beta_2' \end{pmatrix}, \tag{4.66}$$

where

$$\hat{t}_{\alpha R} = \frac{1}{e} \begin{pmatrix} ce - bf \\ -b \end{pmatrix} \quad \text{and} \quad \hat{t}_{jR} = \frac{1}{e} \begin{pmatrix} e^2 - df & f \\ -d & 1 \end{pmatrix}. \tag{4.67}$$

For the left junction, we have

$$\begin{pmatrix} \beta_1' \\ \beta_1 \end{pmatrix} = \hat{t}_{\alpha L} \alpha_1 + \hat{t}_{jL} \begin{pmatrix} \gamma_1 \\ \gamma_1' \end{pmatrix}, \tag{4.68}$$

where

$$\hat{t}_{\alpha L} = \frac{1}{e} \begin{pmatrix} be - cd \\ -c \end{pmatrix} \quad \text{and} \quad \hat{t}_{jL} = \frac{1}{e} \begin{pmatrix} e^2 - df & d \\ -f & 1 \end{pmatrix}. \tag{4.69}$$

The rest of the derivation is completely equivalent with the one above, where we find expressions for α_1' and α_2' as functions of α_1 and α_2. The difference between the asymmetric case and the symmetric case appears when finding these expressions for α_1' and α_2', and in the expressions for the junctions (4.66) and (4.68), since we use (4.9) instead of (4.2). The rest of the work consists of connecting the waves in a concise way with $\hat{t}_1$ and $\hat{t}_2'$, all the way around the ring. Replacing the elements of (4.9) with (4.22) and collecting all the terms of α_1 and α_2 give us

$$\alpha_1' = k_1\alpha_1 + k_2\alpha_2, \quad \alpha_2' = z_1\alpha_1 + z_2\alpha_2. \tag{4.70}$$

As done in (4.63), we can also here find the different coefficients. We have

$$r_{LL} = k_1 = -1 - \frac{\nu^2}{\det\left(\hat{\Pi}\right)} \begin{pmatrix} 1 & 1 \end{pmatrix} \hat{M} \begin{pmatrix} 1 \\ -1 \end{pmatrix}, \tag{4.71}$$

$$t_{LR} = k_2 = \frac{\nu^2 e^{-i(\theta_2)}}{\eta \det\left(\hat{\Pi}\right)} \begin{pmatrix} 1 & 1 \end{pmatrix} \hat{M}\hat{l}_{jL}\hat{t}_2' \begin{pmatrix} 1 \\ -1 \end{pmatrix}, \tag{4.72}$$

$$t_{RL} = z_1 = -\frac{\nu^2 e^{-i(\theta_1)}}{\det\left(\hat{\Pi}\right)} \begin{pmatrix} 1 & 1 \end{pmatrix} \hat{t}_1\hat{M} \begin{pmatrix} 1 \\ -1 \end{pmatrix}, \tag{4.73}$$

and

$$r_{RR} = z_2 = -1 + \frac{\nu^2 e^{-i(\theta_1+\theta_2)}}{\eta \det\left(\hat{\Pi}\right)} \begin{pmatrix} 1 & 1 \end{pmatrix} \hat{t}_1\hat{M}\hat{l}_{jL}\hat{t}_2' \begin{pmatrix} 1 \\ -1 \end{pmatrix}. \tag{4.74}$$

The matrices are given by

$$\hat{\Pi} = e^{-i(\theta_1+\theta_2)}\hat{l}_{jL}\hat{t}_2'\hat{l}_{jR}\hat{t}_1 - \beta^2\eta^2\hat{1} = \begin{pmatrix} \Pi_{11} & \Pi_{12} \\ \Pi_{21} & \Pi_{22} \end{pmatrix} \quad \Longrightarrow \quad \hat{M} = \begin{pmatrix} \Pi_{22} & -\Pi_{12} \\ -\Pi_{21} & \Pi_{11} \end{pmatrix}, \tag{4.75}$$

and

$$\hat{l}_{jL} = \begin{pmatrix} -a & \eta - a \\ -\xi & 1 \end{pmatrix}, \quad \hat{l}_{jR} = \begin{pmatrix} -a & \xi \\ a - \eta & 1 \end{pmatrix}. \tag{4.76}$$

Remember from the discussion on sign in Section 4.1.2 that $a = -\sqrt{1-2\epsilon}$. We can sum this up in a matrix form,

$$\begin{aligned} \hat{s}_a &= \begin{pmatrix} r_{LL} & t_{LR} \\ t_{RL} & r_{RR} \end{pmatrix} \\ &= \begin{pmatrix} -1 - \frac{\nu^2}{\det\left(\hat{\Pi}\right)} \begin{pmatrix} 1 & 1 \end{pmatrix} \hat{M} \begin{pmatrix} 1 \\ -1 \end{pmatrix} & \frac{\nu^2 e^{-i(\theta_2)}}{\eta \det\left(\hat{\Pi}\right)} \begin{pmatrix} 1 & 1 \end{pmatrix} \hat{M}\hat{l}_{jL}\hat{t}_2' \begin{pmatrix} 1 \\ -1 \end{pmatrix} \\ -\frac{\nu^2 e^{-i(\theta_1)}}{\det\left(\hat{\Pi}\right)} \begin{pmatrix} 1 & 1 \end{pmatrix} \hat{t}_1\hat{M} \begin{pmatrix} 1 \\ -1 \end{pmatrix} & -1 + \frac{\nu^2 e^{-i(\theta_1+\theta_2)}}{\eta \det\left(\hat{\Pi}\right)} \begin{pmatrix} 1 & 1 \end{pmatrix} \hat{t}_1\hat{M}\hat{l}_{jL}\hat{t}_2' \begin{pmatrix} 1 \\ -1 \end{pmatrix} \end{pmatrix} \end{aligned} \tag{4.77}$$

This reduces to (4.65) for $\beta = 1$, since

$$\lim_{\beta\to 1} \frac{\nu^2}{\eta} = -1(1 - \sqrt{1-2\epsilon}) = -\frac{\epsilon}{b},$$

and

$$\lim_{\beta\to 1} \nu^2 = \epsilon.$$

4.3 Specific case for transmission and reflection

This section will present explicit expressions for the transmission and reflection coefficients for one specific case of NW's and for two values of the coupling parameter ϵ. We will consider ballistic NW's in the presence of a magnetic field perpendicular to the SNS-junction, where we do not allow the magnetic field to be present in the NW's. This means that we only have to contend with two kinds of phase shifts in the wavefunctions. First, the dynamical phase shift χ for upper and lower arm, due to the energy, and second, the AB-phase shifts, as discussed above. The AB-effect is, of course, present even though we exclude magnetic fields from the actual NW's. Thus, χ_1, θ_1 and χ_2, θ_2 are the phases for the upper and lower arm, respectively. Notice how the AB-effect is already accounted for in our model, e.g. in (4.42). A possible asymmetry in the arm lengths will be described by a parameter λ, see Figure 4.3. We set the length of the upper arm to be $L_1 = L$ and the length of the lower arm to be $L_2 = \lambda L$. $\lambda > 1$ means the lower arm is longer than the upper arm, whereas $\lambda < 1$ means the upper arm is longer than the lower and $\lambda = 1$ means the arms are of equal length.

Since the absence of magnetic fields in the NW's implies that time-reversal symmetry is protected, we have $\hat{t} = \hat{t}'$. Ballistic NW's mean that $T_s = 1$, where T_s is the transmission probability in the NW, which implies $R_s = 1 - T_s = 0$ and therefore $r_1 = r_2 = r_1' = r_2' = 0$ in the arms. We are left with $t = e^{i\chi}$. The transfer matrix (4.25) is therefore, from (4.25), expressed as [72]

$$\hat{t}_k = \begin{pmatrix} e^{i\chi_k} & 0 \\ 0 & e^{-i\chi_k} \end{pmatrix}, \tag{4.78}$$

where $k = 1, 2$ for upper (1) and lower (2) arm. χ_1 represents the dynamical phase acquired in the upper arm of length L_1 and χ_2 represents the dynamical phase acquired in the lower arm of length L_2.

Before we present the coefficients, it is worth discussing how electrons and holes acquire different phases. We start by discussing the dynamical phase. An electron travelling from the left to the right (from $x = 0$ to $x = L$, in the positive direction) will acquire the phase shift $(+k_e)(+L)$. When it travels from the right to the left ($x = L$ to $x = 0$, in the negative direction), it will acquire $(-k_e)(-L) = +k_eL$. This is a general property of the dynamical phase shift: when an electron takes a time-reversed path, it acquires the same dynamical phase as before [35]. The effect of this realisation is that the transmission elements will be the same in the scattering matrix, but opposite in the transfer matrix, as we see in (4.78). The same is true for holes, however, the wave number for holes has the opposite sign from that of electrons and holes will therefore acquire the opposite phase shifts compared to electrons. Let us call the acquired dynamical phase shift for electrons for $\chi_e = k_eL$. We remember that μ is much larger than the electron energy E and write $k_e = \sqrt{\frac{2m}{\hbar^2}(\mu + E)} \approx k_F$, where $k_F = \sqrt{\frac{2\mu m}{\hbar^2}}$. This approximation makes finding the Andreev levels much more feasible. For holes we have $\chi_h = -k_hL$, where we again approximate to $k_h = \sqrt{\frac{2m}{\hbar^2}(\mu - E)} \approx k_F$. With all of this in mind, we conclude that $\chi_e = \chi$ and $\chi_h = -\chi$, where $\chi = k_FL$. Lastly, the AB-phase is $\exp(-iq\Phi/\hbar)$ [64].

For electrons, this will be $2\pi\Phi/\Phi_0$. However, a hole has opposite charge compared to an electron, and the phase acquired by holes is therefore opposite from that acquired by electrons. Thus, we have $\theta_e = \theta$ and $\theta_h = -\theta$. All of this is really only a consequence of the relation between the scattering matrices for electrons and holes [67],

$$\hat{S}_e(E) = \hat{g}^\dagger \hat{S}_h^*(-E)\hat{g},$$

where $\hat{g} = -i\sigma_y$. Since we have assumed no energy dependence and no fields, and thereby do not care about spin, this equation will reduce to $\hat{S}_e = \hat{S}_h^*$, i.e. the coefficients for the holes are the complex conjugate of the coefficients for electrons.

4.3.1 Ballistic nanowires, $\epsilon = \frac{1}{2}$

Complete transmission in the beamsplitters corresponds to $\epsilon = \frac{1}{2}$. The coefficients will, in general, depend on χ, λ, β and θ_B, where $\theta_B = \theta_1 + \theta_2 = 2\pi\Phi/\Phi_0$. For electrons, we have transmission from left to right,

$$t_{RL} = \frac{2ie^{i\theta_2}(\beta^2+1)}{\Lambda_{1/2}}\left(\sin(\chi) + e^{-i\theta_B}\beta^2\sin(\lambda\chi)\right), \tag{4.79}$$

transmission from the right to the left,

$$t_{LR} = \frac{2ie^{i\theta_1}(\beta^2+1)}{\Lambda_{1/2}}\left(e^{-i\theta_B}\sin(\chi) + \beta^2\sin(\lambda\chi)\right), \tag{4.80}$$

and reflection

$$r_{LL} = r_{RR} = \frac{-4\beta^2}{\Lambda_{1/2}}\sin\left(\frac{\chi(\lambda-1)}{2} - \frac{\theta_B}{2}\right)\sin\left(\frac{\chi(\lambda-1)}{2} + \frac{\theta_B}{2}\right). \tag{4.81}$$

The denominator is

$$\Lambda_{1/2} = \beta^4 e^{i\chi(\lambda-1)} + e^{-i\chi(\lambda-1)} - (\beta^2+1)^2 e^{-i\chi(\lambda+1)} + 2\beta^2\cos(\theta_B). \tag{4.82}$$

The coefficients for holes are, if $t_{RL} = t_{eRL}$ etc.,

$$\begin{aligned} t_{hRL} &= t_{eRL}^* \quad t_{hLR} = t_{eLR}^*, \\ r_{hLL} &= r_{eLL}^*, \quad r_{hRR} = r_{eRR}^*. \end{aligned} \tag{4.83}$$

In Figure 4.6 and 4.7, we have plotted the transmission probability T (equal in both directions) and the reflection probability R, respectively, in the N-region for $\chi = 100$. We observe that $T + R = 1$, as it should. It should be noted that we have only plotted for $\chi = 100$. However, both T and R have very strong χ-dependencies.

A closer look at Figure 4.6 reveals that for very low β, the transmission probability will be close to 1 for all lengths of the arms. This is due to the fact that when beta is low, the system will work as if it had mainly one arm and we have minimum reflection from a complete turn around the ring. Also, since $\epsilon = 1/2$, no direct reflection at the beamsplitters is possible. This behaviour is the same for very large β. There are, however, still interference effects, but they are very small. When $\beta \to 1$, we observe that $\lambda = 1$ has overall the strongest interference effects. When both arms are equally preferable, arms of the same length will experience the most complete interference effects.

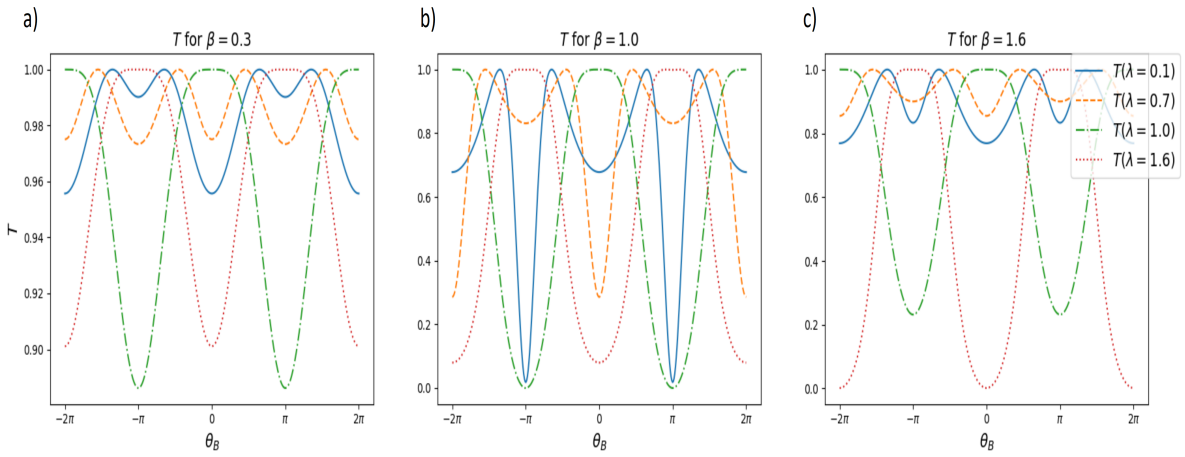

Figure 4.6: Transmission probability for $\epsilon = 1/2$ for a) $\beta = 0.3$, b) $\beta = 1$ and c) $\beta = 1.6$ for $\chi = 100$. Solid line is $\lambda = 0.1$, dashed is $\lambda = 0.7$, dashed-dotted is $\lambda = 1$ and dotted is $\lambda = 1.6$.

For example, the arms can now experience complete destructive interference, making the junction thoroughly opaque. For β close to one, large variations with strong χ-dependencies are observed, greatly influencing which arm lengths experience the most complete interference effects. Observe also how T always is 2π-periodic in θ_B.

We end this section by discussing the different effects of interference. As we can see from Figure 4.6, constructive and destructive interference seems to appear around $\theta_B = [0, \pm\pi]$ (and the same behaviour for $\theta_B = [\pm\pi, \pm 2\pi]$). At $\theta_B = 0$, the only effect will be dynamical interference, which will depend strongly on χ. Incomplete interference effects will therefore induce dips in T, complete constructive interference will have no dip, and thus the junction is completely transparent, and complete destructive interference will make the junction completely opaque. At $\theta = \pm\pi$, the AB-interference is at its, in general, strongest and can therefore induce the same type of effects for different λ's, β's and χ's. The interplay between the dynamical interference and the AB-interference modulates this two extremes, which compete for prominence. This means that depending on their respective interference strengths, they can both partially or completely negate the effects of each other. Because of time limitations, we will not investigate this further.

4.3.2 Ballistic nanowires, $\epsilon = \frac{1}{3}$

Partial transmission and reflection on the beamsplitters is exemplified with $\epsilon = \frac{1}{3}$. For electrons, we have transmission from left to right,

$$t_{RL} = \frac{4ie^{i\theta_2}(\beta^2+1)}{\Lambda_{1/3}}\left(\sin(\chi) + e^{-i\theta_B}\beta^2\sin(\lambda\chi)\right), \tag{4.84}$$

transmission from the right to the left,

$$t_{LR} = \frac{4ie^{i\theta_1}(\beta^2+1)}{\Lambda_{1/3}}\left(e^{-i\theta_B}\sin(\chi) + \beta^2\sin(\lambda\chi)\right), \tag{4.85}$$

and reflection

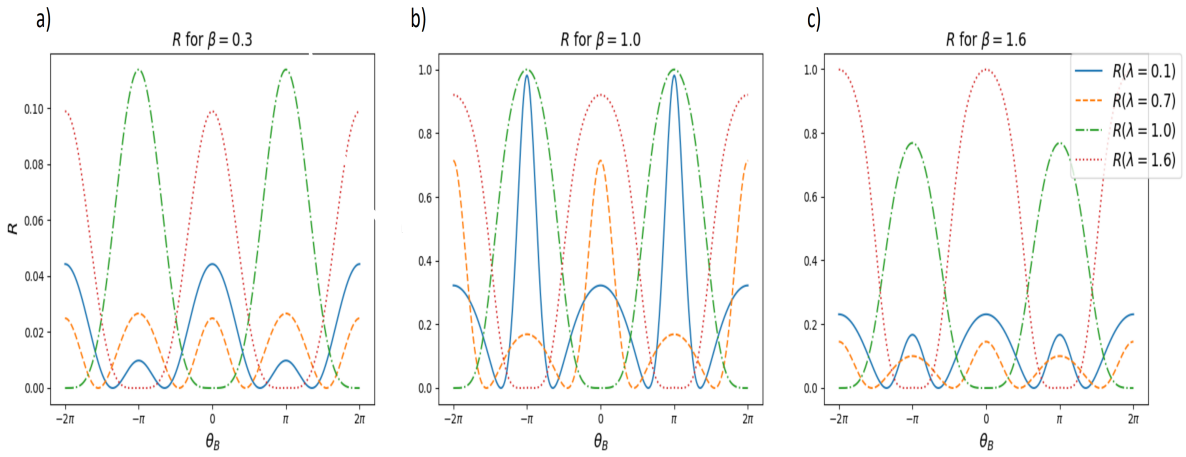

Figure 4.7: Reflection probability for $\epsilon = 1/2$ for a) $\beta = 0.3$, b) $\beta = 1$ and c) $\beta = 1.6$ for $\chi = 100$. Solid line is $\lambda = 0.1$, dashed is $\lambda = 0.7$, dashed-dotted is $\lambda = 1$ and dotted is $\lambda = 1.6$.

$$r_{LL} = r_{RR} = \frac{-2}{\Lambda_{1/3}}\big((\sqrt{3}\beta^4 - 4\beta^2 + \sqrt{3})\cos(\chi(\lambda-1)) - \sqrt{3}(\beta^2+1)^2\cos(\chi(\lambda+1)) + 2\beta^2(2+\sqrt{3})\cos(\theta_B)\big). \tag{4.86}$$

The denominator is

$$\Lambda_{1/3} = (\sqrt{3}\beta^2 - 1)^2 e^{i\chi(\lambda-1)} + (\beta^2 - \sqrt{3})^2 e^{-i\chi(\lambda-1)} + 4\beta^2(2+\sqrt{3})\cos(\theta_B) - (\beta^2+1)^2 e^{i\chi(\lambda+1)} - 3(\beta^2+1)^2 e^{-i\chi(\lambda+1)}. \tag{4.87}$$

In Figure 4.8 and 4.9 we have plotted the transmission probability T (equal in both directions) and the reflection probability R, respectively, in the N-region for $\chi = 100$. We observe that $T+R = 1$, as it should. As before, both T and R have strong χ-dependencies.

Figure 4.8 seems to indicate that the partial reflection and transmission at the beamsplitters have drastically changed the transmission probability compared to complete transmission at the beamsplitters. For example, when β is very small (or very large), we no longer have $T \sim 1$, since direct reflection at the beamsplitters contribute to the total reflection in the junction. However, interference effects are not as prominent and complete for $\beta << 1$ as for β closer to one, since we still mainly only have one arm. In general, there seems to be a trend that the reflection from the beamsplitters make the areas of most interference to be smaller (e.g. steeper dips) or larger (e.g. destructive interference over a larger interval of θ_B). Also, as for $\epsilon = 1/2$, there is a strong dependence on χ and we observe the 2π-periodicity in θ_B.

4.4 Andreev levels, supercurrents and critical currents

Now that we have deduced the transmission and reflection coefficient, we can start to find the Andreev levels $E_n(\phi)$ and from there, the supercurrent $I_S(\phi)$. From the supercurrent,

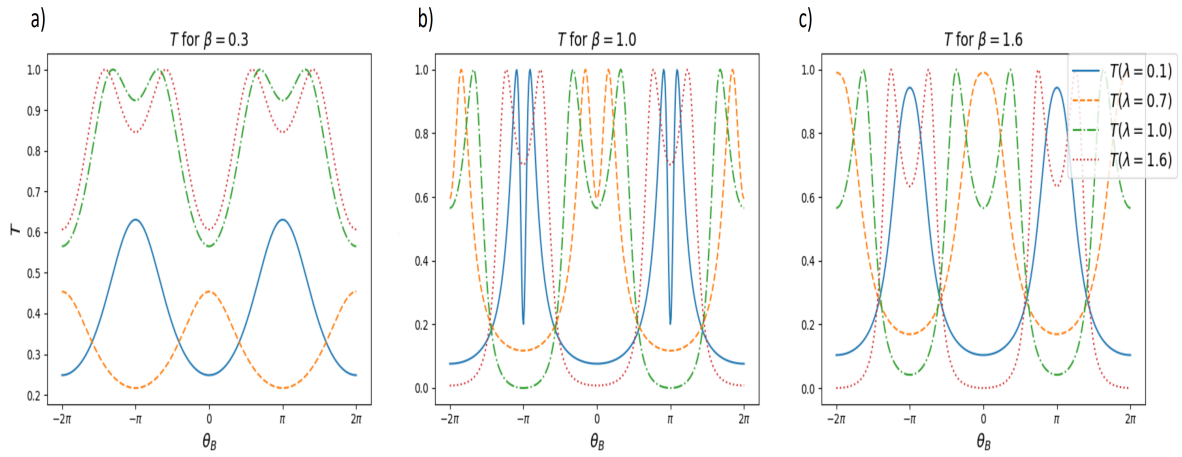

Figure 4.8: Transmission probability for $\epsilon = 1/3$ for a) $\beta = 0.3$, b) $\beta = 1$ and c) $\beta = 1.6$ for $\chi = 100$. Solid line is $\lambda = 0.1$, dashed is $\lambda = 0.7$, dashed-dotted is $\lambda = 1$ and dotted is $\lambda = 1.6$.

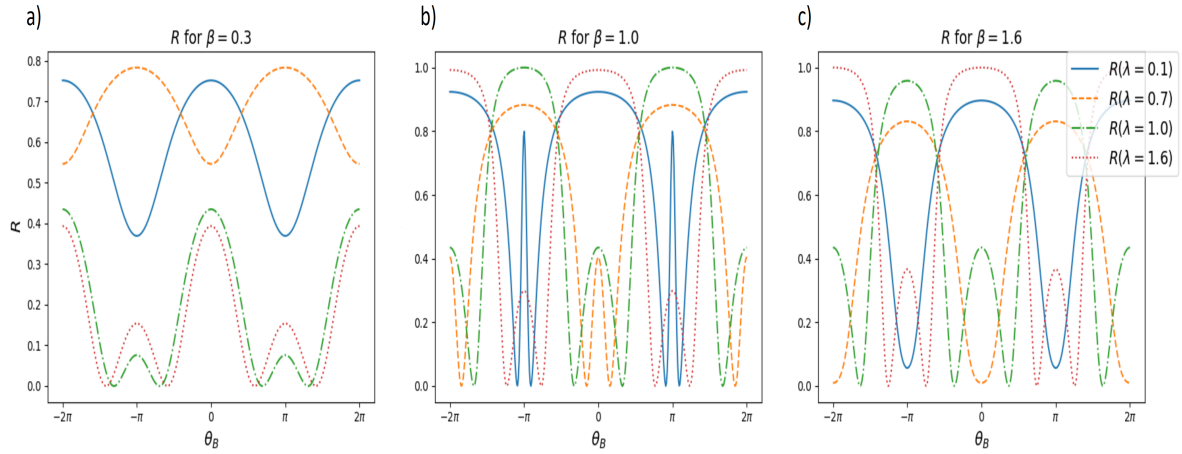

Figure 4.9: Reflection probability for $\epsilon = 1/3$ for a) $\beta = 0.3$, b) $\beta = 1$ and c) $\beta = 1.6$ for $\chi = 100$. Solid line is $\lambda = 0.1$, dashed is $\lambda = 0.7$, dashed-dotted is $\lambda = 1$ and dotted is $\lambda = 1.6$.

we find the critical current as a function of the magnetic flux, $I_C(\theta_B)$. If we recall Chapter 1, the supercurrent experienced asymmetries upon inversion of the perpendicular field, i.e. the flux. We will investigate the critical current with our model to discover whether the ingredients presented so far are enough to reproduce these asymmetries.

Section 4.4.1 will present the setup of the problem and a solution method to find an equation for the Andreev levels. Note that, since we have suppressed the spin indices, all energy levels will have a two-fold degeneracy, as we experienced in Section 3.2. Section 4.4.2 will present the results for the Andreev levels and the resulting supercurrent for several different magnetic fluxes, as well as the critical current as a function of the flux.

4.4.1 Solution for Andreev levels

We can express the wavefunction inside the junction for four different situations: incoming (I) or outgoing (U) from the ring, on either the left or the right side of the ring in the N-region. If we write $\boldsymbol{\alpha} = (\alpha_e, \alpha_h)^T$ as the wavevector with electron and hole components, we can correspondingly write $\boldsymbol{\alpha}_{UR}$, $\boldsymbol{\alpha}_{UL}$, $\boldsymbol{\alpha}_{IR}$ and $\boldsymbol{\alpha}_{IL}$ for waves outgoing on the right side, outgoing on the left side, incoming on the right side and incoming on the left side, respectively, as shown in Figure 4.10. With this, we write the wavevectors in the N-region as

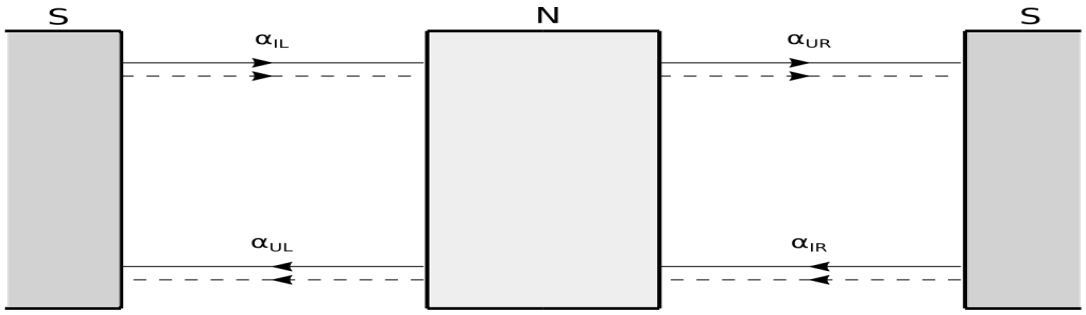

Figure 4.10: Conceptual illustration of SNS-junction with wavevectors on the right and left sides. Scale of arms outside the ring (represented by a square in the middle) is heavily oversized. Solid lines are electrons, dashed lines are holes.

$$\boldsymbol{\alpha}_{UR} = \hat{t}_{RL}\boldsymbol{\alpha}_{IL} + \hat{r}_{RR}\boldsymbol{\alpha}_{IR}, \tag{4.88}$$

and

$$\boldsymbol{\alpha}_{UL} = \hat{t}_{LR}\boldsymbol{\alpha}_{IR} + \hat{r}_{LL}\boldsymbol{\alpha}_{IL}, \tag{4.89}$$

where

$$\hat{t}_{RL} = \begin{pmatrix} t_{eRL} & 0 \\ 0 & t_{hRL} \end{pmatrix}, \quad \hat{t}_{LR} = \begin{pmatrix} t_{eLR} & 0 \\ 0 & t_{hLR} \end{pmatrix}, \quad \hat{r}_{RR} = \begin{pmatrix} r_{eRR} & 0 \\ 0 & r_{hRR} \end{pmatrix}, \quad \hat{r}_{LL} = \begin{pmatrix} r_{eLL} & 0 \\ 0 & r_{hLL} \end{pmatrix}. \tag{4.90}$$

t_{eLR} etc. are the transmission and reflection coefficients calculated earlier. If we assume that the beamsplitters are placed directly at the NS-interfaces, i.e. the two paths across the junction spans the entire N-region, the Andreev reflection can be written as

$$\boldsymbol{\alpha}_{IL} = \hat{A}_L\boldsymbol{\alpha}_{UL}, \quad \boldsymbol{\alpha}_{IR} = \hat{A}_R\boldsymbol{\alpha}_{UR}, . \tag{4.91}$$

Here

$$\hat{A}_L = e^{-i\arccos\left(\frac{E}{|\Delta|}\right)} \begin{pmatrix} 0 & e^{i\phi_L} \\ e^{-i\phi_L} & 0 \end{pmatrix}, \quad \hat{A}_R = e^{-i\arccos\left(\frac{E}{|\Delta|}\right)} \begin{pmatrix} 0 & e^{i\phi_R} \\ e^{-i\phi_R} & 0 \end{pmatrix}. \tag{4.92}$$

We can absorb the left- and right-components of $\boldsymbol{\alpha}$ into a common wavevector, by writing

$$\boldsymbol{\alpha}_U = \begin{pmatrix} \alpha_{eUR} \\ \alpha_{hUR} \\ \alpha_{eUL} \\ \alpha_{hUL} \end{pmatrix} = \hat{N} \begin{pmatrix} \alpha_{eIR} \\ \alpha_{hIR} \\ \alpha_{eIL} \\ \alpha_{hIL} \end{pmatrix} = \hat{N}\boldsymbol{\alpha}_I, \tag{4.93}$$

for the N-region and

$$\boldsymbol{\alpha}_I = \hat{A}\boldsymbol{\alpha}_R, \tag{4.94}$$

for the Andreev reflection. The matrices are

$$\hat{N} = \begin{pmatrix} \hat{r}_{RR} & \hat{t}_{RL} \\ \hat{t}_{LR} & \hat{r}_{LL} \end{pmatrix}, \quad \text{and} \quad \hat{A} = \begin{pmatrix} \hat{A}_R & 0 \\ 0 & \hat{A}_L \end{pmatrix}. \tag{4.95}$$

The effect of the N-region is illustrated in Figure 4.11 and the Andreev reflection is illustrated in Figure 4.12.

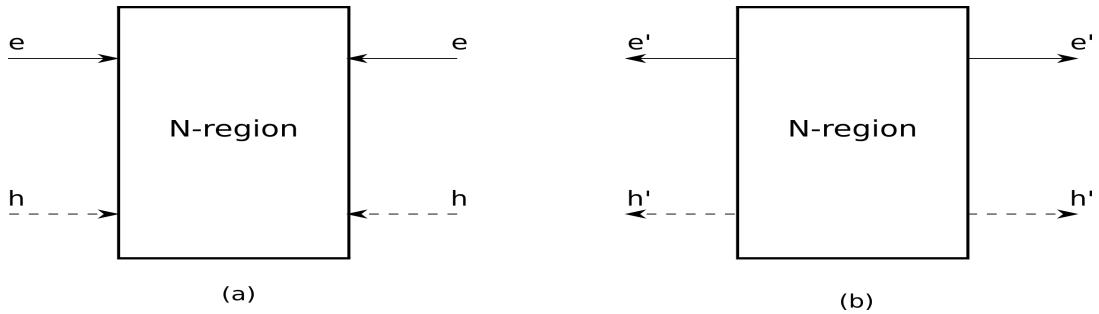

Figure 4.11: Illustration of the effect of the N-region, or how the incoming waves are related to the outgoing waves. (a) is the incoming situation, (b) is the outgoing situation.

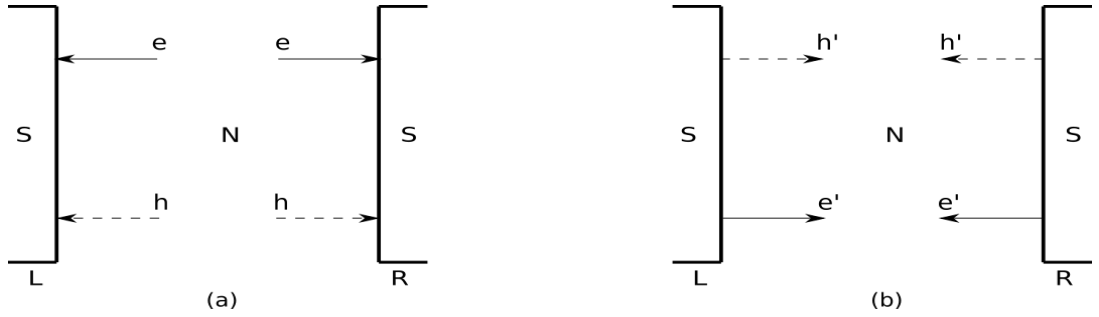

Figure 4.12: Illustration of the effect of the Andreev reflection at the NS-interfaces, or how the incoming waves are related to the outgoing waves. (a) is the incoming situation, (b) is the outgoing situation.

By insertion of (4.94) into (4.93), we get

$$\boldsymbol{\alpha}_U = \hat{N}\boldsymbol{\alpha}_I = \hat{N}\left(\hat{A}\boldsymbol{\alpha}_U\right) \implies \left(\hat{1} - \hat{N}\hat{A}\right)\boldsymbol{\alpha}_U = 0, \tag{4.96}$$

so that the localisation condition for the Andreev bound state becomes

$$\det\left(\hat{1} - \hat{N}\hat{A}\right) = 0. \tag{4.97}$$

(4.97) gives us

$$-u_1 e^{-i\phi}\alpha^2 - u_2 e^{i\phi}\alpha^2 - u_3\alpha^2 + u_4\alpha^4 = -1 \tag{4.98}$$

where

$$u_1 = t_{eLR}t_{hRL}, \tag{4.99}$$
$$u_2 = t_{eRL}t_{hLR}, \tag{4.100}$$
$$u_3 = r_{eLL}r_{hLL} + r_{eRR}r_{hRR}, \tag{4.101}$$
$$u_4 = (r_{eLL}r_{eRR} - t_{eLR}t_{eRL})(r_{hLL}r_{hRR} - t_{hLR}t_{hRL}). \tag{4.102}$$

By closer investigating, we see that u_4 is actually only the product of the determinants of the scattering matrix for electrons $\hat{S}$ and the scattering matrix for holes $\hat{S}_h$. Since scattering matrices are unitary, their determinant will just equal a phase term $e^{i\xi}$. However, as we have already discussed, $\hat{S}_h = S_e^*$ (in the absence of energy and spin dependence), and thus

$$\begin{aligned} u_4 &= (r_{eLL}r_{eRR} - t_{eLR}t_{eRL})(r_{hLL}r_{hRR} - t_{hLR}t_{hRL}) = \det\left(\hat{S}_e\right)\det\left(\hat{S}_h\right) \\ &= \det\left(\hat{S}_e\right)\det\left(\hat{S}_e^*\right) = e^{i\xi}e^{-i\xi} = 1. \end{aligned} \tag{4.103}$$

Solving (4.98) with this in mind produces

$$E = \pm|\Delta|\cos\left(\frac{1}{2}\arccos\left(\frac{u}{2}\right)\right), \tag{4.104}$$

where

$$u = u_1 e^{-i\phi} + u_2 e^{i\phi} + u_3. \tag{4.105}$$

Keep in mind that we here have spin degeneracy, thus actually four solutions.

4.4.2 Results and discussion

This section will present the the solutions of (4.104), as well as the supercurrent and the critical current, for different values of the magnetic flux. For each case ($\epsilon = 1/2$ and $\epsilon = 1/3$), we discuss the Andreev levels E, the resulting supercurrent I_S and the critical current I_C. The critical current is presented as a function of the magnetic flux, plotted for the two possible directions of the (perpendicular) magnetic field through the ring. I_{C+} is the critical current in the positive direction while I_{C-} is the critical current in the negative direction.

Before we proceed, we set $\theta_1 = \theta_2$. This is justified since it doesn't matter where we assume the phase shift to happen. The gauge-invariant, and thus observable, quantity of importance is the magnetic phase accumulated along the closed path, i.e. $\theta_B = \theta_1 + \theta_2 = 2\pi\Phi/\Phi_0$. Generally speaking, any periodic dependence on this quantity is called the Aharanov-Bohm effect.

Results for $\epsilon = \frac{1}{2}$

Figure 4.13 and Figure 4.14 present the Andreev levels and the supercurrent for $\lambda = 1$ and $\lambda = 1.7$, respectively, for complete transmission at the beamsplitters. We plotted for three values of magnetic field and three values of β.

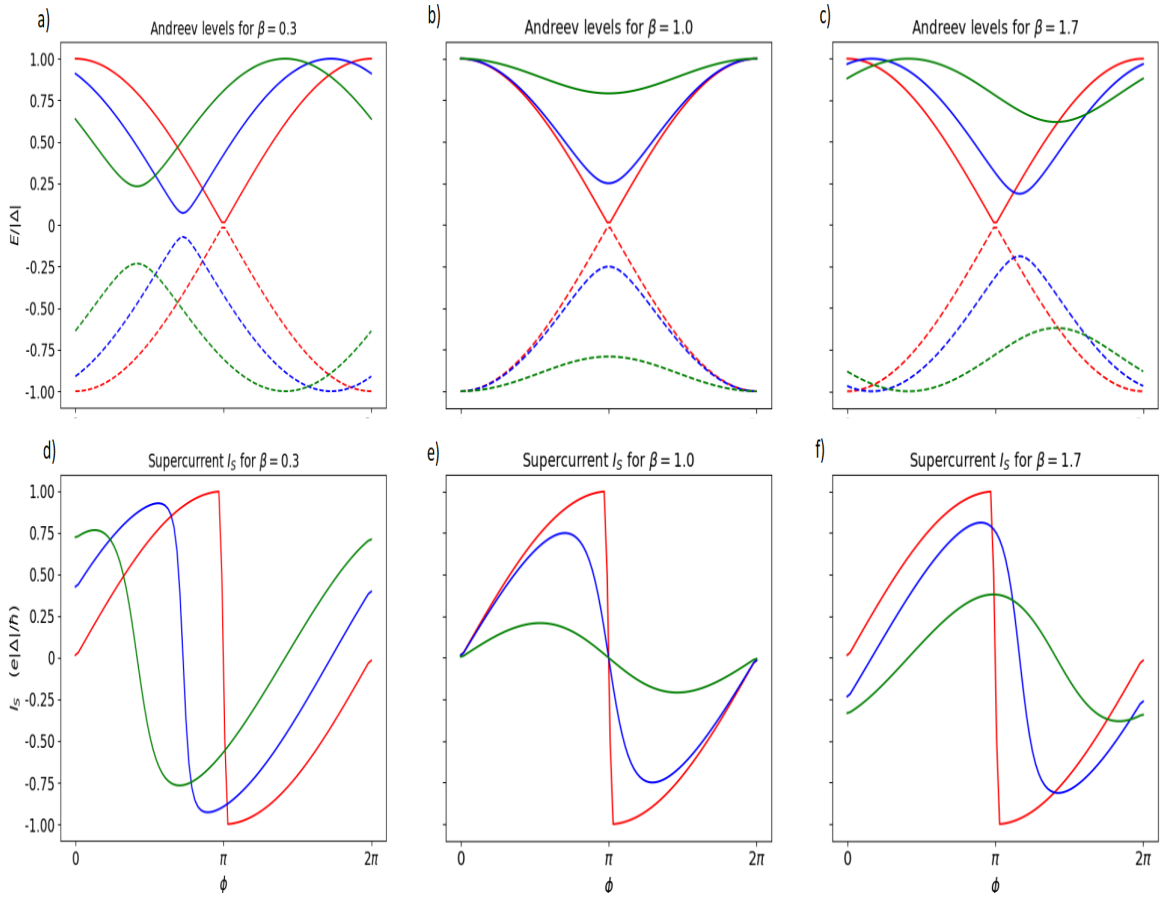

Figure 4.13: The figure shows the Andreev spectrum for a) $\beta = 0.3$, b) $\beta = 1$ and c) $\beta = 1.7$, and the supercurrent I_S for d) $\beta = 0.3$, e) $\beta = 1$ and f) $\beta = 1.7$ as a function of the phase difference ϕ. Plotted for $\theta_B = 0$ (red), $\theta_B = 1$ (blue) and $\theta_B = 2$ (green) with $\chi = 100$, $\lambda = 1$ and $\epsilon = 1/2$.

For $\lambda = 1$, in Figure 4.13, we see that when $\theta_B = 0$, I_S has a form equal that of the no fields-case for 1D NW's (1D-behaviour) in Chapter 3. This is explained by that we can interpret our system to be, in effect, as a 1D NW with a scatterer. Take $\beta = 1$ as an example: when there is no enclosed flux, the combined interference effects of electrons and holes cancel each other out out and we have a ballistic NW, exactly the same as we investigated in Section 3.2. Increasing θ_B will, in effect, decrease the transmission probability, as we now have an effective scatterer, and the supercurrent is reduced, as we see in Figure 4.13 e). The same is true for other β's, however, here the effects are not as clear because of the interplay between the dynamical interference and the AB-interference, as one of the arm is preferred over the over.

When $\lambda = 1.7$, we no longer have complete the 1D-behaviour, as the asymmetry in the arm lengths allows for incomplete interference effects, even for $\beta = 1$. Small β is close to the $\lambda = 1$-case as we still mainly have one arm. Dynamical interference effects will

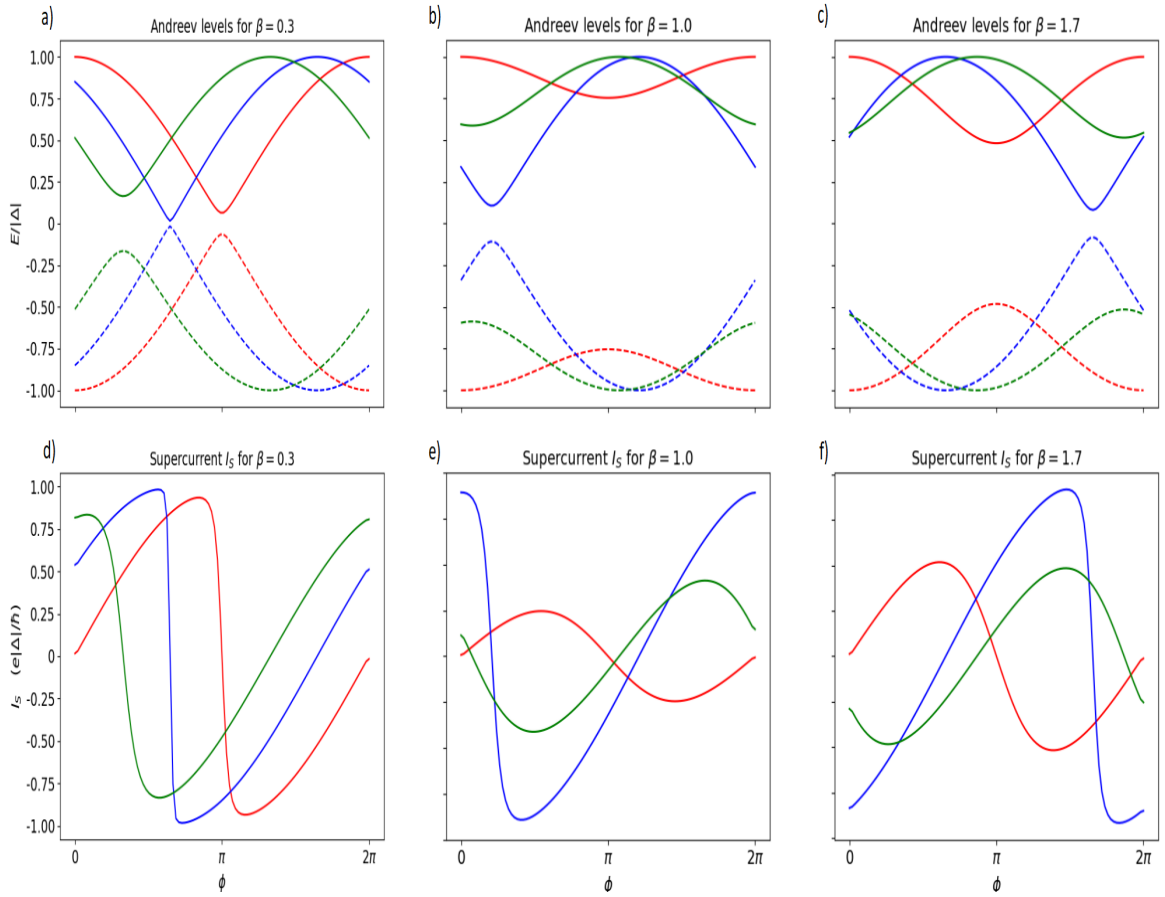

Figure 4.14: The figure shows the Andreev levels E for a) $\beta = 0.3$, b) $\beta = 1$ and c) $\beta = 1.7$, and the supercurrent I_S for d) $\beta = 0.3$, e) $\beta = 1$ and f) $\beta = 1.7$ as a function of the phase difference ϕ. Plotted for $\theta_B = 0$ (red), $\theta_B = 1$ (blue) and $\theta_B = 2$ (green) with $\chi = 100$, $\lambda = 1.7$ and $\epsilon = 1/2$.

now become more prominent, so we have a stronger χ-dependence here than for $\lambda = 1$. Again, time limitations limit our discussion on the χ-θ_B-interplay.

Figure 4.15 shows the critical current as a function of θ_B for different arm lengths and different probability injections. We see that, for symmetric arms, I_C will be a smooth curve, with destructive interference around $\theta_B = \pm\pi$. As expected, this is caused by the AB-effect. At symmetric injection, $I_C \sim \cos^2(\theta_B/2)$, which again is as expected. Changing β results in incomplete destructive interference. As we still have a strong dependence on χ, other values of β, λ and χ will induce sharper dips around $\theta_B = \pm\pi$ and $\theta_B = 0$, larger oscillations in value for I_C, different shapes, sometimes more or less complete interference effects, but they all have some things in common. $\lambda = 1$ preserves the smooth curve, they all have a 2π-periodic behaviour and $I_C(\theta_B) = I_C(-\theta_B)$, i.e. *the critical current is symmetric with respect to inversion of the perpendicular magnetic field.*

Results for $\epsilon = \frac{1}{3}$

Figure 4.16 and Figure 4.17 present the Andreev levels and the supercurrent for $\lambda = 1$ and $\lambda = 1.7$, respectively, for partial transmission and reflection at the beamsplitters. We plotted for three values of magnetic field and three values of β.

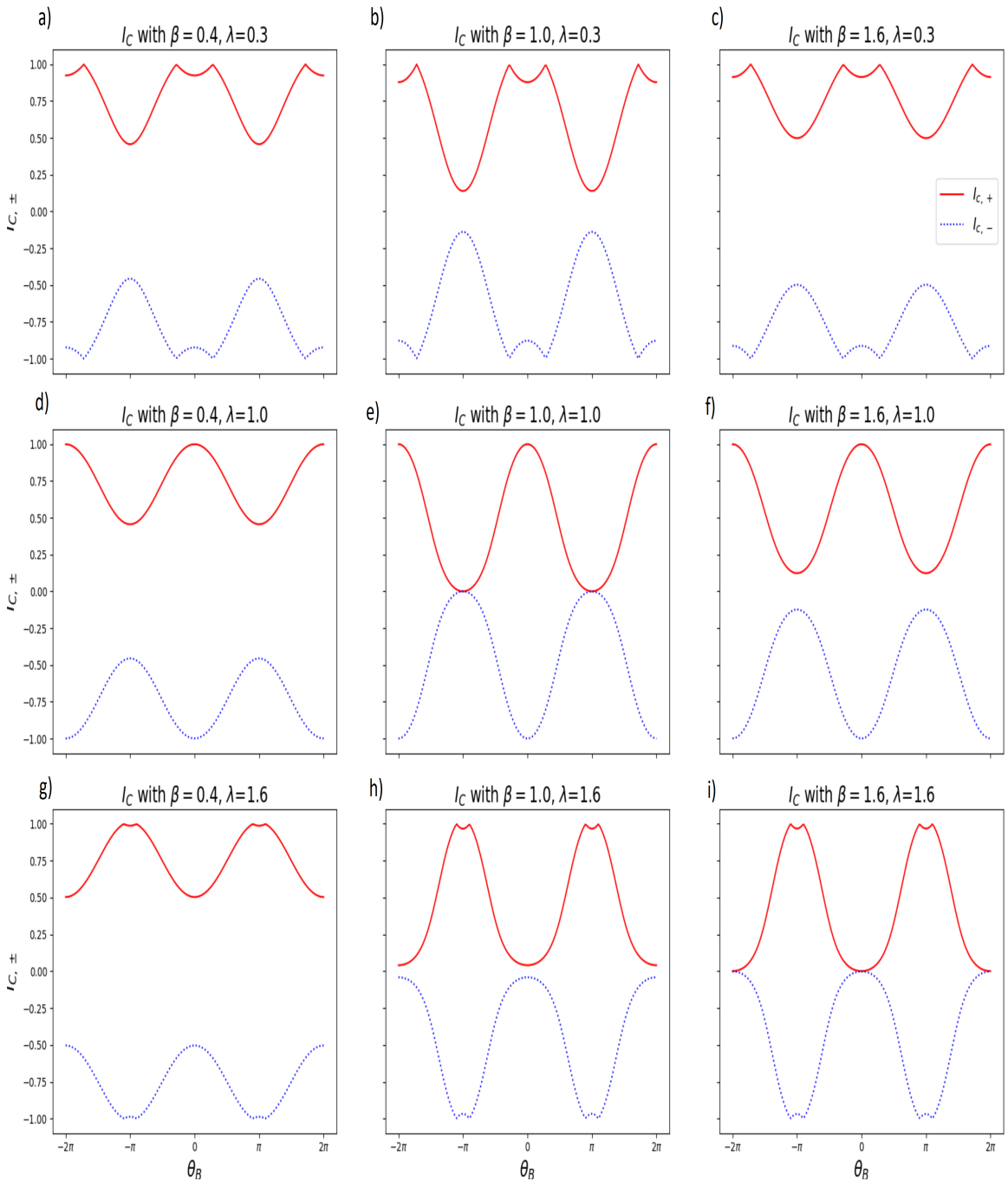

Figure 4.15: The figure shows the critical current for $\lambda = 0.3$ with a) $\beta = 0.4$, b) $\beta = 1$, c) $\beta = 1.6$, $\lambda = 1$ with d) $\beta = 0.4$, e) $\beta = 1$, f) $\beta = 1.6$ and $\lambda = 1.6$ with g) $\beta = 0.4$, h) $\beta = 1$, i) $\beta = 1.6$. Plotted with $\chi = 100$ and $\epsilon = 1/2$.

With partial transmission and reflection at the beamsplitters, we will never observe the ballistic behaviour from $\epsilon = 1/2$, even when $\lambda = 1$, $\beta = 1$. This mimics the description of our system as a NW with a scatterer. Now, we can never have zero reflection, and therefore we will never have a completely ballistic NW. The χ-dependence is even more prevalent now than for $\epsilon = 1/2$, and even more so for $\lambda = 1.7$.

For $\epsilon = 1/3$, I_C has changed shapes, e.g. $\lambda = 1$ are no longer are smooth, but allows for destructive interference at $\theta_B = 0$. We observe larger areas of complete destructive

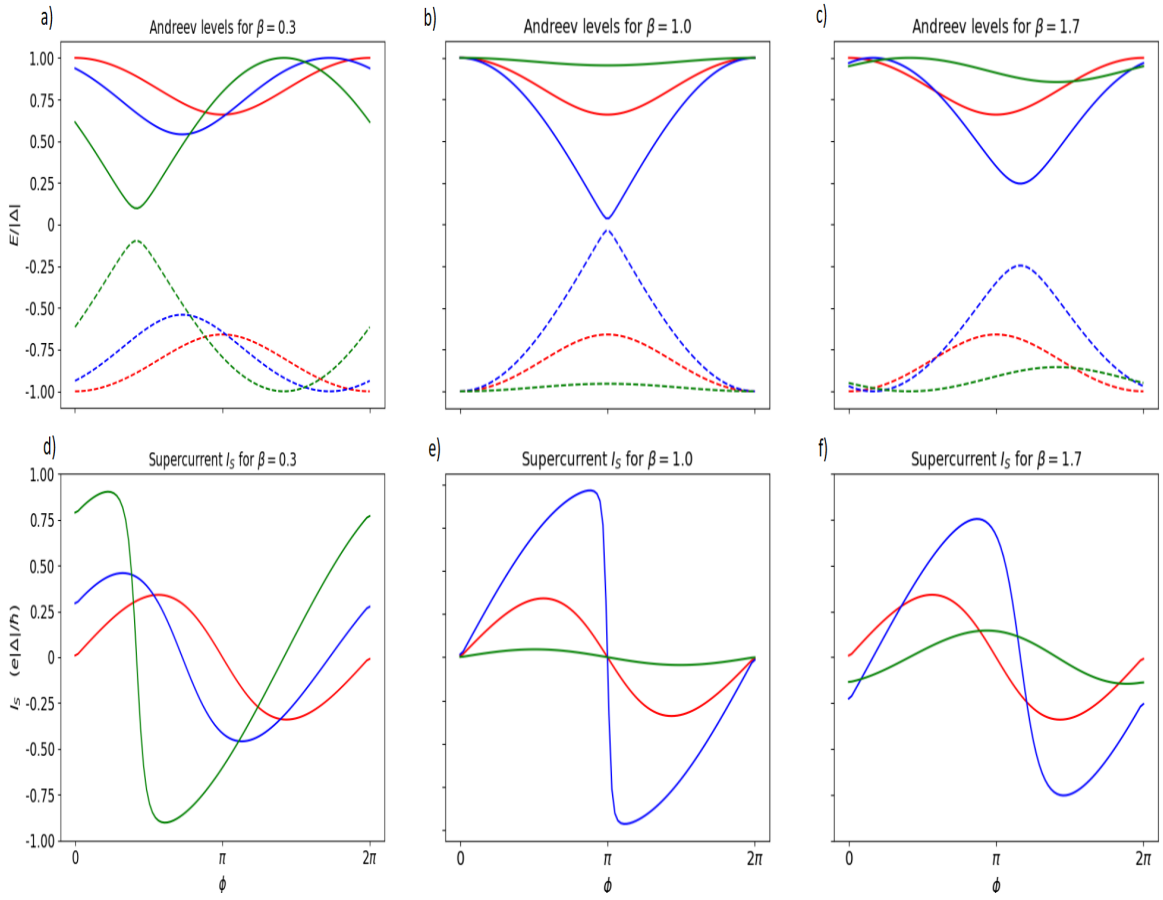

Figure 4.16: The figure shows the Andreev spectrum for a) $\beta = 0.3$, b) $\beta = 1$ and c) $\beta = 1.7$, and the supercurrent I_S for d) $\beta = 0.3$, e) $\beta = 1$ and f) $\beta = 1.7$ as a function of the phase difference ϕ. Plotted for $\theta_B = 0$ (red), $\theta_B = 1$ (blue) and $\theta_B = 2$ (green) with $\chi = 100$, $\lambda = 1$ and $\epsilon = 1/3$.

interference and thus, overall weaker supercurrents. However, as for $\epsilon = 1/2$, they all have a strong dependence on χ, 2π-periodic behaviour and $I_C(\theta_B) = I_C(-\theta_B)$, i.e. *the critical current is symmetric with respect to inversion of the perpendicular magnetic field.*

General trends

In general, we observe a few points worth summing up at the end. First, I_C is weaker for $\epsilon = 0.3$ than for $\epsilon = 0.5$, owing to larger areas of destructive interference and less coupling between the nanowires and the interfaces. Second, $\epsilon = 1/3$ does not have as prominent 1D-behaviour (as seen in Section 3.2.3) as $\epsilon = 1/2$, due to the fact that the ballistic NW-case can never be achieved when direct reflection at the beamsplitters is possible. Third, I_C is symmetric for all θ_B's with respect to inversion of the perpendicular magnetic field.

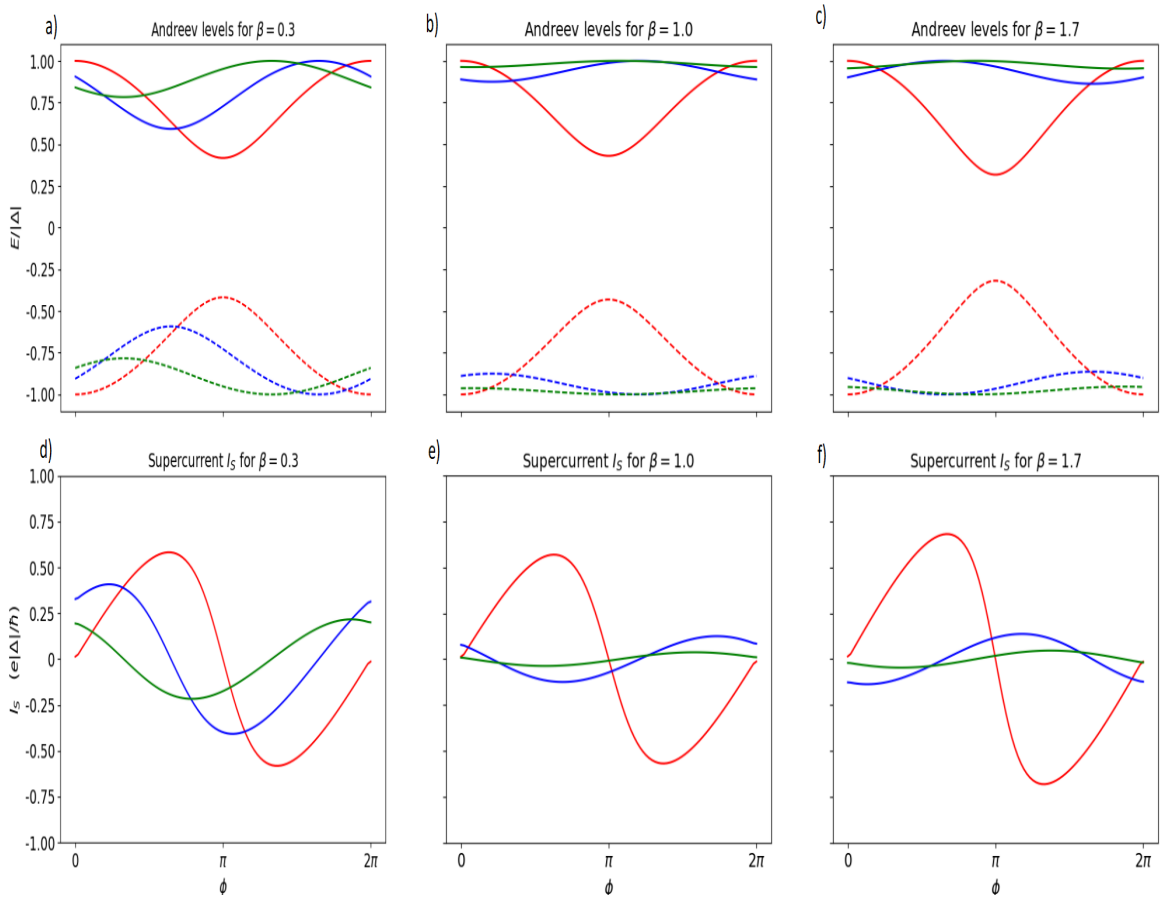

Figure 4.17: The figure shows the Andreev spectrum for a) $\beta = 0.3$, b) $\beta = 1$ and c) $\beta = 1.7$, and the supercurrent I_S for d) $\beta = 0.3$, e) $\beta = 1$ and f) $\beta = 1.7$ as a function of the phase difference ϕ. Plotted for $\theta_B = 0$ (red), $\theta_B = 1$ (blue) and $\theta_B = 2$ (green) with $\chi = 100$, $\lambda = 1.7$ and $\epsilon = 1/3$.

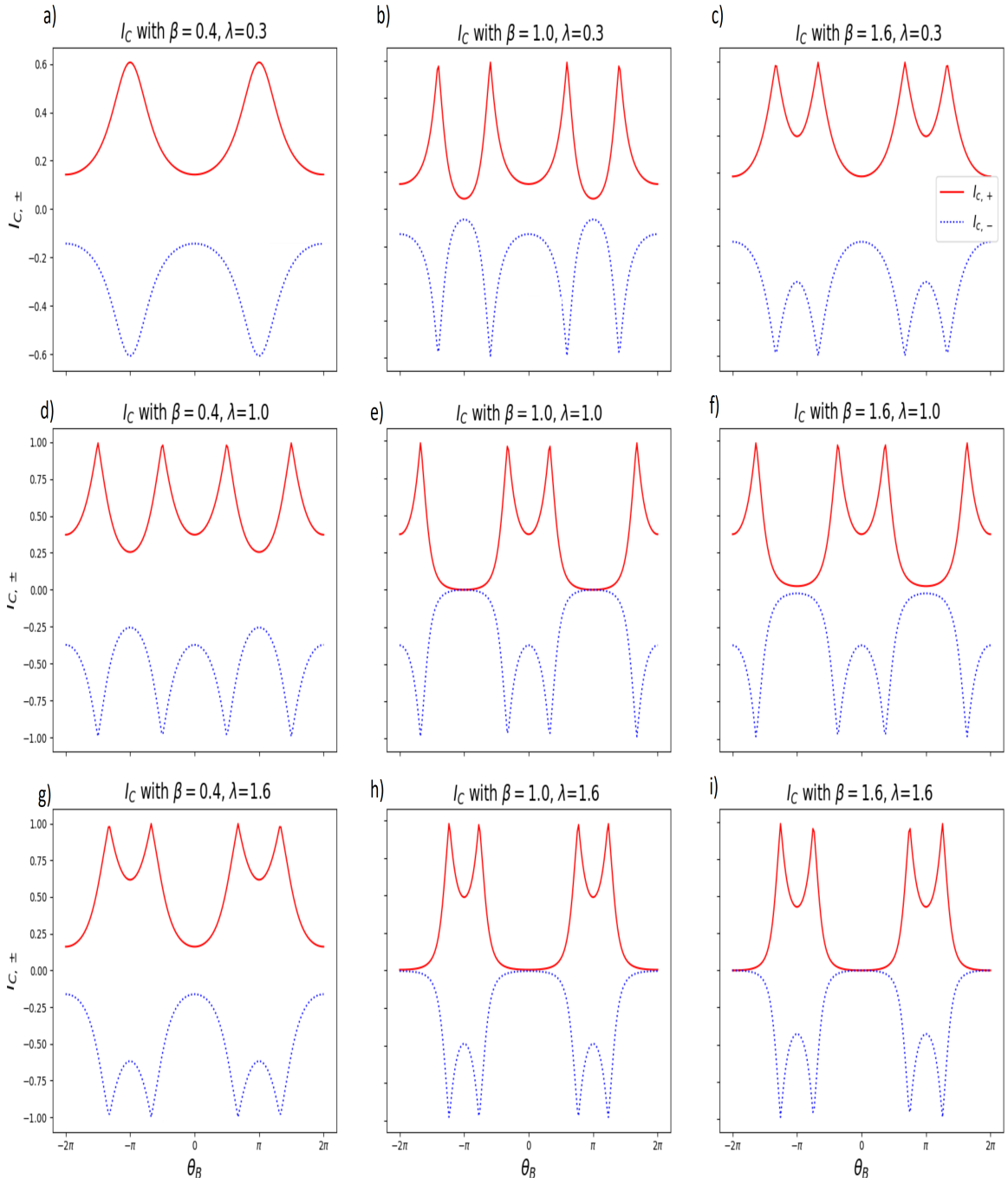

Figure 4.18: The figure shows the critical current for $\lambda = 0.3$ with a) $\beta = 0.4$, b) $\beta = 1$, c) $\beta = 1.6$, $\lambda = 1$ with d) $\beta = 0.4$, e) $\beta = 1$, f) $\beta = 1.6$ and $\lambda = 1.6$ with g) $\beta = 0.4$, h) $\beta = 1$, i) $\beta = 1.6$. Plotted with $\chi = 100$ and $\epsilon = 1/3$.

5 — Conclusion

The purpose for this research was to explain the asymmetries in the Fraunhofer-like patterns of the critical current as a function of applied magnetic field. A proposed possibility for these asymmetries is, apart from SOI and Zeeman interactions, system disorder. We have investigated the possibility of this phenomenon with a toy model to simulate disorder, modelling two possible paths across the junction by ballistic nanowires, split at the NS-interfaces by beamsplitters.

To better understand SNS-junctions and the supercurrents that flow through them, we started out by investigating the Andreev reflection at the NS-interfaces. We showed how the conversion of an electron to a hole, (and vice versa) follows naturally from the BdG-equation for superconductors and subsequently how the electrons and holes with certain spin orientation are converted into their corresponding counterparts with opposite spin. From this, we were able to calculate the energy levels in one-dimensional nanowires sandwiched between two superconductors, which had analytical expressions in the short-junction limit, and hence, the DC supercurrent. Correspondingly, we developed a model which included a magnetic field and a general SO-field, with contributions only from the lowest order in $\mathbf{k}$, into effective fields for electrons and holes. In finding a matrix expression equivalent to the BdG-equation, we found the energy levels of this system expressed with a single parameter combining the effects of magnetic field and SOI. An oscillatory behaviour in the supercurrent as a function of the angle between the magnetic field and the SO-field was observed, where the effect of both of these nearly cancelled when they were perpendicular and the SOI was in the intermediate or strong regimé. Also, we found no anomalous Jospehson current, which we attributed to the fact that we were considering a single conduction channel in a ballistic NW.

From this understanding of nanowires and Andreev reflection, we built a toy model for a two-dimensional SNS-junction at zero temperature. The model consisted of two possible paths across the normal material, connected by beamsplitters at the NS-interfaces. The paths were modelled as one-dimensional, ballistic nanowires. By developing a method for concisely connecting wavefunctions in the normal material, we found expressions for the outgoing waves (from the normal region) related to the incoming waves. The method involved scattering matrices for the beamsplitters and transfer matrices for the nanowires, in such a way that we could adjust the asymmetry between the length of, and the probability injection relation between, the nanowires. The scattering matrix approach to the beamsplitters also allowed us to decide on the coupling between the nanowires and the NS-interface. A magnetic field perpendicular to the junction was allowed to penetrate the region enclosed by the two nanowires, but not the nanowires themselves, so that the Aharanov-Bohm effect was present in our system. Thereafter, we found the transmission and reflection coefficients for the junction in both directions, which we combined with the Andreev reflection to find the Andreev energy levels of this system and thus, the

supercurrent.

However, we found that, in the absence of SOI and Zeeman interaction in the NW's, the critical current was symmetric with respect to the inversion of the perpendicular magnetic field. This was irrespective of combinations of the asymmetry of the injection probability, different path lengths, modifications of the chemical potential or NS-interface coupling strength. Thus, we conclude that either our toy model was not sufficiently complex, e.g. more than two interfering trajectories across the junction is necessary to explain the asymmetries, or that disorder at the NS-interfaces alone is not enough to explain these asymmetries. Further research is required in order to determine which conclusion is correct.

The obvious next step is to try to find these asymmetries by including magnetic fields in the nanowires, both perpendicular and parallel. Spin effects would then have to be taken into account because of the Zeeman effect, possibly also the magnetic shift in the momentum operators. This would mean that the time-reversal symmetry would no longer be valid in nanowires, and thus $\hat{t} \neq \hat{t}'$. Other possible ideas could be to include scatterers and spin-orbit interaction in the nanowires. We emphasise here that all of these ingredients are easily incorporated into our model, as they would all be included in the transfer matrices $\hat{t}$. In addition, in Section 3.4, we derived the transfer matrices for ballistic NW's when including both SOI and the Zeeman effect. Thus, most of this work is already done, and the main piece of further work would be to expand the basis by a factor of 2 to include spin. Other possibilities for improving our model is to include more than two paths across the junction, disorder in the normal region as well as on the interfaces, spatial extension of the nanowires to include more than one conduction channel or nonzero temperatures.

References

[1] Žutić, I., Fabian, J., and Das Sarma, S. *Reviews of Modern Physics* **76**(2), 323–410 (2004).

[2] Duy, L., Alexei, B., Edwin, P., Miguel, I., Iori, T., Takashi, K., Conrad, T., Ludwig, B., Talat, S. R., and Peter, A. D. *Journal of Physics: Condensed Matter* **27**(18), 182201 (2015).

[3] Datta, S. and Das, B. *Applied Physics Letters* **56**(7), 665–667 (1990).

[4] Bellucci, S. and Onorato, P. *Physical Review B* **78**(23), 235312 (2008).

[5] Földi, P., Benedict, M. G., Kálmán, O., and Peeters, F. M. *Physical Review B* **80**(16), 165303 (2009).

[6] Nitta, J., Akazaki, T., Takayanagi, H., and Enoki, T. *Physical Review Letters* **78**(7), 1335–1338 (1997).

[7] Schultz, M., Heinrichs, F., Merkt, U., Colin, T., Skauli, T., and Løvold, S. *Semiconductor Science and Technology* **11**(8), 1168 (1996).

[8] Manchon, A., Koo, H. C., Nitta, J., Frolov, S. M., and Duine, R. A. *Nature Materials* **14**, 871 (2015).

[9] Kohda, M., Nakamura, S., Nishihara, Y., Kobayashi, K., Ono, T., Ohe, J.-i., Tokura, Y., Mineno, T., and Nitta, J. *Nature Communications* **3**, 1082 (2012).

[10] Debray, P., Rahman, S. M. S., Wan, J., Newrock, R. S., Cahay, M., Ngo, A. T., Ulloa, S. E., Herbert, S. T., Muhammad, M., and Johnson, M. *Nature Nanotechnology* **4**, 759 (2009).

[11] Nazarov, Y. V. and Danon, J. *Advanced Quantum Mechanics : A Practical Guide*. Cambridge : Cambridge University Press, Cambridge, (2013).

[12] Nowack, K. C., Koppens, F. H. L., Nazarov, Y. V., and Vandersypen, L. M. K. *Science* **318**(5855), 1430–1433 (2007).

[13] Nadj-Perge, S., Frolov, S. M., Bakkers, E. P. A. M., and Kouwenhoven, L. P. *Nature* **468**, 1084 (2010).

[14] Chirolli, L. and Burkard, G. *Advances in Physics* **57**(3), 225–285 (2008).

[15] Kitaev, A. Y. *Physics-Uspekhi* **44**(10S), 131 (2001).

[16] Bravyi, S. B. and Kitaev, A. Y. *Annals of Physics* **298**(1), 210–226 (2002).

[17] Liu, C. and Jia, J. *National Science Review* **1**(1), 36–37 (2014).

[18] Kittel, C. and McEuen, P. *Introduction to solid state physics.* Wiley, Hoboken, N.J, 8th. edition, (2005).

[19] Drozdov, A. P., Eremets, M. I., Troyan, I. A., Ksenofontov, V., and Shylin, S. I. *Nature* **525**, 73 (2015).

[20] Beenakker, C. *Annual Review of Condensed Matter Physics* **4**(1), 113–136 (2013).

[21] Fu, L. and Kane, C. L. *Phys. Rev. Lett.* **100**, 096407 Mar (2008).

[22] Masatoshi, S. and Yoichi, A. *Reports on Progress in Physics* **80**(7), 076501 (2017).

[23] Das, A., Ronen, Y., Most, Y., Oreg, Y., Heiblum, M., and Shtrikman, H. *Nature Physics* **8**, 887 (2012).

[24] Finck, A. D. K., Van Harlingen, D. J., Mohseni, P. K., Jung, K., and Li, X. *Physical Review Letters* **110**(12), 126406 (2013).

[25] Williams, J. R., Bestwick, A. J., Gallagher, P., Hong, S. S., Cui, Y., Bleich, A. S., Analytis, J. G., Fisher, I. R., and Goldhaber-Gordon, D. *Physical Review Letters* **109**(5), 056803 (2012).

[26] Ruby, M., Pientka, F., Peng, Y., von Oppen, F., Heinrich, B. W., and Franke, K. J. *Physical Review Letters* **115**(19), 197204 (2015).

[27] Hell, M., Leijnse, M., and Flensberg, K. *Physical Review Letters* **118**(10), 107701 (2017).

[28] Hell, M., Flensberg, K., and Leijnse, M. *Physical Review B* **96**(3), 035444 (2017).

[29] Litinski, D. and von Oppen, F. arXiv: 1801.08143v1, 2018.

[30] Mourik, V., Zuo, K., Frolov, S. M., Plissard, S. R., Bakkers, E. P. A. M., and Kouwenhoven, L. P. *Science* **336**(6084), 1003–1007 (2012).

[31] Deng, M. T., Yu, C. L., Huang, G. Y., Larsson, M., Caroff, P., and Xu, H. Q. *Nano Letters* **12**(12), 6414–6419 (2012).

[32] Yurgens, A. A. *Superconductor Science and Technology* **13**(8), R85 (2000).

[33] Andreev, A. F. *Journal of Experimental and Theoretical Physics* **19**(5), 1823 (1964).

[34] Andreev, A. F. *Journal of Experimental and Theoretical Physics* **22**(2), 655 (1966).

[35] Nazarov, Y. V. and Blanter, Y. M. *Quantum Transport: Introduction to Nanoscience.* Cambridge University Press, Cambridge, (2009).

[36] Josephson, B. D. *Physics Letters* **1**(7), 251–253 (1962).

[37] Buzdin, A. *Physical Review Letters* **101**(10), 107005 (2008).

[38] Liu, J.-F. and Chan, K. S. *Physical Review B* **82**(12), 125305 (2010).

[39] Pablo, S.-J., Jorge, C., Elsa, P., and Ramón, A. *New Journal of Physics* **15**(7), 075019 (2013).

[40] Bezuglyi, E. V., Rozhavsky, A. S., Vagner, I. D., and Wyder, P. *Physical Review B* **66**(5), 052508 (2002).

[41] Ketterson, J. B. and Song, S. N. *Superconductivity*. Cambridge University Press, Cambridge, (1999).

[42] Dynes, R. C. and Fulton, T. A. *Physical Review B* **3**(9), 3015–3023 (1971).

[43] Hui, H.-Y., Lobos, A. M., Sau, J. D., and Das Sarma, S. *Physical Review B* **90**(22), 224517 (2014).

[44] Shabani, J., Kjaergaard, M., Suominen, H. J., Kim, Y., Nichele, F., Pakrouski, K., Stankevic, T., Lutchyn, R. M., Krogstrup, P., Feidenhans'l, R., Kraemer, S., Nayak, C., Troyer, M., Marcus, C. M., and Palmstrøm, C. J. *Physical Review B* **93**(15), 155402 (2016).

[45] Kjaergaard, M., Nichele, F., Suominen, H. J., Nowak, M. P., Wimmer, M., Akhmerov, A. R., Folk, J. A., Flensberg, K., Shabani, J., Palmstrøm, C. J., and Marcus, C. M. *Nature Communications* **7**, 12841 (2016).

[46] Suominen, H. J., Danon, J., Kjaergaard, M., Flensberg, K., Shabani, J., Palmstrøm, C. J., Nichele, F., and Marcus, C. M. *Physical Review B* **95**(3), 035307 (2017).

[47] Rasmussen, A., Danon, J., Suominen, H., Nichele, F., Kjaergaard, M., and Flensberg, K. *Physical Review B* **93**(15), 155406 (2016).

[48] Fetter, A. L. and Walecka, J. D. *Quantum theory of many-particle systems*. Dover Publications, Mineola, N.Y, (2003).

[49] Onnes, H. K. *Commun. Phys. Lab., Univ. Leiden* **Suppl. 34**(b), 133–134 (1913).

[50] Meissner, W. and Ochsenfeld, R. *Naturwissenschaften* **21**(44), 787–788 (1933).

[51] Henyey, F. S. *Physical Review Letters* **49**(6), 416–416 (1982).

[52] File, J. and Mills, R. G. *Physical Review Letters* **10**(3), 93–96 (1963).

[53] Bardeen, J., Cooper, L. N., and Schrieffer, J. R. *Physical Review* **108**(5), 1175–1204 (1957).

[54] G. de Gennes, P. *Superconductivity of metals and alloys / P. G. de Gennes*. (1966).

[55] Bardeen, J., Kümmel, R., Jacobs, A. E., and Tewordt, L. *Physical Review* **187**(2), 556–569 (1969).

[56] Beenakker, C. W. J. *Phys. Rev. Lett.* **67**, 3836–3839 Dec (1991).

[57] Yokoyama, T. and Yu, V. N. *EPL (Europhysics Letters)* **108**(4), 47009 (2014).

[58] Timm, C.

[59] Winkler, R. *Spin-orbit coupling effects in two-dimensional electron and hole systems*, volume vol. 191 of *Springer tracts in modern physics*. Springer, Berlin, (2003).

[60] Telegdi, V. *Beiträge zur Entwicklung der Physik: Festgabe zum 70. Geburtstag von Professor Paul Scherrer, 3. Februar 1960* **5**, 249 (1960).

[61] Kálmán, O. *Quantum Interference in Semiconductor Rings*. Phd thesis, (2009).

[62] Joyce, H., Boland, J. L., Davies, C. L., Baig, S. A., and Johnston, M. B. *Semiconductor Science and Technology* **31**(10), 103003 (2016).

[63] Kulik, I. O. *Journal of Experimental and Theoretical Physics* **30**(5), 944 (1969).

[64] Hemmer, P. *Kvantemekanikk*. Tapir akademisk forlag, 5. edition, (2005).

[65] Golubov, A. A., Kupriyanov, M. Y., and Il'ichev, E. *Reviews of Modern Physics* **76**(2), 411–469 (2004).

[66] van Heck, B., Väyrynen, J. I., and Glazman, L. I. *Physical Review B* **96**(7), 075404 (2017).

[67] Yokoyama, T., Eto, M., and Nazarov, Y. V. *Physical Review B* **89**(19), 195407 (2014).

[68] Beri, B., Bardarson, J. H., and Beenakker, C. W. J. *Phys. Rev. B* **77**, 045311 Jan (2008).

[69] Krive, I. V., Gorelik, L. Y., Shekhter, R. I., and Jonson, M. *Low Temperature Physics* **30**(5), 398–404 (2004).

[70] Yokoyama, T., Eto, M., and V. Nazarov, Y. *Journal of the Physical Society of Japan* **82**(5), 054703 (2013).

[71] Shapiro, B. *Physical Review Letters* **50**(10), 747–750 (1983).

[72] Büttiker, M., Imry, Y., and Azbel, M. Y. *Physical Review A* **30**(4), 1982–1989 (1984).

[73] Markos, P. and Soukoulis, C. M. *Wave Propagation From Electrons to Photonic Crystals and Left-Handed Materials*. Princeton University Press, stu - student edition edition, (2008).

[74] Cattapan, G. and Lotti, P. *Physica E: Low-dimensional Systems and Nanostructures* **43**(1), 293–301 (2010).